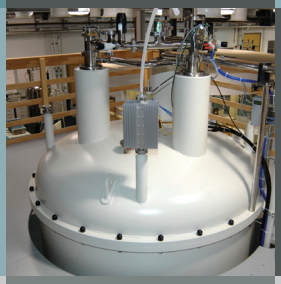

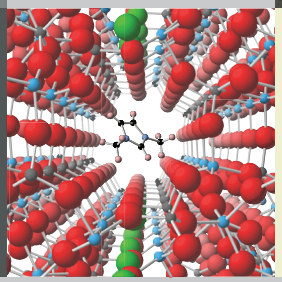

The UK 850 MHz Solid-State NMR Facility

Annual Report 2010

The UK 850 MHz solid-state NMR facility at the University of Warwick was formally opened by David Delpy, Chief Executive of EPSRC on Thursday 28th October 2010. The occasion was marked by a symposium with lectures by internationally-leading members of the solid-state NMR community: Marc Baldus, Utrecht University, The Netherlands, "Solid-state NMR on complex biomolecules"; Rod Wasylishen, University of Alberta, Canada, "NMR investigations of solids at high magnetic field strengths: new opportunities for interrogating quadrupolar nuclei in solids"; Clare Grey, University of Cambridge, U.K, "Following Function in Real Time: New NMR Methods for Studying Structure and Dynamics in Batteries and Fuel Cells". The event attracted an excellent turnout with 86 registered delegates from across the UK.

Photo: The National Management Committee with David Delpy. From left to right: Front: Steven Brown (Warwick, NMC Chair), David Delpy (EPSRC), Sharon Ashbrook (St Andrews), Robin Harris (Durham), Mark Smith (Warwick). Back: Stephen Wimperis (Glasgow), Ray Dupree (Warwick), Jeremy Titman (Nottingham), Melinda Duer (Cambridge), Dinu Iuga (Facility Manager)

Contents

Introduction

The detailed planning of the UK's first high-field solid-state NMR facility began in January 2009, following a £3.7 M grant from EPSRC (including a contribution from BBSRC) to a consortium of UK solid-state NMR spectroscopists who form the National Management Committee of the Facility, with additional financial contributions from the University of Warwick (in part through the Birmingham Science City Advanced Materials Projects 1 and 2, supported by Advantage West Midlands and the European Regional Development Fund).

The purpose of the Facility is not only to underpin world-class research in chemistry, materials, earth sciences, biology and physics in the UK, but to stimulate new research. The 850 MHz magnet at the heart of the Facility allows experiments to be performed that simply cannot be done successfully at lower fields. The linebroadening associated with quadrupolar nuclei, for instance, decreases markedly with increasing magnetic field strength, whilst the signal-to-noise ratio increases, presenting a win-win situation for the spectroscopist. Thus a structural study that would simply not be possible at lower field becomes tractable at 850 MHz. For instance, observing ^{17}O at natural abundance becomes possible at 850 MHz, which has led to a surge of interest in studying this nucleus for a wide range of applications from examining hydrogen bonding to studying the structure and molecular dynamics in geological minerals. Section 7 of this report contains detailed descriptions of the research enabled by the Facility in its first year of operation. The Facility also provides a focus for solid-state NMR spectroscopy in the UK with the Facility implementing new solid-state NMR experiments as they appear in the literature for the benefit of the UK science community and the Facility Manager available for advice to those less familiar with the technique.

Installation of the Facility's Bruker 850 MHz wide bore spectrometer in the new Magnetic Resonance Centre of Millburn House at the University of Warwick began in July 2009, overseen by newly-appointed Facility Manager, Dr Dinu Iuga. The magnet came to field on 14th August 2009 and testing of the spectrometer and commissioning of the probes began in September 2009. Testing continued until January 2010, during which time 11 of the 12 probes at the Facility were commissioned (the remaining probe, for double-rotation experiments, as supplied by the Samoson group in Tallinn, Estonia, was made available to facility users at the start of 2011) and a wide range of solid-state NMR pulse sequences were setup and tested on a range of different nuclei and samples that represented the broad spectrum of samples expected at the Facility.

The first call for time on the Facility went out to the UK science community in autumn 2009 with the Facility welcoming the first users on 1st February 2010. 80% of the spectrometer time is allocated by a three-person Time-Allocation Panel (TAP) and is available to any UK academic or spectroscopist working in industry of similar standing. In its first year of operation, the Facility was heavily oversubscribed with applications with a total of 525 days of time being requested and only 302 available. A total of 19 Principal Investigators carried out work on 44 projects over the year, a hugely successful beginning.

Further details of the Facility can be found at the Facility website:
http://go.warwick.ac.uk/850mhz/

Organization and Management of the Facility

The UK National High-field Solid-state NMR Facility was established with the aid of several linked research grants from EPSRC. The eight investigators on the grant comprise the National Management Committee (NMC) which determines the strategic objectives for the Facility and the procedures by which these are to be achieved. The NMC meets twice a year, communicating informally more frequently as the need arises. The operation of the Facility is the responsibility of the Local Management Team comprising the Facility Manager who is an ex-officio member of the NMC and the Warwick-based NMC chair. The duties of the Facility Manager include maintaining the instrumentation and assisting visitors to the Facility with their experiments. The management of the Facility is overseen by the International Advisory Board (IAB) which is made up of three eminent solid-state NMR spectroscopists from overseas: Marc Baldus (Utrecht), Arno Kentgens (Nijmegen), Roderick Wasylishen (Alberta).

Time Allocation Process

All UK academics who are eligible to apply for Research Council funding, as well as UK researchers of similar standing in industry, may apply for an allocation of spectrometer time at the Facility. Users are expected to run their own experiments with the assistance of the Facility Manager, so personnel with previous solid-state NMR experience must be identified to visit the Facility and carry out the research. A minimum of 80 % of the available time is allocated by an independent Time Allocation Panel (TAP) which comprises three UK scientists, including one member of the NMC, as well as the Facility Manager in an ex-officio capacity. The balance is allocated by the NMC and is reserved for fast-track applications, measurements referred from the EPSRC solid-state NMR service, the Facility Manager's designated research time and to compensate users who were unable to take up their allocated time because of instrument down-time. Members of the TAP normally serve for a two-year term.

There are two allocation rounds each year for time, each covering a six-month period, starting in either February or August. Deadlines for receipt of proposal are published on the Facility website and normally occur two months prior to the start of the allocation period. Previous users of the Facility are normally notified of these deadlines by email. Further details of future deadlines, previous time allocations and instructions for applicants are given on the Facility website (http://go.warwick.ac.uk/850mhz/). The main criterion for allocating time is overall scientific merit, as well as the quality of the case made for high-field solid-state NMR. Where appropriate, the TAP will consider additional factors, such as the quality of publications arising from previous allocations of time and whether the research is supported by peer-reviewed grants or involves students funded by EPSRC or BBSRC. The TAP is charged with ensuring that the balance of the allocated time broadly reflects the research objectives of the original grant and with providing feedback for unsuccessful applicants. During the TAP meeting, the Facility Manager gives advice on the feasibility of the proposed experiments and the spectrometer time required.

The maximum time that can be requested by an individual applicant during any allocation round is 28 days, but this can be split between several applications. It is a condition that the Facility is mentioned in any publication arising wholly or partly from an allocation of time. Furthermore, an experimental report must be produced by the original applicant no later than three months after the end of the specific six-month time-allocation period. Applications are not accepted from users who have outstanding experimental reports from previous allocations of time. The code for all NMR pulse sequences implemented by users on the Facility's spectrometer must be deposited in a shared database. If the experiment is a new one, the code will only be made available to other users after the pulse sequence has been published. Reasonable travel costs associated with the use of the facility will be paid to academic users. The Facility rents accommodation on the University of Warwick campus for use by Facility visitors.

TAP membership (2010): non-NMC members: Mike Anderson (Manchester) & David Middleton (Liverpool). Chair: 2010: Robin Harris (Durham); from the February 2011 allocation round onwards: Jeremy Titman (Nottingham).

What is the Facility?

UK 850 MHz solid-state NMR facility probes

No	Probe
1	1.3 mm probe HXY (+19F) conventional insert design H13863
2	2.5 mm HXY DBB (double-broadband) H13856
3	2.5 mm HX (+19F) H13889
4	2.5 mm HFX H13894
5	3.2 mm HXY DBB (double-broadband) H13857
6	3.2 mm HXY low E field for biosolids LLC H13900
7	3.2 mm HXY conventional insert design H13888
8	4 mm HXY conventional insert design (+19F) H13694
9	4 mm HX (low gamma) H13892
10	7 mm X (low gamma) H13895
11	Static
12	DOR probe (produced by Samoson group, Tallinn, Estonia)

Probes 1 to 11 were supplied by Bruker. Maximum MAS frequencies: 4 mm probes 15 kHz; 3.2 mm probes 24 kHz, 2.5 mm probes 35 kHz; 1.3 mm probe 65 kHz. All 3.2 mm and 4 mm MAS probes are equipped with DVT stators and can operate between -140 ^{O}C + 150 ^{O}C.

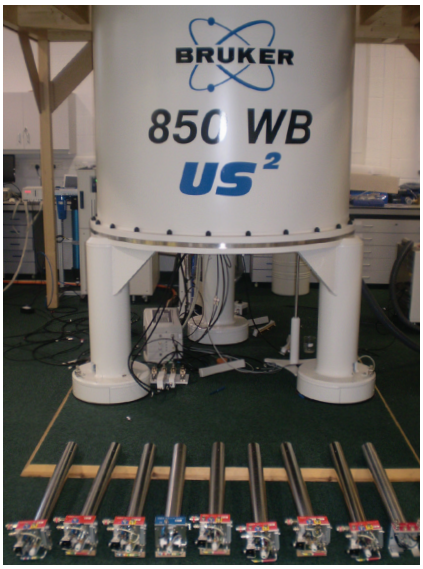

850 MHz spectrometer and probes

Probes usage 2010

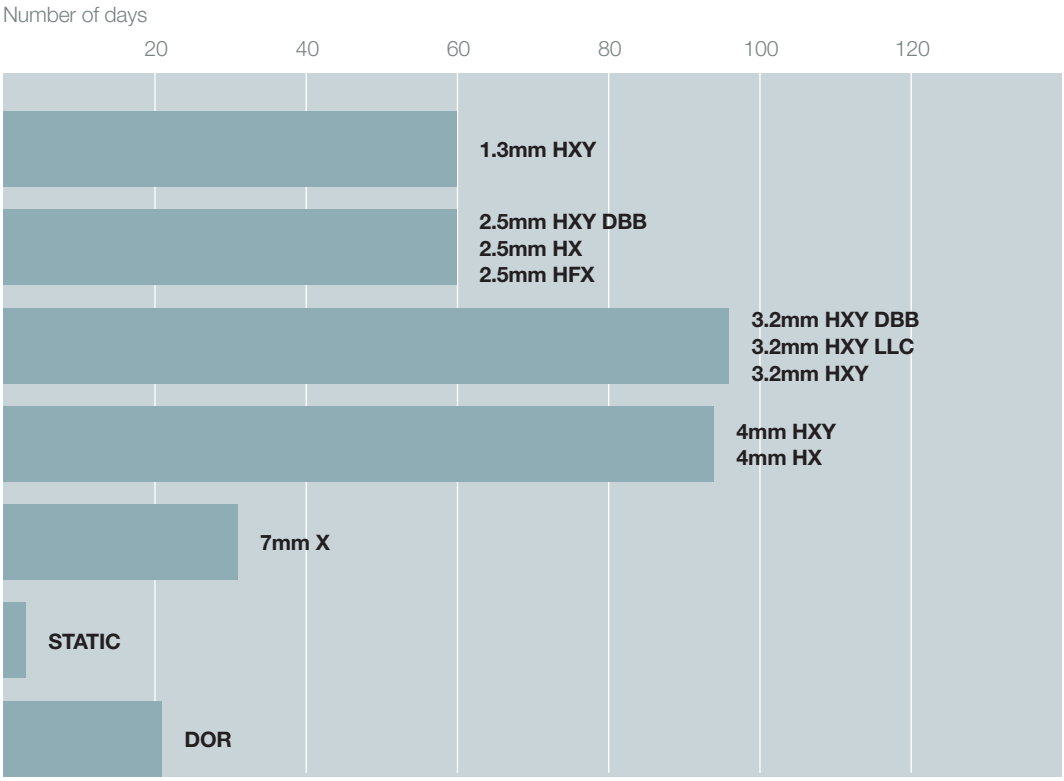

Nuclei tested in Double Resonance Mode

Probe in double Resonance mode	Mode	X-Nucleus																		
		^{31}P	^{87}Rb	^{11}B	^{71}Ga	^{23}Na	^{27}Al	^{13}C	^{79}Br	^{93}Nb	^{29}Si	^{2}H	^{17}O	^{15}N	^{35}Cl	^{14}N	^{43}Ca	^{25}Mg	^{89}Y	^{39}K	^{87}Sr
1.3 mm probe HXY (+19F) conventional insert design	DR ^{1}H-X DR ^{19}F-X ●				■	✸	✸	■ ■	■	■	✸	✸	■	■	✸	■					
2.5 mm HX (+19F) 2.5 mm HFX 2.5mm HXY DBB	DR ^{1}H-X DR ^{19}F-X ●	■	✸	✸	■	✸	✸ ■	■ ■	■	✸	✸	✸	■	■	✸	■	✸	■			
3.2 mm HXY low E field for biosolids LLC	DR ^{1}H-X		✸	✸	✸	✸	✸	■	■	✸	✸	✸	✸	■	✸	✸					
3.2 mm HXY conventional insert design 3.2mm HXY DBB	DR ^{1}H-X		■	■	■	✸	■	■	✸	✸	✸	✸	■	■	✸	■					
4 mm HXY conventional insert design (+19F)	DR ^{1}H-X DR ^{19}F-X ●	■	✸	✸	✸	■	■	■ ■	✸	✸	■	✸	✸	■ ■	✸	✸					
4 mm HX (low gamma)	DR ^{1}H-X							■	■	■	✸	■	■	■	✸	■	✸	■	■	✸	
7 mm X (low gamma)	X												✸	✸	■	■	■	✸	■	■	■
Static	X	■	✸	✸	✸	✸	✸	■	✸	✸	✸	■	✸	✸	■	■	✸	✸	✸	■	

■ *experiments performed at the facility to date.*
✸ *bench tests indicate should be possible;*
● *Other ^{19}F- X DR combinations have not yet been investigated.*
For triple-resonance capabilities, refer to the facility website.

The UK 850 MHz Solid-State NMR Facility PhD Travel Fund

Supported by Bruker

The UK 850 MHz Solid-State NMR Facility PhD travel fund supported by Bruker provides funding for: (a) attendance at an internationally recognised, high-profile conference where a PhD student presents results he/she obtained at the 850 MHz Facility, or (b) a "start-up" visit to another lab to learn new methods to be implemented at the 850 MHz Facility. For further details see: **http://go.warwick.ac.uk/850mhz/travel_fund/**

2010 awards

Mr Garrick F. Taylor (University of Southampton) awarded £800 to attend the Joint EUROMAR 2010 and 17th ISMAR Conference in Florence, Italy (4-9 July 2010) and present a poster entitled *Insights into the structure of beta-2 microglobulin fibrils and the role of serum amyloid-P component in their stabilisation*.

Mr Jonathan Bradley (University of Warwick) awarded £900 to attend the Rocky Mountain Conference on Analytical Chemistry in Snowmass, Colorado (1-5 August 2010) and present a talk entitled *^{1}H double-quantum build-up curves from DQ filtered ^{1}H-^{13}C correlation spectra of indomethacin-gamma*.

Time Allocation

525 days requested by 21 PI from 11 different institutions (Cambridge, Cardiff, Glasgow, King's College London, Liverpool, Nottingham, Queen Mary College London, Southampton, St. Andrews, University College London and Warwick). 302 days allocated by the Time Allocation Panel.

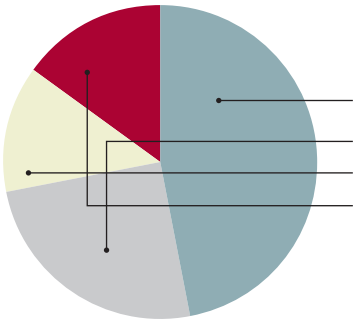

Requested time

Outside Warwick and non-NMC **47%**
NMC outside Warwick **25%**
Warwick NMC **13%**
Warwick non NMC **15%**

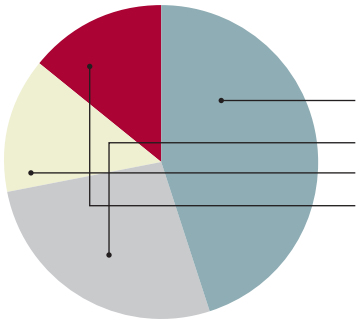

Allocated time

Outside Warwick and non-NMC **45%**
NMC outside Warwick **27%**
Warwick NMC **14%**
Warwick non NMC **14%**

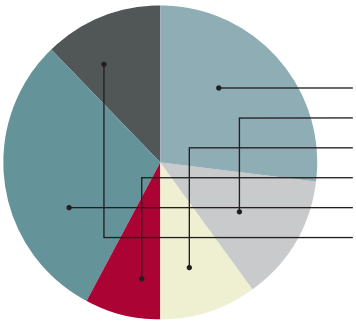

Requested time

Advanced materials **27%**
Bio materials **13%**
Energy materials **10%**
Methods development **8%**
Proteins **30%**
Pharmaceuticals and supramolecular chemistry **12%**

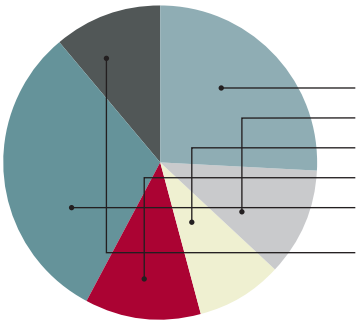

Allocated time

Advanced materials **26%**
Bio materials **11%**
Energy materials **9%**
Methods development **12%**
Proteins **31%**
Pharmaceuticals and supramolecular chemistry **11%**

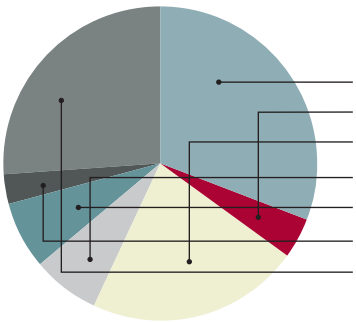

Requested time

EPSRC grants **31%**
BBSRC grants **4%**
EPSRC PhD **22%**
BBSRC PhD **7%**
Other agencies **7%**
Industrial PhD funding **3%**
No external funding **26%**

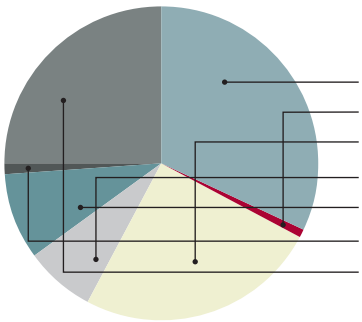

Allocated time

EPSRC grants **32%**
BBSRC grants **1%**
EPSRC PhD **25%**
BBSRC PhD **7%**
Other agencies **9%**
Industrial PhD funding **1%**
No external funding **25%**

Projects with more than one funding source were counted only once. Other agencies that are funding facility users are: Medical Research Council, Science and Technology Funding Council, Wellcome Trust, British Heart Foundation, EU ERC and Royal Society.

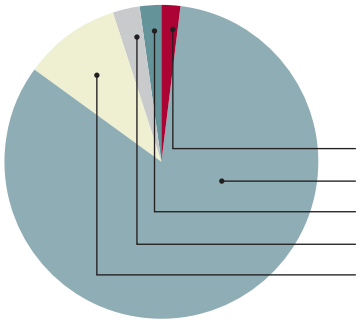

Spectrometer time

Feb 1 2010 – Jan 31 2011
(the facility operates 24 hours a day 7 days a week)

Fast track **2%**
TAP allocated days **83%**
Compensation **2%**
Maintenance **3%**
Facility manager research **10%**

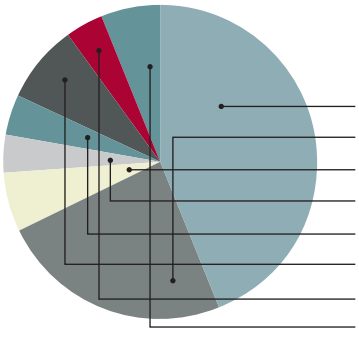

Facility users

Feb 1st 2010 – Jan 31 2011

21 PIs + 1 UK academic
12 EPSRC PhD students*
3 BBSRC PhD students
2 industrial funded PhD students
2 other PhD students**
4 PDRA***
2 permanent research staff
3 overseas collaborators

**Some students were partially funded by industry, STFC or the corresponding university*
***1 Overseas (USA) funded PhD and 1 self funded*
****1 EPSRC funding, 1 BBSRC funding, 1 Wellcome Trust funding and 1 EU funding*

Results from User Questionnaire Feb 2010 – Jan 2011

Feedback questionnaires are provided for each visit to the facility and contain a series of questions and the opportunity for visitors to make comments and suggestions. The responses are graded from 1 (least satisfied) to 5 (most satisfied). Figure 1 shows the average scores based on results from 39 responses from visits over the period February 2010 to January 2011.

Section 1 to be completed by the PI

Application for time

1 The ease of the application process
2 The transparency of the application process
3 The feedback on any unsuccessful time requests

Scheduling of time awarded

4 The scheduling of your time by the facility

Section 2 to be completed by the visitor

Accommodation

5 The ease of arranging accommodation
6 The quality of the accommodation
7 The location of the accommodation

At the 850 facility

8 The support from the facility manager upon arrival
9 The support from the facility manager throughout your visit
10 The quality of the NMR facilities
11 The quality of the office facilities
12 The quality of the sample preparation area and storage facilities
13 The ease of access to the facility out of hours
14 Your overall time at the facility

Post visit experience

15 The arrangements for accessing data
16 The arrangements for returning any samples
17 Reimbursement of any expenses

Average scores from feedback questionnaire over period Feb 2010 – Jan 2011

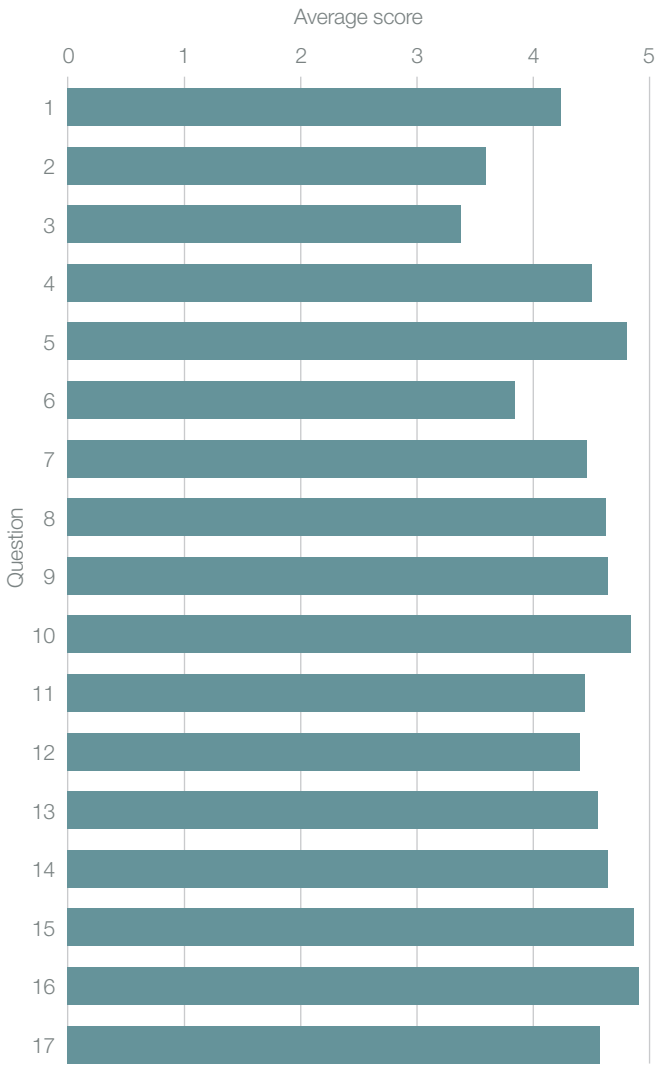

The Reports

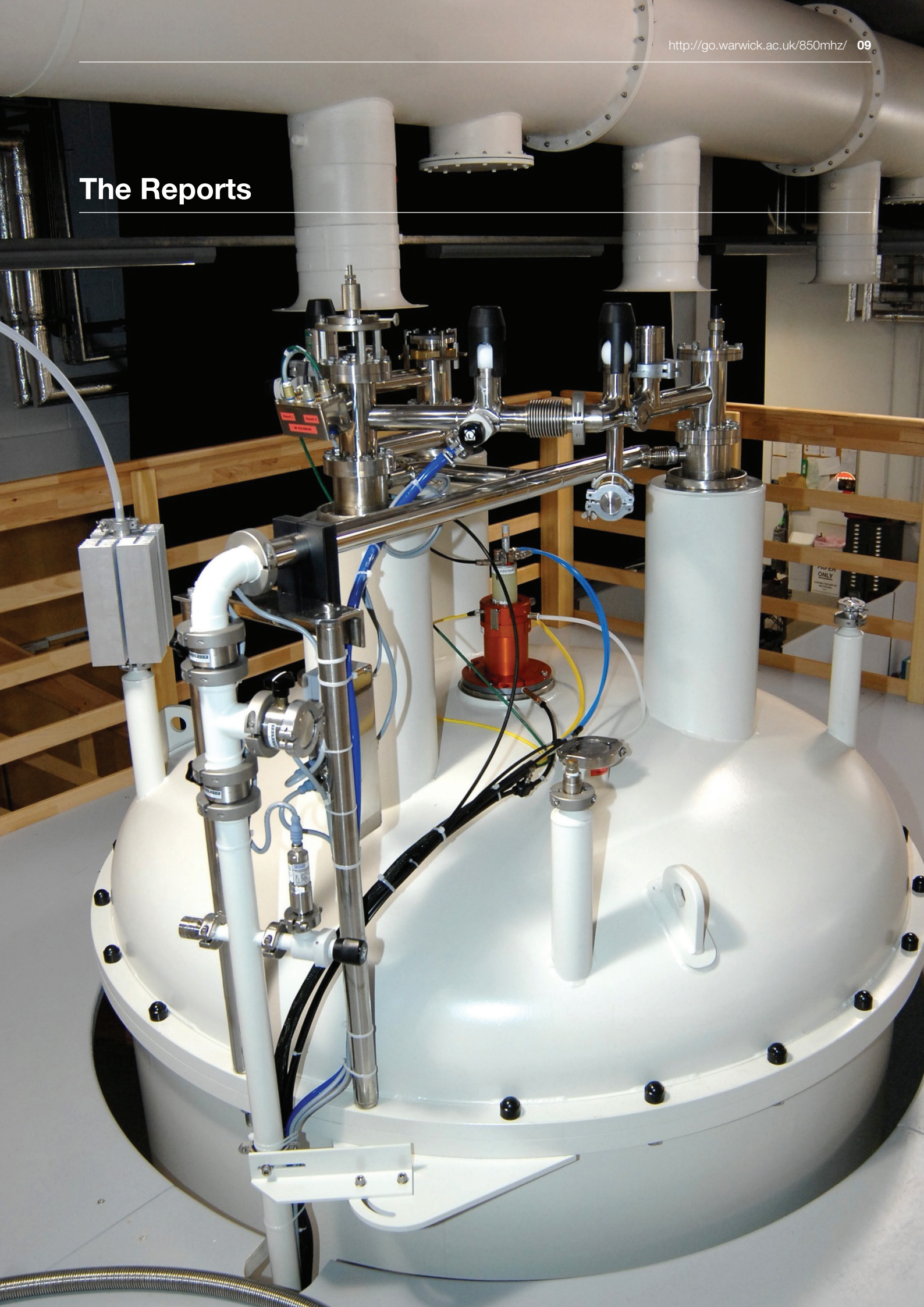

Natural Abundance Deuterium NMR for Molecular Dynamics Studies and Proton Chemical Shift Measurements in Solids

Abil E. Aliev,[1] Sam E. Mann,[1] Dinu Iuga[2] and Kenneth D. M. Harris[3]

[1]Department of Chemistry, University College London, [2]Department of Physics, University of Warwick, [3]School of Chemistry, Cardiff University

Overview

One of the reasons why solid-state NMR is not as widely employed as its solution-state counterpart is that such a common nucleus as ^{1}H shows little or no resolution in NMR spectra of solids due to strong homonuclear ^{1}H···^{1}H dipole-dipole interactions. Selective averaging of these anisotropic interactions is associated with significant experimental challenges and a number of advanced NMR strategies have been devised for this purpose, allowing information on isotropic ^{1}H NMR chemical shifts to be accessed and exploited.[1] An alternative simple approach for accessing information on ^{1}H chemical shifts in solids is to exploit the fact that proton (^{1}H) and deuterium (^{2}H) chemical shifts are essentially the same, except for small second-order shifts which are considerably less significant at very high magnetic fields. The more routine nature of this approach emanates from the fact that acquisition of high-resolution ^{2}H NMR spectra for solids only requires averaging of the anisotropic heteronuclear ^{2}H···^{1}H dipole-dipole interactions, which is readily achieved using standard ^{1}H decoupling techniques. Other anisotropic interactions of ^{2}H are readily averaged by magic angle spinning (MAS). As a consequence, the routine measurement of high-resolution NMR spectra for solids is significantly more straightforward for ^{2}H NMR than for ^{1}H NMR. However, the major drawback of ^{2}H NMR is its inherently low sensitivity, and for this reason, ^{2}H NMR studies of solids are virtually always carried out on isotopically-enriched materials, which imposes limitations with regard to materials synthesis and preparation. Clearly, it would be highly desirable to be able to carry out ^{2}H NMR studies on solid materials with natural isotopic abundances.

Background

Natural-abundance (NA) solid-state ^{2}H NMR was first explored by us in 1994, and it was shown that this technique represents a feasible approach for establishing ^{1}H chemical shifts of solids.[2] In particular, we showed that the signals from inequivalent sites in solids could be successfully resolved in solid-state NA ^{2}H MAS NMR spectra. In some favourable cases, chemical shift differences as small as 0.1 ppm were resolved, and it was shown that relative peak intensities could be used in peak assignment in a similar manner to the analysis of routine solution-state ^{1}H NMR spectra. In order to address the low sensitivity of ^{2}H NMR, we carried out detailed studies of ^{1}H–^{2}H CP dynamics for NA samples, leading to the first demonstration that ^{2}H CPMAS NMR can provide up to a six-fold sensitivity enhancement in comparison with single-pulse ^{2}H MAS NMR.[2] In another publication, we had earlier shown that solid-state NA ^{2}H NMR spectra can be recorded for rotator phase solids, as well as for the rigid phases of the same materials below their rotator-phase transition temperatures.[3] To date, however, very few solids have been probed using ^{2}H MAS NMR, and there is a clear need for extending these studies in order to assess the potential of the technique. Another less explored feature of solid-state ^{2}H MAS NMR is that the measured spectra are expected to reflect motional averaging effects with frequencies of the order of 10^{5} – 10^{7} Hz, thus providing efficient means for assessing dynamic processes in solid materials.

Preliminary results

From the ^{2}H MAS NMR spectra of amino acids, the sensitivity of ^{2}H NMR chemical shifts to the existence of N–H···O and C–H···O close contacts was revealed. By measuring NA ^{2}H MAS NMR spectra for the α and γ polymorphs of glycine, we showed that the isotropic ^{2}H chemical shift and linewidth of the signal due to the NH_3^+ group can be used for easy identification of polymorphic form. The NH_3^+ signal for the α polymorph, for example, is detected in less than 3 mins of acquisition. In contrast to the situation for motionally mobile NH_3^+ groups (as in glycine polymorphs) and CH_3 groups (as in L-alanine), however, we were unable to detect signals due to deuterons in motionally static methine and methylene groups in amino acids by NA ^{2}H MAS NMR. The half-height linewidths of the NH_2D^+ signal for the α polymorph (70 Hz) and γ polymorph (180 Hz) of glycine were found to be significantly different, which is attributed to the difference in rotational mobility of the NH_2D^+ group in the two polymorphs. The rotation frequencies at 298 K for the NH_3^+ group about the C^{α}–N bond in the α and γ polymorphs of glycine have been determined previously to be 77 GHz and 3 GHz respectively. For L-alanine, the signal due to the NH_2D^+ group in the NA ^{2}H MAS NMR spectrum is very broad (~700 Hz), correlating well with the much lower rotation frequency (*ca*. 7 MHz) for the NH_3^+ group in L-alanine

compared to glycine. For L-alanine, the rotation frequency approaches the same order of magnitude as the static ^{2}H coupling constant, thus leading to significant line broadening in ^{2}H MAS NMR spectra. These findings indicate that NA ^{2}H MAS NMR is a promising technique for routine characterization of solid-state dynamics in materials with natural isotopic abundances (e.g., polymorphs of drugs), and we plan to explore this issue in more depth in the future.

We also undertook preliminary NA ^{2}H MAS NMR measurements for a solid protein, collagen (molecular weight ~300 kDa). Specifically, the collagen-containing material that we studied was 62 mg of a new parchment sample made of calf skin. The NA ^{2}H MAS NMR spectrum obtained after 7 h of acquisition showed two well-resolved peaks attributed to the NH_2D^+ peptide end-groups and the methyl CH_2D groups in collagen. Other aliphatic peaks were also detected, but were not well resolved. It is noteworthy that the NA ^{2}H MAS NMR spectrum has sharper lines than the ^{1}H MAS NMR spectrum of the same material.

A number of organic solids were also studied. No signals were detected in some cases for rigid solids within one hour of acquisition, but well-resolved spectra were obtained in other materials known (or expected) to have a higher degree of molecular mobility. For example, comparison of ^{1}H and ^{2}H MAS NMR spectra of camphor showed that considerably sharper lines are observed in ^{2}H spectra than in ^{1}H spectra. As in the case of NH_3^+ and CH_3 groups, phenyl rings and various substituted derivatives often undergo large-amplitude motions in solids. Indeed, the NA ^{2}H MAS NMR spectrum of benzyl triethylchloride showed signals due to both methyl and phenyl deuterons, while no signal was detected for deuterons in the aromatic ring of *p*-toluenesulfonic acid monohydrate, probably due to the dynamics of the aromatic ring being slow or intermediate (relative to the ^{2}H NMR timescale) in this case.

A noteworthy result for deuterated solids is that the ^{2}H MAS NMR spectrum of glycine-d_5 ($ND_3^+CD_2COO^-$) shows a characteristic Pake-like pattern for a dipolar coupled ^{2}H···^{2}H pair in the CD_2 group, the width of which is significantly reduced due to the MAS employed. The reduced Pake-like pattern is indicative of strong ^{2}H···^{2}H dipolar coupling, since the distance between the geminal CD_2 deuterons is only 1.7 Å and, unlike the ND_3^+ group, the CD_2 group is motionally static in glycine-d_5.

Conclusion and outlook

Our preliminary results demonstrate that natural-abundance solid-state ^{2}H MAS NMR spectra can be recorded within a few hours of acquisition using a standard 4 mm double-resonance probe-head. Such functionalities as methyl, NH_3^+ and phenyl groups are particularly straightforward to detect, as the large amplitude motions characteristic for these groups lead to considerable motional averaging of the ^{2}H quadrupolar couplings, and reduced spin-lattice relaxation times. Combined together, these two effects provide favourable conditions for detecting ^{2}H signals in solids. The detection of all different ^{2}H environments, including methylene, methine and hydroxyl functionalities, is straightforward for plastic crystalline solids and other materials for which overall motions of molecules lead to considerable reduction of anisotropic interactions. Comparison of the ^{1}H and ^{2}H MAS NMR spectra of camphor shows that considerably sharper lines can be obtained in ^{2}H spectra compared to ^{1}H spectra.

For conventional crystalline organic solids, the detection of static functionalities such as methylene, methine, amino and hydroxyl groups is still problematic and may require the application of ultrafast MAS frequencies, as well as examination and optimization of various ^{1}H-^{2}H CP strategies for ^{2}H signal enhancement. On a positive note, however, this limitation of routine ^{2}H MAS NMR measurements can be advantageously explored as a means of easy detection of the relative dynamics of different functional groups in new materials, and for assessing the extent of overall motions of molecules in solids prior to more detailed multinuclear NMR and diffraction studies. As an example, natural-abundance ^{2}H MAS NMR measurements of solids may successfully complement routine powder X-ray diffraction characterization, as dynamically disordered solids are often not readily amenable to study by diffraction-based techniques.

References

1. Brown, S.P. *Prog. Nucl. Magn. Reson. Spectrosc.* **2007**, *50*, 199.

2. Aliev, A.E.; Harris, K.D.M.; Apperley, D.C. *Chem. Phys. Lett.* **1994**, *226*, 193.

3. Aliev, A.E.; Harris, K.D.M. *Mendeleev Commun.* **1993**, 153.

Polymorphism of Alzheimer's Ac-Aβ$_{(16-22)}$-NH$_2$ Amyloid Fibrils Explored by Solid-State ^{15}N{^{17}O} REAPDOR NMR

Oleg N. Antzutkin,[1,2] Andrei V. Filippov,[2] Dinu Iuga,[1] Johanna Baldus-Becker,[1] Steven P. Brown,[1] and Ray Dupree[1]

[1]Department of Physics, University of Warwick, [2]Chemistry of Interfaces, Luleå University of Technology, Sweden.

Overview

Different polymorphs of amyloid fibrils[1] and in particular small amyloid aggregates (oligomers)[2] have been shown to cause death of nerve cell cultures *in vitro*. Therefore, these amyloid species may be key toxic species for brain neurons causing a variety of neurodegenerative diseases. Toxic amyloid species are rich in different types of β-sheet or/and β-hairpin structures. However, a special challenge in such structures is to determine how peptides or proteins are packed against each other and whether parallel or anti-parallel β-sheets or β-hairpin structures are formed. To resolve this issue, ^{13}C MQ NMR methodology has been applied to specifically ^{13}C labelled Alzheimer's Aβ$_{(1-40)}$ amyloid fibrils where it has revealed in-registry parallel β-sheet supramolecular structure in this system.[3] Another approach was based on measurements of the hydrogen bonding interactions indirectly using ^{13}CO…^{15}N correlations.[4] However, these are very insensitive experiments because of the very small dipolar coupling (< 45 Hz), and can only be recorded in favourable cases where narrow lines lead to sufficient signal intensity. In this work an alternative "direct" approach of exploring hydrogen bonding contacts between the carbonyl oxygen and the amide nitrogen atoms is developed. The characteristic dipolar coupling for this type of N-H…O hydrogen bonding (^{15}N…^{17}O interspin distance of *ca* 2.8 Å) is *ca* 75 Hz, which, when found, is a direct indication of the connection. Previously, we have shown that it is possible to measure the ^{15}N-^{17}O dipolar and *J* couplings in hydrogen bonded model compounds.[5] One of these novel solid state NMR tools, ^{15}N{^{17}O} REAPDOR, was employed to obtain additional important structural information in amyloid fibrils and small toxic amyloid aggregates. Fmoc solid phase peptide synthesis was used to incorporate ^{17}O and ^{15}N at selective sites into peptides and a variety of solid-state NMR measurements were performed at lower fields. Experiments at high magnetic fields are very useful because of the higher sensitivity, improved resolution (^{15}N), and the line narrowing of the quadrupolar line (^{17}O).

^{15}N{^{17}O} REAPDOR NMR of amyloid fibrils

We report on yet unknown polymorphism of amyloid fibrils formed by a seven-residue peptide *N*-acetyl-Lys-Leu-Val-Phe-Phe-Ala-Glu-NH$_2$, Ac-Aβ$_{(16-22)}$-NH$_2$, which is a "key" amyloidogenic central fragment of Alzheimer's β-amyloid peptide. Structural measurements on these fibrils invoked a new "direct" approach in solid-state NMR, i.e., exploring of intermolecular hydrogen bonding contacts between the carbonyl oxygen and the amide nitrogen atoms using ^{15}N{^{17}O} REAPDOR NMR. We were able for the first time to detect ^{15}N…^{17}O dipole-dipole interactions between the amide nitrogen in Phe20 and the carbonyl oxygen in Val18 in a sample of amyloid fibrils of Alzheimer's Ac-Aβ$_{(16-22)}$-NH$_2$, which forms in-registry antiparallel β-sheets.[6] We collected ^{15}N{^{17}O} REAPDOR data (with dephasing times from 2 to 9 ms) on ca. 2 mg of selectively ^{15}N (98%) and ^{17}O (15%) labelled Ac-Aβ$_{(16-22)}$-NH$_2$ amyloid fibrils prepared in a PBS buffer at pH 7. The data correlate with the expected value of the dipole-dipole coupling constant *d*(^{15}N,^{17}O) ≈ 75 Hz (for Val18-Phe20 intermolecular bonds) when the enrichment level of ^{17}O is taken into account. A sample of 3.0 mg of unfibrillised Ac-Aβ$_{(16-22)}$-NH$_2$ did not show diminution of ^{15}N NMR signal in the ^{15}N{^{17}O} REAPDOR for mixing times between 2 and 9 ms (spectra not shown here), proving that the intramolecular Phe20(^{15}N)…(^{17}O)Val18 dipole-dipole interaction corresponding to the ^{15}N-^{17}O interspin distances of *ca* 5 Å (~15 Hz) produces insignificant dephasing of the ^{15}N NMR signal. Thus, the observed dephasing in the Ac-Aβ$_{(16-22)}$-NH$_2$ fibrillised sample is due to intermolecular hydrogen bonds Val18-C=O…HN-Phe20 (^{15}N-^{17}O interspin distance of ca 2.8 Å) as originally suggested from other solid-state NMR measurements on Ac-Aβ$_{(16-22)}$-NH$_2$ amyloid fibrils.[6] For one of the Ac-Aβ$_{(16-22)}$-NH$_2$ samples a few different polymorphs of amyloid fibrils were detected. Further studies on supramolecular structure of new polymorphs of Ac-Aβ$_{(16-22)}$-NH$_2$ fibrils using a combination of ^{13}C, ^{15}N and ^{17}O selective labeling with a variety of solid-state NMR experiments, including ^{15}N{^{17}O} REAPDOR, are currently in progress.

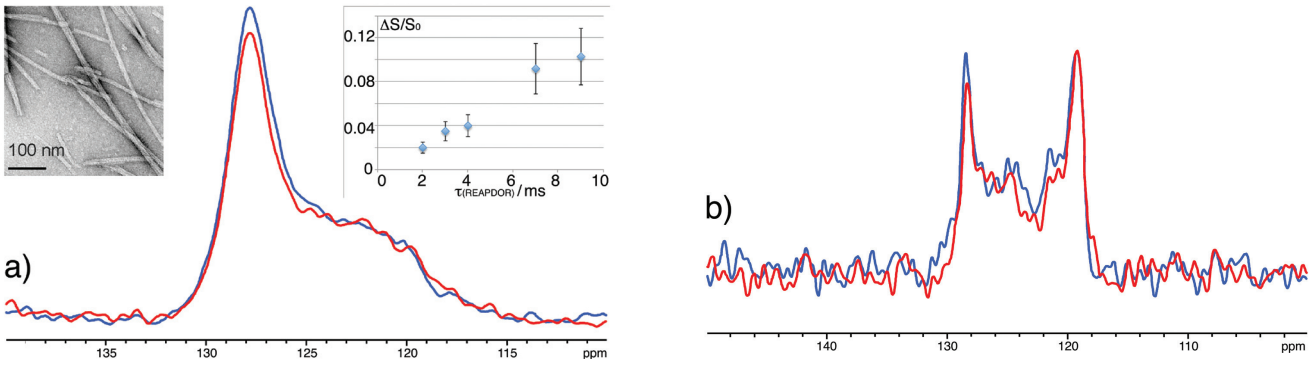

Figure 1. (a) $^{15}N\{^{17}O\}$ REAPDOR spectra of amyloid fibrils (TEM image, left inset) formed by selectively Val18-^{17}O (enrichment 15%) and Phe20-^{15}N (enrichment 98%) labelled fragment of Alzheimer's peptide Ac-A$\beta_{(16-22)}$-NH_2 and (b) a polymorphic sample of fibrils of the same peptide. Spectra correspond to the experiment with adiabatic ^{17}O pulse and mixing time 7 ms (S, red lines) and without the ^{17}O pulse (S_0, blue lines). REAPDOR dephasing ($(S_0-S)/S_0$) for the sharp feature (amyloid fibrils) in (a) at different mixing times is shown in the inset. A broad spectral feature in (a) in the range 120-125 ppm corresponds to non-fibrillar (amorphous) aggregates, which do not show diminution of ^{15}N NMR signal in the $^{15}N\{^{17}O\}$ REAPDOR for mixing times 2-9 ms.

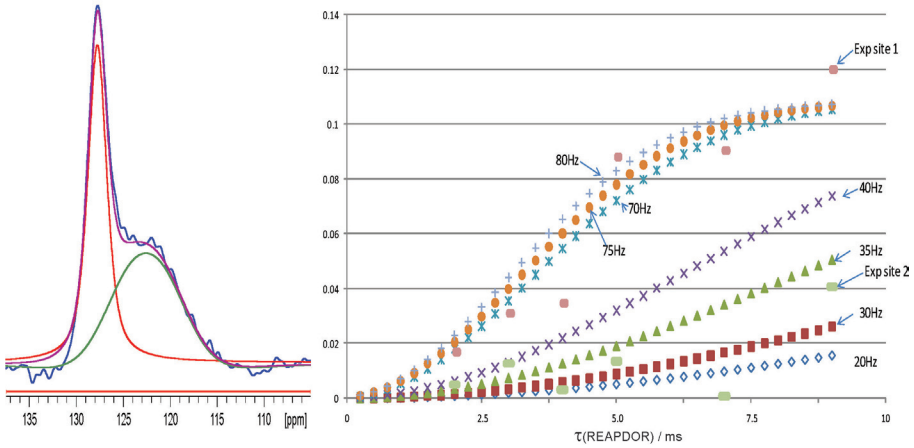

Figure 2. (left) A representative deconvolution of a REAPDOR NMR spectrum shown in Figure 1a. (right) SIMPSON simulations of experimental data for the narrow resonance peak (128 ppm, Exp. site 1, amyloid fibrils, $^{15}N\ldots^{17}O$ dipole-dipole coupling 75 Hz) and the broad resonance line (123 ppm, Exp. site 2, amorphous aggregates).

References

1. Petkova, A. T.; Leapman, R. D.; Guo, Z.; Yau, W.-M.; Mattson, M. P.; Tycko, R.; *Science* **2005**, *307(5707)*, 262.
2. Sandberg, A.; Luheshi, L. M.; Söllvander, S.; Pereira de Barros, T.; Macao, B.; Knowles, T. P. J.; Biverstål, H.; Lendel, C.; Ekholm-Petterson, F.; Dubnovitsky, A.; Lannfelt, L.; Dobson, C. M.; Härd, T.; *Proc. Natl. Acad. Sci. U.S.A.* **2010**, *107(35)*, 15595.
3. Antzutkin, O. N.; Balbach, J. J.; Leapman, R. D.; Rizzo, N. W.; Reed, J.; Tycko, R.; *Proc. Natl. Acad. Sci. U.S.A.* **2000**, *97*, 13045.
4. Wasmer, C.; Lange, A.; Van Melckebeke, H.; Siemer, A. B.; Riek, R.; Meier, B. H.; *Science* **2008**, *319*,1523.
5. Hung, I.; Uldry A.-C.; Becker-Baldus, J.; Webber, A. L.; Wong, A.; Smith, M. E.; Joyce, S. A.; Yates, J. R.; Pickard, C. J.; Dupree, R.; Brown, S. P.; *J. Am. Chem. Soc.* **2009**, *131(5)*, 1820.
6. Balbach J. J.; Ishii, Y.; Antzutkin, O. N.; Leapman, R. D.; Rizzo, N. W.; Dyda, F.; Reed, J.; Tycko, R.; *Biochemistry* **2000**, *39*, 13748.

High-Field ^{25}Mg Solid-State NMR for the Study of Inner-Earth Minerals

John M. Griffin and Sharon E. Ashbrook

School of Chemistry and EaStCHEM, University of St Andrews

Overview

^{25}Mg solid-state NMR should be a powerful probe of local bonding geometry and coordination; however, the typically large linewidths combined with the low gyromagnetic ratio and natural abundance (10%) of the ^{25}Mg nucleus present significant hindrances to the acquisition of high-quality NMR spectra. However, the inverse dependence of the second-order quadrupolar interaction upon magnetic field strength means that significant enhancement of the ^{25}Mg NMR signal can be obtained by the use of high-field spectrometers. Experimental methods such as the Carr-Purcell Meilboom-Gill (CPMG) sequence can also offer substantial gains in signal intensity by focusing the signal into a 'spikelet' manifold. Furthermore, isotopic enrichment in ^{25}Mg can provide a direct, albeit expensive, method to considerable enhancement of the NMR signal.[1]

^{25}Mg multiple-quantum MAS NMR of wadsleyite

Wadsleyite (β-Mg_2SiO_4) is a magnesium silicate phase present in the Earth's mantle transition zone and has received much interest due to its high capacity for the incorporation of water within its structure. While ^{17}O and ^{29}Si NMR parameters for wadsleyite have been determined,[2] the ^{25}Mg NMR parameters have never been measured experimentally, largely due to the challenging nature of ^{25}Mg solid-state NMR and the very small sample sizes (~10 mg) that result from the high-pressure synthesis procedure. However, with the aim of determining the feasibility and limits of ^{25}Mg solid-state NMR for the study of this system, we have prepared a sample 99%-enriched in ^{25}Mg. The crystal structure of wadsleyite, shown in Figure 1a, contains three distinct magnesium sites, with quadrupolar coupling constants (C_Q) of 8.1, 3.4 and 5.3 MHz predicted from CASTEP DFT calculations. A ^{25}Mg MAS NMR spectrum of ^{25}Mg-enriched wadsleyite recorded at 20 T, shown in Figure 1b, exhibits a lineshape in agreement with a simulated spectrum. A ^{25}Mg MQMAS NMR spectrum, shown in Figure 1c, was recorded in 3.6 days. This spectrum, shows intensity consistent with the C_Q = 3.4 and 5.3 MHz sites. However, the broadening observed in the indirect dimension confirms the presence of disorder in the structure.

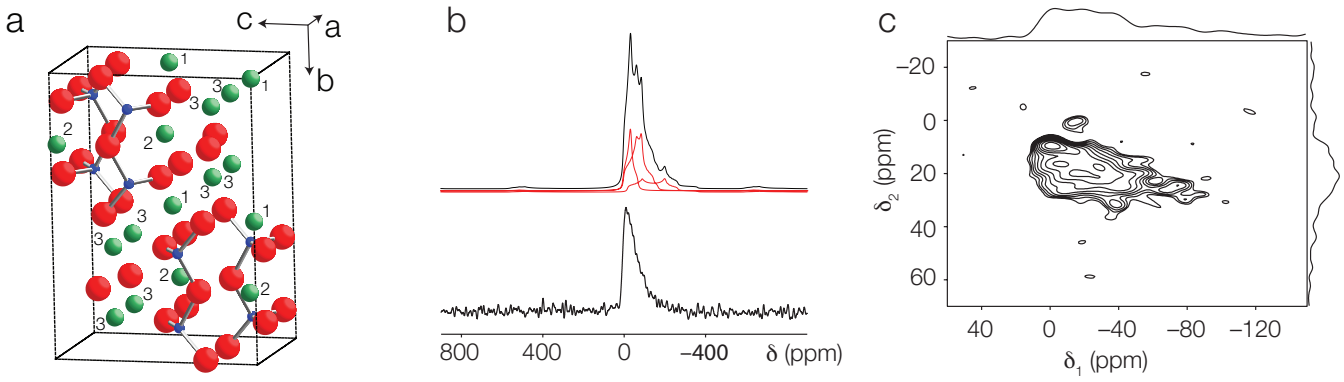

Figure 1. (a) Crystal structure of wadsleyite indicating the 3 distinct Mg sites. (b) ^{25}Mg MAS (20 T) NMR spectrum of wadsleyite and simulated spectrum (shown above). (c) ^{25}Mg MQMAS (20 T) NMR spectrum of wadsleyite recorded in 3.6 days.

Observation of 'hidden' magnesium in clinoenstatite

Clinoenstatite ($MgSiO_3$) is a magnesium silicate phase present in the upper mantle. The crystal structure has two distinct Mg sites, Mg1 and Mg2, which are both nominally octahedrally coordinated to 6 surrounding oxygens, as shown in Figure 2a. Although the chemical environments of these two sites appear similar, the Mg2 site has a more distorted bonding arrangement, and a larger quadrupolar coupling interaction should be expected. In a ^{25}Mg MAS NMR spectrum of clinoenstatite recorded in a previous study, only the Mg1 site was observed, with a C_Q of approximately 2.4 MHz.[3] It is possible that the distortion of the Mg2 site results in a much larger quadrupolar coupling interaction, broadening it beyond detection; indeed, CASTEP DFT calculations predict the Mg1 and Mg2 sites to have C_Q values of 2.7 and 13.9 MHz, respectively. In order to fully characterise the Mg environments in clinoenstatite, we have recorded ^{25}Mg MAS and static CPMG NMR spectra at 20 T. These spectra, shown in Figure 2b, are dominated by a single peak corresponding to the Mg1 site, with a C_Q of 2.8 MHz, in good agreement with the value of 2.4 MHz determined in previous work. However, upon closer inspection of ^{25}Mg static NMR spectrum, low intensity signal appears to be present across the width of the spectrum. A frequency-stepped wideline CPMG spectrum, shown in Figure 2c, reveals that this intensity corresponds to a second resonance that is extensively broadened by the second-order quadrupolar interaction. From lineshape analysis, this site is found to have a C_Q of 12.8 MHz, in good agreement with the value predicted by the DFT calculations.

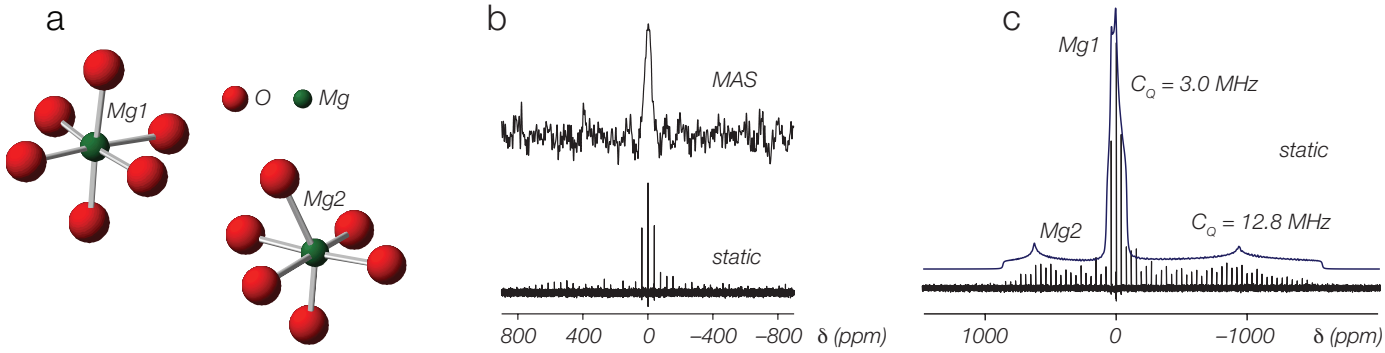

Figure 2. (a) Octahedrally-coordinated magnesium sites Mg1 and Mg2 in the crystal structure of clinoenstatite. (b) ^{25}Mg MAS and static CPMG NMR spectra of clinoenstatite recorded at 20.0 T. (c) Wideline frequency-stepped ^{25}Mg static NMR spectrum of clinoenstatite, recorded at 20 T. A fit to the spikelet manifold is shown in blue.

References

1. Shimoda, K.; Nemoto, T.; Saito, K. *J. Phys. Chem. B* **2008**, *112*, 6747.
2. Ashbrook, S. E.; Berry, A. J.; Hibberson, W. O.; Steuernagel, S.; Wimperis, S. *J. Am. Chem. Soc.* **2003**, *125*, 11824.
3. Mackenzie, K. J. D.; Meinhold, R. H.; *Am. Mineral*. **1994**, *79*, 250.

High-Field ^{27}Al and ^{31}P Solid-State NMR for the Study of Aluminophosphate STA-2

Valerie R. Seymour, John M. Griffin, Paul A. Wright and Sharon E. Ashbrook

School of Chemistry and EaStCHEM, University of St Andrews

Overview

Aluminophosphates (AlPOs) are porous framework materials with a range of applications. First synthesized by Wilson *et al.* in the 1980s,[1] AlPOs consist of alternating corner sharing AlO_4 and PO_4 tetrahedra. AlPOs are synthesized using template molecules, which are often charged, requiring the incorporation into the structure of charge-balancing anions. It is often difficult to determine the charged state of the template and location and ordering of charge-balancing anions by diffraction. In contrast, solid-state NMR is an excellent probe of local structure and order, particularly suited to the study of AlPOs, as the basic components of the framework are NMR active, as are those of the templates molecules. ^{27}Al NMR is particularly useful because the quadrupolar and chemical shift parameters are very sensitive to the local environment, and ^{27}Al-^{31}P correlation experiments can give detailed information about connectivities in the framework. In this way we can compare the framework structures in templated and calcined materials to provide insight into the location and order of the charge-balancing anionic species.

STA-2

The AlPO STA-2 (St Andrews 2) has been the focus of recent study with the aim of 'designing' a template material which will not only allow the formation of the desired microporous material, but is a fraction of the cost to the current alternatives. Two templates have been used to synthesise STA-2; bis-diazabicyclooctane-butane (BQNB), made from expensive starting materials, and bis-quinuclidine-butane (BDAB), shown in Figure 1a, proposed as a cheaper alternative. The templates, BQNB and BDAB both have a 2^+ charge, which is balanced by hydroxyls in the STA-2 structure. Solid-state NMR studies indicate that they result in the same structure,[2] and therefore BDAB is suitable as a cheaper template. The dehydrated, calcined structure contains two crystallographically-distinct sites for both Al and P. Previous solid-state NMR studies of this material revealed well-resolved sites in a ^{27}Al Multiple-Quantum (MQ) MAS spectrum, and a subsequent ^{27}Al-^{31}P MQ-INEPT experiment[3] allowed the framework structure to be investigated. For STA-2 templated with BDAB, a range of sites is observed. A ^{27}Al MQMAS NMR spectrum resolves two tetrahedrally-coordinated Al sites, with shoulders indicating additional sites, along with AlO_5/AlO_6 sites.

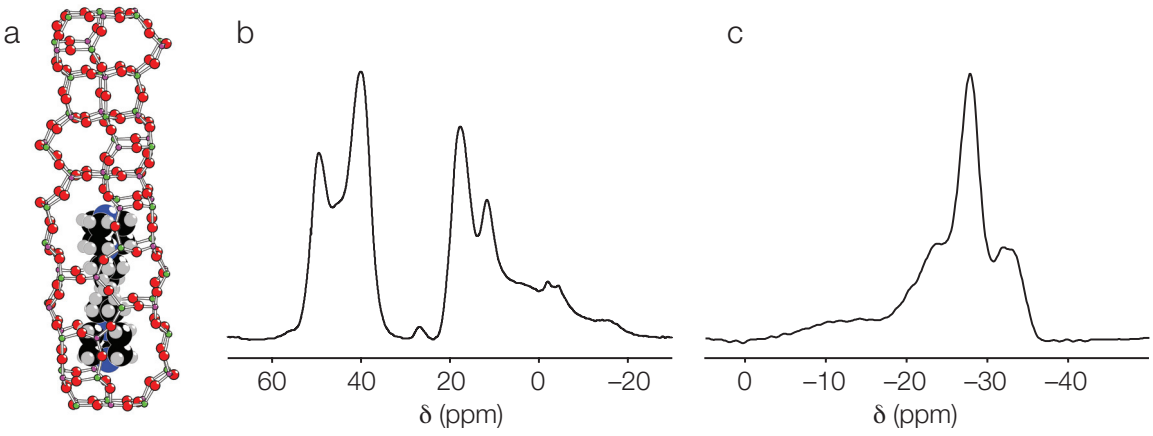

Figure 1. (a) A BDAB template molecule within a pore of STA-2, (b) ^{27}Al MAS and (c) ^{31}P MAS NMR spectra of STA-2 (BDAB) recorded at 20.0 T with a MAS frequency of 12.5 kHz.

The aim of this work was to perform high-resolution INEPT heteronuclear correlation experiments at 20.0 T. The high-resolution obtained by the resolution and sensitivity advantages at high magnetic field should enable us to probe in more detail connectivities within the framework. This will lead to a more confident assignment of the distinct Al and P sites in the structure and help us to fully characterize the location and ordering of the OH^- species.

Results

High-quality one-dimensional spectra, shown in Figures 1b and 1c for STA-2 (BDAB), were obtained for the two materials. ^{27}Al-^{31}P INEPT correlation spectra, shown in Figure 2, were recorded for STA-2 (BDAB) and STA-2 (BQNB), with different J evolution delays, τ. The different τ delays give small variation in the finer detail of the spectra. The two STA-2 materials gave very similar spectra. Conventional two-dimensional ^{27}Al-^{31}P INEPT correlation experiments performed worked well and resulted in higher resolution spectra than those already obtained on the same materials at 14.1 T. Work is currently underway to assign these spectra and to relate this information to the structural role of the template ion. We intend to carry out ^{27}Al-^{31}P MQ-INEPT experiments at high field, to see if the ^{27}Al resolution can be further improved by reducing the quadrupolar broadening and therefore provide further insight into the structure.

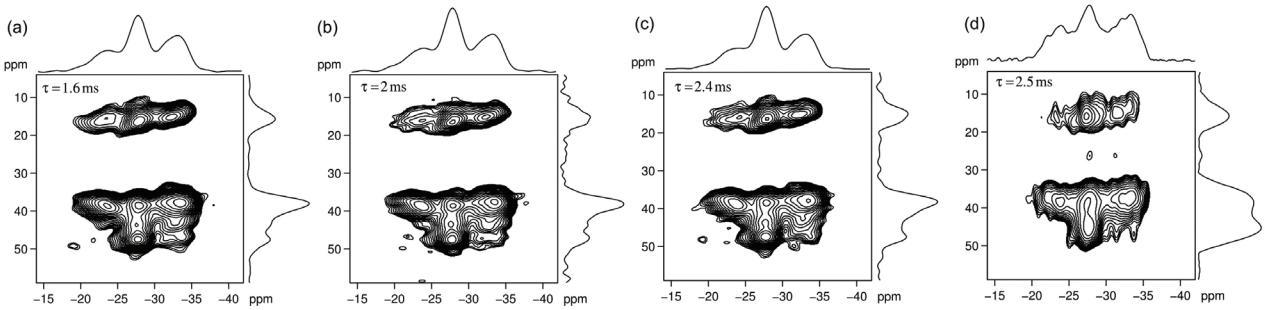

Figure 2: ^{27}Al-^{31}P INEPT NMR spectra of STA-2 (BDAB) recorded at magnetic field strengths of (a-c) 20.0 T and (d) 14.1 T. ^{27}Al is shown in the F_1 dimension and ^{31}P in the F_2 dimension.

References

1. Wilson, S.T.; Lok, B. M.; Messina, C. A.; Cannan, T. R.; Flanigen, E. M. *J. Am. Chem. Soc.* **1982**, *104*, 1146.
2. Castro, M.; Seymour, V. R.; Carnevale, D.; Griffin, J. M.; Ashbrook, S. E.; Wright, P. A.; Apperley, D. C.; Parker, J. E.; Thompson, S. P.; Fecant, A.; Bats, N. *J. Phys. Chem. C* **2010**, *114*, 12698.
3. Wiench, J. W.; Pruski, M. *Solid State Nucl. Magn. Reson*. **2004**, *26*, 51.

Structural Characterization of $NaNbO_3$ Polymorphs by ^{93}Nb Solid-State NMR

Karen E. Johnston, John M. Griffin and Sharon E. Ashbrook

School of Chemistry and EaStCHEM, University of St Andrews

Overview

Perovskites (ABX_3) are an important and attractive area of materials chemistry. Such structures are extremely flexible in their composition and can be distorted with relative ease producing a range of useful physical and chemical properties. The $NaNbO_3$-$KNbO_3$ (KNN) system currently receives much attention as a potential 'green' replacement for the most widely used piezoelectric PZT ($PbZr_{1-x}Ti_xO_3$).[1] Despite its rapidly growing significance in recent years, the basic structural chemistry of the KNN system is poorly understood, and much of this can be traced back to the Na end-member, $NaNbO_3$. A number of contradictory and inconsistent suggestions have been proposed regarding the structure of the room temperature phase. Crystallographic data reports that $NaNbO_3$ adopts a $\sqrt{2} \times \sqrt{2} \times 4$ supercell in the space group *Pbcm* (Figure 1a), with two crystallographically-distinct Na sites and a single Nb site.[2] Whilst some materials appear to be in agreement with this model, many samples synthesized in our laboratory appear to contain a second Na-bearing phase, the amount of which varies depending on the synthesis route.[3] This phase cannot be easily observed using lab-based powder X-ray diffraction. However, the presence of this phase is clearly evident in a high-resolution ^{23}Na multiple-quantum (MQ) MAS NMR spectrum of a sample prepared by a solid-state synthesis method recorded at 9.4 T (Figure 1b), where four distinct ^{23}Na sites are observed. We have been able to identify samples prepared by molten salt and sol-gel synthesis methods that appear to be close to phase pure, each with only two prominent Na sites observed in ^{23}Na MQMAS NMR spectra (Figure 1b). For the molten salt sample, refinement confirms the *Pbcm* structure, while for the sol-gel sample, the structure is better described $P2_1ma$. The polar nature of the $P2_1ma$ space group makes this material potentially ferroelectric.

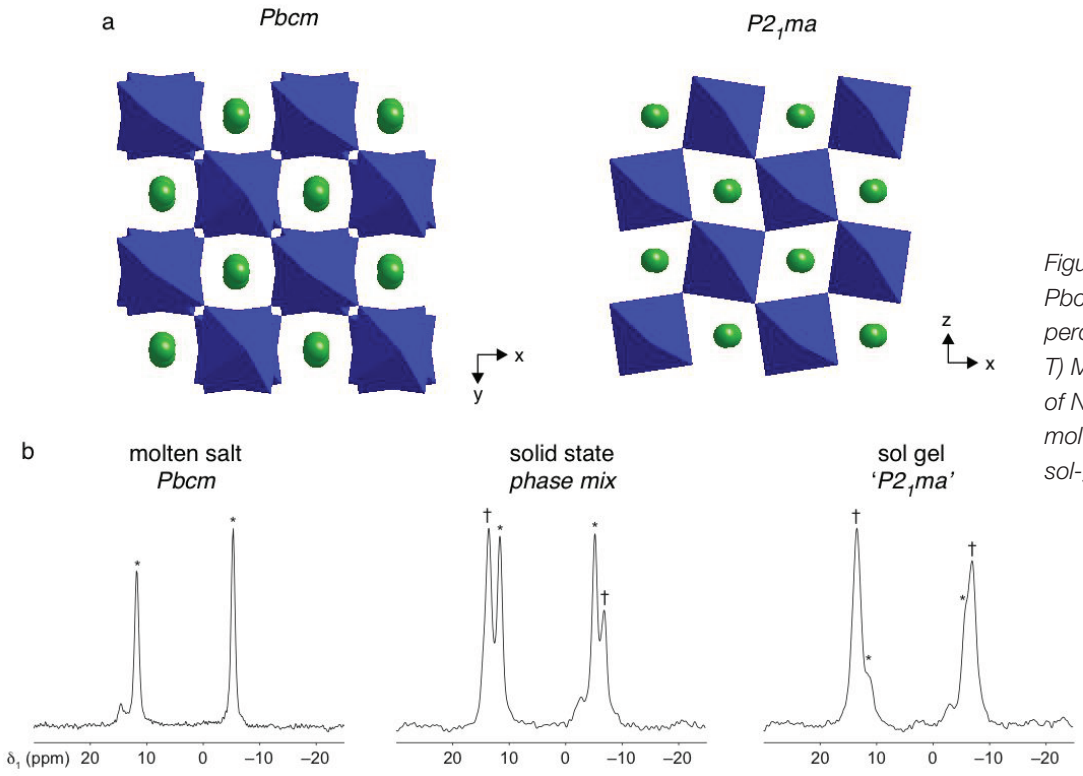

Figure 1. (a) Structures of Pbcm and $P2_1ma$ $NaNbO_3$ perovskites and (b) ^{23}Na (9.4 T) MQMAS NMR spectra of $NaNbO_3$ prepared using molten salt, solid-state and sol-gel approaches.

^{93}Nb solid-state NMR of $NaNbO_3$

Although ^{23}Na NMR is able to provide information on the number of perovskite phases present, the ^{23}Na NMR parameters are very similar for the different phases, hindering an unambiguous identification. Figure 2 shows ^{93}Nb (I = 9/2) wideline spectra of static samples of perovskite $NaNbO_3$ prepared by molten salt and sol-gel synthesis at 9.4 T and 20.0 T. For static samples, spectra contain information on both the quadrupolar coupling and the CSA (i.e., the anisotropy and asymmetry and the relative orientation of the two tensors). Although providing much information, this results in a complex lineshape and spectra are often acquired at variable field, exploiting the differing field dependencies of the quadrupolar and CSA interactions (proportional to $1/B_0$ and B_0, respectively). Figure 2 shows that the NMR spectra for $NaNbO_3$ prepared by molten salt and sol-gel routes (almost phase pure *Pbcm* and $P2_1ma$ perovskites, respectively) are very similar, demonstrating that the local Nb environment does not change significantly in the two phases. In contrast, the ^{93}Nb spectra obtained for the ilmenite polymorph of $NaNbO_3$, prepared by a hydrothermal route, is considerably different. The quadrupolar and CSA parameters of the molten salt material at 9.4, 14.1 (not shown) and 20.0 T are in good agreement with those obtained from planewave GIPAW calculations for the *Pbcm* phase. While poor agreement is initially obtained between the experimental parameters for the sol-gel sample and those calculated for the $P2_1ma$ structure, the calculated forces on the atoms are high and geometry optimization is required. Subsequently, there is very good agreement between calculation and experiment.

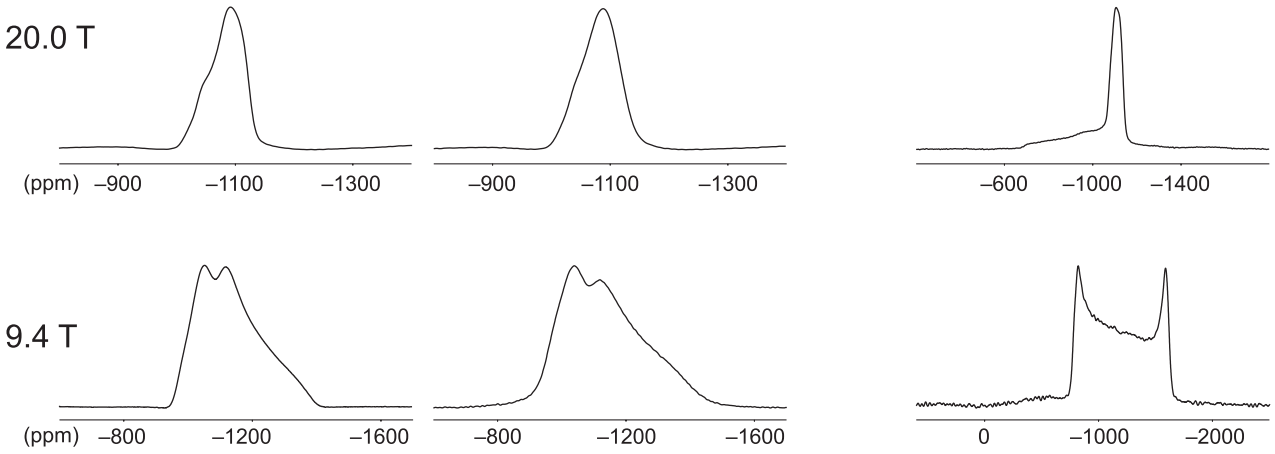

Figure 2. ^{93}Nb wideline spectra, acquired using a spin-echo pulse sequence at 9.4 and 20.0 T, for $NaNbO_3$ prepared using molten salt, sol-gel and hydrothermal synthesis. In the first two cases perovskite phases are formed, while in the latter the ilmenite polymorph is obtained.

Conclusions

Variable field wideline ^{93}Nb spectra for $NaNbO_3$ polymorphs have demonstrated that it is difficult to distinguish between the different perovskite (*Pbcm* and $P2_1ma$) polymorphs in this way. In contrast, the ilmenite polymorph of $NaNbO_3$ has considerably different spectra and a much larger CSA contribution. Good agreement can be obtained between the NMR parameters extracted from the experiment and those calculated using structure from the literature, but only after geometry optimization of the initial models.

References

1. Cross, E. *Nature* **2004**, *432*, 24.
2. Johnston, K. E.; Tang, C. C.; Parker, J. E.; Knight, K. S.; Lightfoot, P.; Ashbrook, S. E. *J. Am. Chem. Soc.* **2010**, *132*, 8732.

Measurement of Chemical Shift Anisotropies in Disordered Pyrochlore Ceramics

Martin R. Mitchell and Sharon E. Ashbrook

School of Chemistry and EaStCHEM, University of St Andrews

Overview

Pyrochlore materials with the general formula $A_2B_2O_7$ currently find important application as components of SYNROC, a ceramic wasteform that is used to safely encapsulate the radioactive actinides and lanthanides present in nuclear waste. Titanate-based pyrochlores exhibit good chemical durability; however, it has recently been shown that the introduction of tin to these pyrochlores results in an increased tolerance to radiation damage.[1] The high sensitivity of the ^{89}Y chemical shift to local environment in makes it a highly informative probe of structure and disorder. This has recently been demonstrated both experimentally and through the use of DFT calculations for members of the $Y_2Ti_{2-x}Sn_xO_7$ solid-solution.[2,3] However, there are also several challenges associated with yttrium NMR. Although ^{89}Y has spin quantum number I = 1/2, it has a low gyromagnetic ratio of $\gamma = -1.3 \times 10^7$ radT^{-1}s^{-1} and a receptivity of 0.7 relative to ^{13}C. This low sensitivity, coupled with typically long T_1 relaxation times can lead to impractically long experimental times, necessitating the use of higher magnetic field strengths.

In recent work we have demonstrated the use of first-principles calculations to aid the assignment of specific resonances in ^{89}Y MAS NMR spectra.[3] Whilst the isotropic shifts are indicative of the local structure, a second parameter such as the chemical shift anisotropy (CSA) would give greater confidence in the assignment. However, the CSA is removed by magic-angle spinning (MAS), provided the MAS rate is sufficiently rapid. Although measurement of the CSA by means of slow spinning MAS experiments is possible for simple materials, this may yield inaccurate results due to the ineffective removal of dipolar couplings and the overlap of spectral resonances. There are, however, a number of methods that allow faster MAS rates to be employed, whilst also generating the CSA spinning sideband pattern which would be obtained at a reduced MAS frequency in the indirect dimension, e.g., the CSA-amplified PASS experiment of Orr and Duer.[4] This type of experiment has been widely applied for the determination of ^{13}C CSAs in organic materials, but the time-consuming nature of this two-dimensional approach would necessitate high magnetic field strengths for sufficient sensitivity.

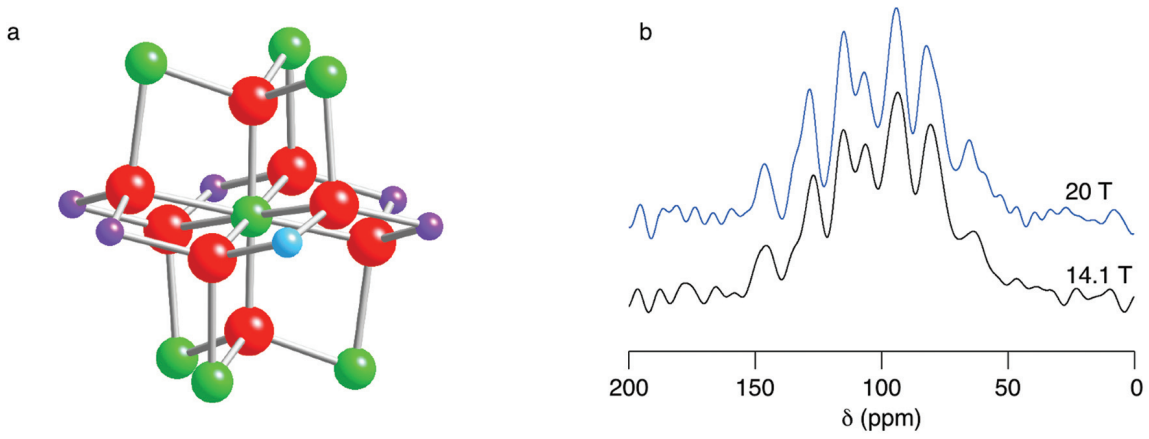

Figure 1. (a) Cluster showing the local environment around an Y^{3+} cation (green) with surrounding O (red) and six NNN B-site cations (Sn^{4+} or Ti^{4+}). (b) ^{89}Y MAS (14 kHz) NMR spectra of $Y_2Ti_{1.2}Sn_{0.8}O_7$ at 14.1 T and 20.0 T.

^{89}Y solid-state NMR of $Y_2(Sn,Ti)_2O_7$ pyrochlores

In a recent ^{89}Y MAS NMR study of the $Y_2Ti_{2-x}Sn_xO_7$ solid-solution, it was found that the ^{89}Y chemical shift is a clear indicator of the number of Sn^{4+} and Ti^{4+} next nearest neighbours (NNN), as shown in Figure 1 for $Y_2Ti_{1.2}Sn_{0.8}O_7$.[3] There appears to be no increase in resolution in the spectrum recorded at higher B_0 field, reflecting the presence of distributions of chemical shift in this disordered material. In both cases, the intensities of the observed resonances are consistent with those predicted by a random distribution of Sn^{4+} and Ti^{4+} cations on the B-site.

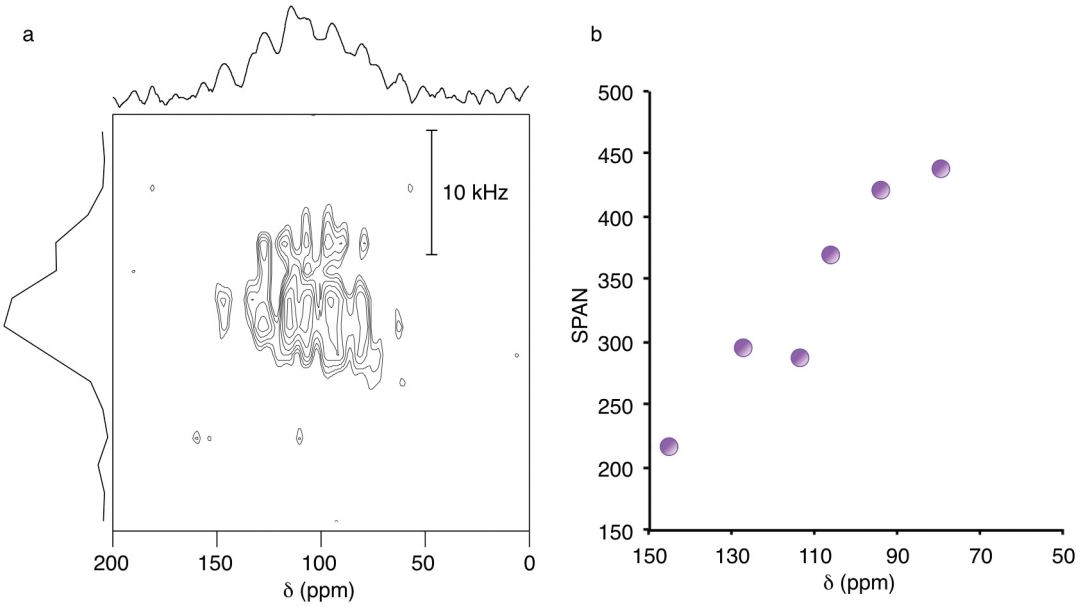

Figure 2. (a) ^{89}Y (20 T) 2D CSA-Amplified PASS NMR spectrum of $Y_2Ti_{1.2}Sn_{0.8}O_7$. (b) Plot showing the correlation between the isotropic and anisotropic (span, Ω) chemical shift for the distinct spectral resonances.

Figure 2a shows a 2D CSA-Amplified PASS NMR spectrum of $Y_2Ti_{1.2}Sn_{0.8}O_7$, recorded at 20.0 T, using a 14 kHz MAS rate. The total acquisition time was 5.5 days. CSA parameters (principally the span, Ω) can be extracted from the sideband intensities contained in the projections for each of the distinct spectral resonances, as shown in Figure 2b. This shows a clear increase in the shielding anisotropy as the isotropic chemical shift decreases. While accurate information can be obtained for many of the resonances, a spectrum with better signal-to-noise would be required to improve the confidence in the values extracted for some of the less intense resonances. The experimental CSA values will be compared to those obtained from planewave DFT calculations to ascertain whether the CSA is a sensitive probe of the local environment around Y. It is anticipated that the combination of information on both the isotropic and anisotropic chemical shift will aid in the assignment and interpretation of ^{89}Y NMR spectra of pyrochlore ceramics, and result in a better understanding of the nature of the disorder observed.

References

1. Lumpkin, G. R.; Smith, K. L.; Blackford, M. G.; Whittle, K. R.; Harvey, E. J.; Redfern, S. A. T. *Chem. Mater.* **2009**, *21*, 2746.
2. Ashbrook, S. E.; Whittle, K. R.; Lumpkin, G. R.; Farnan, I. *J. Phys. Chem.* **2006**, *110*, 10358.
3. Reader, S. W.; Mitchell, M. R.; Johnston, K. E.; Pickard, C. J.; Whittle, K. R.; Ashbrook, S. E. *J. Phys. Chem*. **2009**, *113*, 18874.
4. Orr, R. M.; Duer, M. J.; Ashbrook, S. E. *J. Magn. Reson.* **2005**, *174*, 301.

Structural Analysis of Mersacidin/Lipid II Complexes in Lipid Membranes

Judicaël Parisot,[1] Dinu Iuga,[3] David C. Griffin,[1] Eefjan Breukink,[4] Hans-Georg Sahl,[2] Gabrielle Bierbaum,[2] Boyan B. Bonev[1]

[1]School of Biomedical Sciences, University of Nottingham, [2]Microbiologie, Universität Bonn, Germany, [3]Department of Physics, University of Warwick, [4]Biochemistry, Utrecht University

Overview

Resistance to antibiotics is a major problem for the clinical management of infectious diseases, which are still a major cause of human mortality. Lanthionine antibiotics are one class of compounds with high activity against Gram-positive pathogens and low toxicity. This high therapeutic ratio stems from their mode of action, which relies on specific recognition of lipid II, the mature bacterial cell wall intermediate.[1] Lipid II is extremely well-conserved across eubacteria and lipid II-mediated antibiotic action forms the basis of low resistance to lanthionine antibiotics. Methicillin-resistant *S. aureus* (MRSA) and *C. difficile*, for example, have been shown to be susceptible to mersacidin[4].

$^{13}C/^{13}C$ NOESY-MAS NMR study of mersacidin/lipid II complexes

Mersacidin is a 20 aminoacid residue Class II lanthionine antibiotic of particular interest, as it is amongst the very few known inhibitors of transglycosylation[5]. It targets lipid II in its action but not undecaprenyl pyrophosphate, which points to a unique recognition site, most likely residing on the disaccharide-pentapeptide moiety of lipid II. We seek the structure of lipid II in its membrane complex with mersacidin, as well as the antibiotic/target interface to create a template for computational screening of synthetic macrocyclic antibiotics[6].

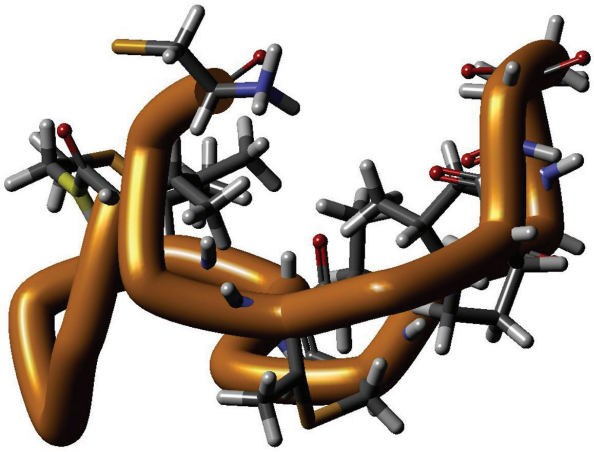

Figure 1. Solution NMR structure of mersacidin (1MQZ)[7]

Membrane samples containing $^{13}C,^{15}N$-labelled lipid II and $^{13}C,^{15}N$-labelled mersacidin were prepared for investigation by $^{13}C,^{13}C$ solid-state MAS NMR correlation spectroscopy. Spectral assignment of lipid II was carried out previously from ^{13}C-labelled lipid II in membrane complexes with unlabelled antibiotic, using R14 2Q-1Q correlation spectroscopy[8]. Resonance assignment from mersacidin is sought, as well as structural information from its membrane complexes with lipid II. Hydrated lipid membranes were studied by NOESY-MAS solid-state NMR to obtain two-dimensional $^{13}C,^{13}C$ correlation spectra. Figure 2 shows a high-resolution spectrum from the membrane complex, obtained with 100 ms mixing at –56°C and 12.5 kHz MAS. Multiple internal molecular correlations are observed from lipid II and mersacidin, as well as intermolecular couplings.

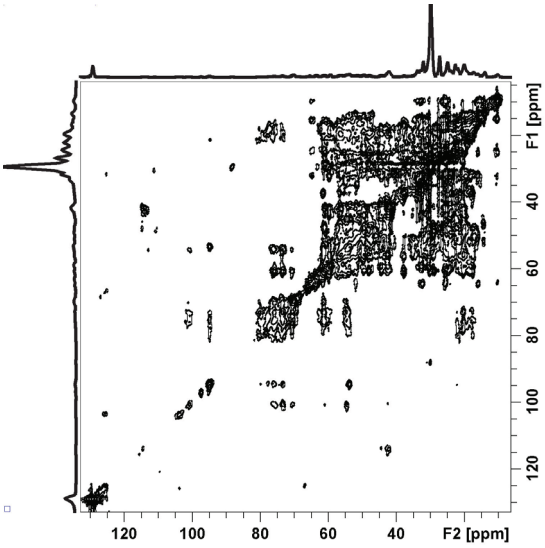

Figure 2. $^{13}C,^{13}C$-NOESY-MAS NMR spectrum from labelled mersacidin/lipid II complexes in lipid membranes.

Correlations within the disaccharide region of lipid II allow resonance assignment in connectivity interpretation. A large number of well-resolved resonances are observed from mersacidin, as well. Further spectral editing, using the ^{15}N-labels, is required to assign the hydrocarbon region of the antibiotic. Additional NOESY spectra need to be acquired at shorter and longer mixing times to obtain a complete picture of the intermolecular connectivity with the membrane complex.

References

1. Breukink, E.; Wiedemann, I.; van Kraaij, C.; Kuipers, O. P.; Sahl, H. G.; de Kruijff, B. *Science* **1999**, *286* (5448), 2361-2364.
2. Bonev, B. B.; Breukink, E.; Swiezewska, E.; De Kruijff, B.; Watts, A. *Faseb Journal* **2004**, *18* (15), 1862-1869.
3. Parisot, J. L.; Carey, S.; Breukink, E.; Chan, W. C.; Narbad, A.; Bonev, B. *Antimicrobial Agents and Chemotherapy* **2008**, *52* (2), 612-618.
4. Kruszewska, D.; Sahl, H. G.; Bierbaum, G.; Pag, U.; Hynes, S. O.; Ljungh, A. *J. Antimicrob. Chemother.* **2004**, *54* (3), 648-653.
5. Brotz, H.; Bierbaum, G.; Leopold, K.; Reynolds, P. E.; Sahl, H. G. *Antimicrob. Agents Chemother.* **1998**, *42* (1), 154-160.
6. Turpin, E. R.; Bonev, B. B.; Hirst, J. D. *Biochemistry* **2010**, *49* (44), 9594-9603.
7. Hsu, S. T. D.; Breukink, E.; Bierbaum, G.; Sahl, H. G.; de Kruijff, B.; Kaptein, R.; van Nuland, N. A. J.; Bonvin, A. *J. Biol. Chem.* **2003**, *278* (15), 13110-13117.
8. Carravetta, M.; Eden, M.; Zhao, X.; Brinkmann, A.; Levitt, M. H. *Chem. Phys. Lett.* **2000**, *321* (3-4), 205-215.

Fast MAS ^{1}H Spectroscopy of ^{1}H-Diluted Membrane Peptide

David C. Griffin[1], Dinu Iuga[2] and Boyan B. Bonev[1]

[1]School of Biomedical Sciences, University of Nottingham; [2]Department of Physics, University of Warwick

Overview

Subtilin is a 32 aminoacid Class I lanthionine antibiotic, which acts *via* lipid II-mediated membrane poration[1] to inhibit cell wall biosynthesis, deregulate bacterial division and cell wall formation, akin to nisin[2]. High specificity in bacterial target recognition by both subtilin and nisin is conferred by pyrophosphate recognition of mature peptidoglycan intermediates lipid II and undecaprenyl pyrophosphate found in the outer leaflets of bacterial membranes[3]. Class I lanthionine antibiotics subtilin and nisin act through target-mediated multimeric binary transmembrane pores pore-formation, most likely composed of four antibiotic/target 2:1 binary hetero-trimers. N-terminal Trp has been shown to play a key role in target recognition by enzymatic deletion[1], while backbone amino protons are involved in pyrophosphate recognition[4].

High-speed MAS in deuterated antimicrobial peptide in lipid membranes

Proton MAS NMR resolution in peptides is dominated by field-independent isotropic line broadening, which results from strong interproton dipolar couplings. Such isotropic broadening is approximately inversely proportional to the MAS speed[5] and responds to multipulse homonuclear decoupling. In addition, management of interproton dipolar couplings can be facilitated in partially deuterated samples, where the average coupling strength is significantly reduced[6].

Subtilin was deuterated randomly at 70% proton replacement. Membrane complexes of 0.7^{2}H-subtilin and protonated membrane target, undecaprenyl pyrophosphate (11PP), were prepared and investigated under fast MAS. Within the one day experiment, focus fell on investigation of the effects of spinning. The phospholipid/antibiotic/target sample was lyophilised at first and ^{1}H spectra were acquired at MAS speed between 58 kHz and 20 kHz. A notable improvement in proton linewidth is seen at high spinning speeds. Proton decoupling is expected to aid significantly in resolution enhancement, although significant contribution from inhomogeneous line broadening in dehydrated samples is likely to be present.

Hydrated (D_2O) samples were also investigated. The intrinsic linewidth in this case was markedly lower but the achievable spinning speeds were limited by spinning instability in the hydrated sample. Within the one day time limit an undecoupled ^{1}H NOESY-MAS was acquired. The feasibility of the approach was demonstrated although a high quality spectrum could not be acquired and severe t_1 truncation is evident. Longer acquisitions and the use of windowed decoupling should enhance significantly spectral resolution.

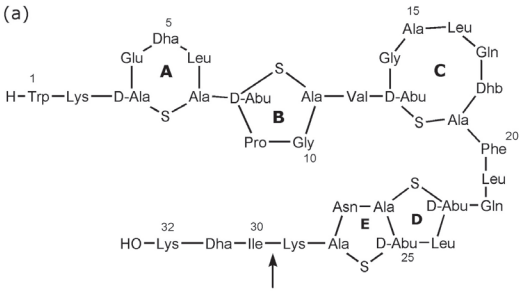

Figure 1. Structure of subtilin[1]

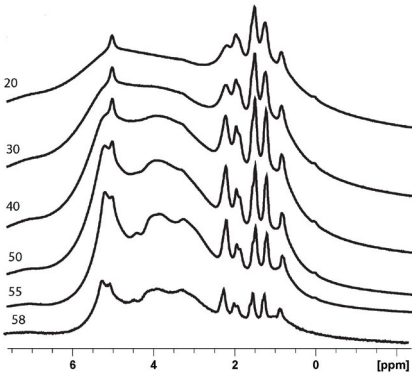

Figure 2. Undecoupled ^{1}H MAS NMR spectra of dry lipid/deuterated antibiotic/target sample following a single pulse excitation. MAS speed was varied between 58 KHz (bottom), 55, 50, 40, 30 and 20 kHz (top).

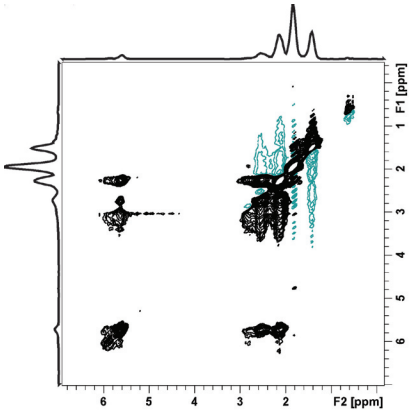

Figure 3. Proton NOESY-MAS spectrum of D_2O hydrated 0.7^{2}H-subtilin/11PP complexes in lipid membranes.

References

1. Parisot, J. L.; Carey, S.; Breukink, E.; Chan, W. C.; Narbad, A.; Bonev, B. *Antimicrobial Agents and Chemotherapy* **2008**, *52* (2), 612-618.
2. Hyde, A. J.; Parisot, J.; McNichol, A.; Bonev, B. B. *Proceedings of the National Academy of Sciences of the United States of America* **2006**, *103* (52), 19896-19901.
3. Bonev, B. B.; Breukink, E.; Swiezewska, E.; De Kruijff, B.; Watts, A. *Faseb Journal* **2004**, *18* (15), 1862-1869.
4. Hsu, S. T. D.; Breukink, E.; Tischenko, E.; Lutters, M. A. G.; de Kruijff, B.; Kaptein, R.; Bonvin, A.; van Nuland, N. A. J. *Nature Structural & Molecular Biology* **2004**, *11* (10), 963-967.
5. Maricq, M. M.; Waugh, J. S. *J. Chem. Phys.* **1979**, *70* (7), 3300-3316.
6. Zhou, D. H.; Graesser, D. T.; Franks, W. T.; Rienstra, C. M. *J. Magn. Reson.* **2006**, *178* (2), 297-307.

^{14}N-^{1}H Correlation Spectra of Organic Solids

Andrew Tatton,[1] Dinu Iuga,[1] Tran N. Pham,[2] Fred G. Vogt,[2] and Steven P. Brown[1]

[1]Department of Physics, University of Warwick, [2]GlaxoSmithKline

Overview

^{14}N-^{1}H solid-state NMR experiments offer the opportunity to probe N-H correlations for organic solids without recourse to isotopic labelling.[1,2] We present here ^{14}N-^{1}H spectra recorded using a HMQC pulse sequence with R^3 recoupling of the ^{14}N-^{1}H dipolar coupling.[1] Specifically, it was found that optimum performance was achieved using the 1.3 mm probe that allows MAS at 60 kHz and a ^{14}N nutation frequency of 120 kHz.

^{14}N-^{1}H spectra

Figure 1 presents ^{14}N-^{1}H spectra of (a) the dipeptide β-AspAla and (b) nicotinamide. The experimental ^{14}N skyline projections (solid lines) are compared to simulated spectra that use the isotropic chemical shifts and the ^{14}N quadrupolar coupling constants, C_Q, that have been calculated using CASTEP: C_Q = 1.2 MHz (NH_3) and 3.3 MHz (NH) for the dipeptide and 2.7 MHz (NH_2) and 4.0 MHz (N) for nicotinamide. Importantly, the simulations take into account the second-order isotropic quadrupolar shifts, that are large for sites with C_Q over 2 MHz, e.g. over 200 ppm for the NH site in the dipeptide for which the CASTEP-calculated C_Q is 3.3 MHz.

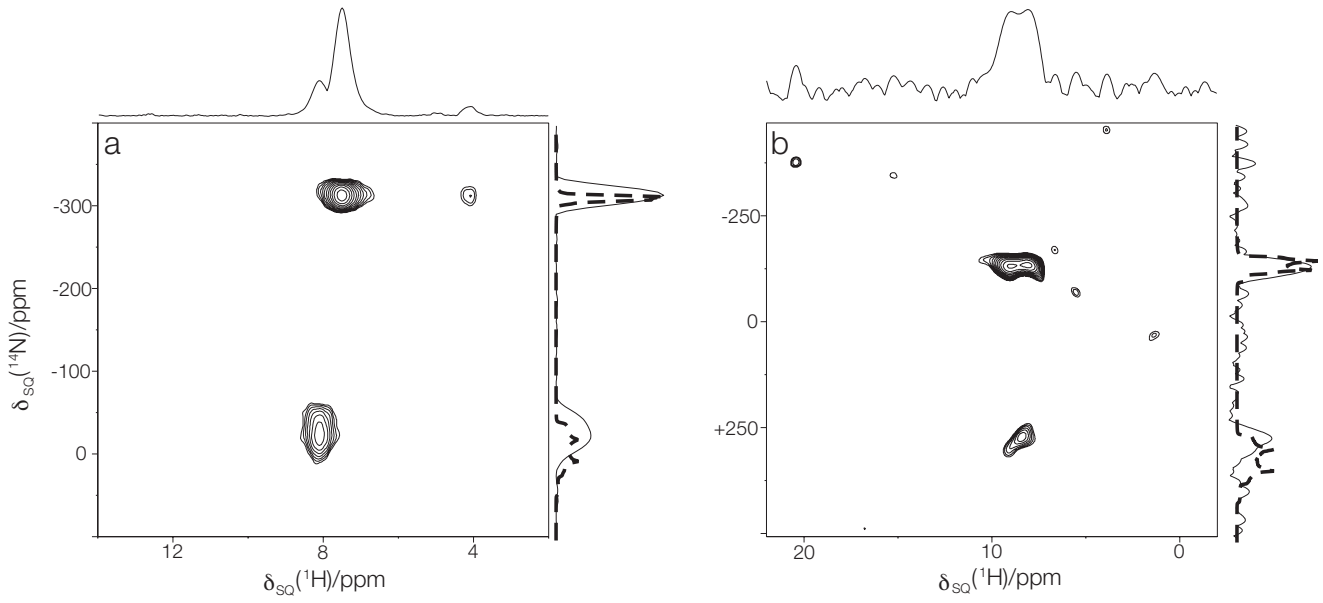

Figure 1. ^{14}N–^{1}H HMQC (850 MHz, 60 kHz MAS) spectra with skyline projections of (a) the dipeptide β-AspAla and (b) nicotinamide. Simulations of the ^{14}N spectra for ^{14}N quadrupolar coupling constants, C_Q, and isotropic chemical shifts that have been calculated using CASTEP are shown as dashed lines, with the simulations importantly taking into account the second-order isotropic quadrupolar shifts.

Figure 2 presents ^{14}N-^{1}H spectra of the deoxyguanosine derivative, dG(C3)$_2$, recorded with two different recoupling times. For the shorter recoupling time in (a), only one-bond N-H correlations are observed between N1 & the NH proton and between N2 & the NH_2 protons. In (b), additional peaks due to correlations with the non-protonated N7 ^{14}N resonance are observed for the case of the longer recoupling time.

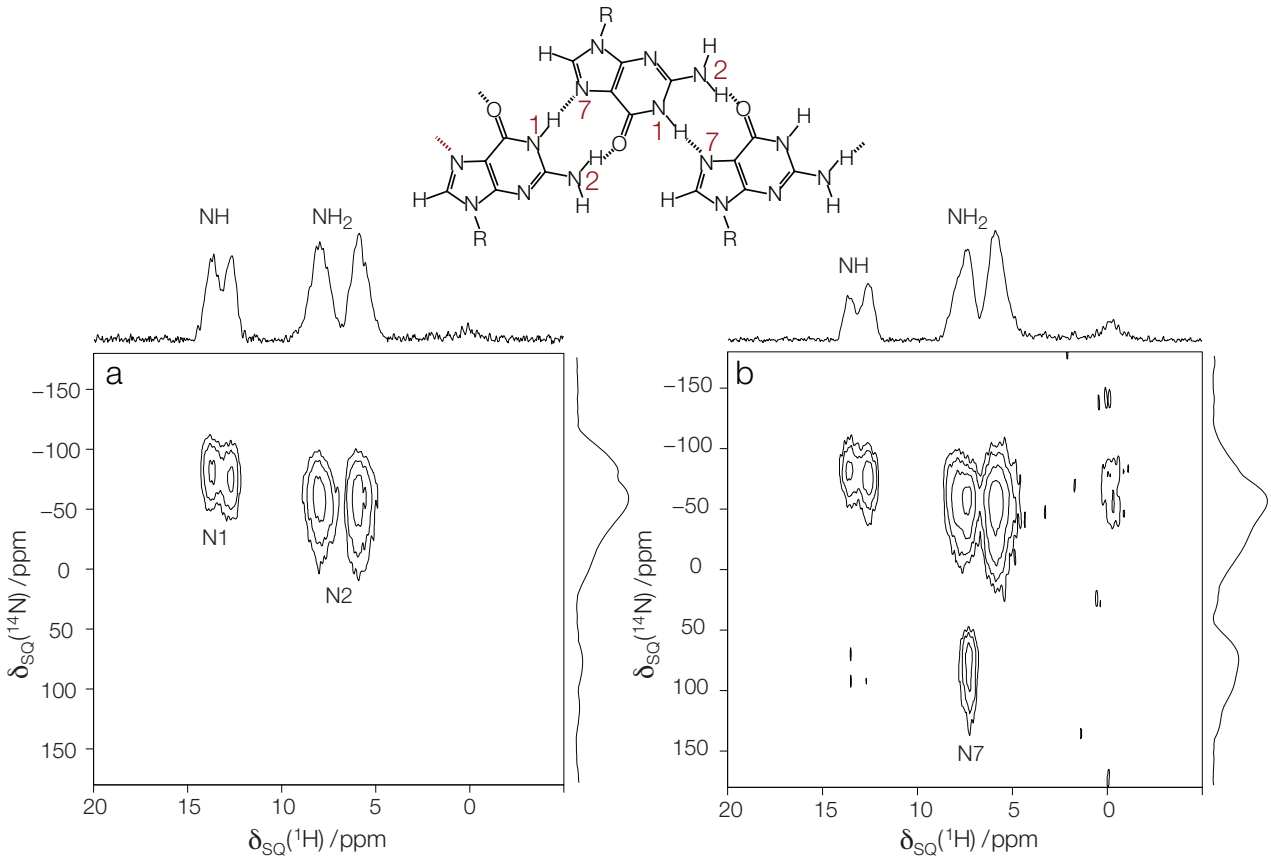

Figure 2. ^{14}N–^{1}H HMQC (850 MHz, 60 kHz MAS) spectra with skyline projections of the deoxyguanosine derivative, dG(C3)$_2$, recorded with recoupling times of (a) 333 μs and (b) 800 μs.

References

1. Gan, Z. H.; Amoureux, J. P.; Trebosc, J. *Chem. Phys. Lett.* **2007**, *435*, 163.

2. Cavadini, S.; Abraham, A.; Bodenhausen, G. *Chem. Phys. Lett.* **2007**, *445*, 1.

Applications of ^{1}H Double-Quantum Solid-State NMR to Pharmaceuticals and Supramolecular Self-Assembly

Jonathan P. Bradley,[1] Amy L. Webber,[1] Les Hughes,[2] Dave Martin,[2] Sitaram Velaga,[3] Oleg N. Antzutkin,[1,3] and Steven P. Brown[1]

[1]Department of Physics, University of Warwick, [2]Astra Zeneca, [3]Luleå University, Sweden

Overview

^{1}H double-quantum (DQ) spectroscopy is a powerful method for probing proton-proton proximities in the solid state structures adopted by organic molecules.[1] In 2004, it was shown that much enhanced resolution can be achieved for a dipeptide using a ^{1}H DQ CRAMPS experiment at 12.5 kHz MAS as compared to MAS alone at 30 kHz.[2] Recently, a ^{1}H DQ CRAMPS – ^{13}C refocused INEPT experiment has been presented that enables better resolution of ^{1}H DQ resonances via the ^{13}C dimension.[3] We present here, first, a comparison of the resolution achievable at 850 MHz and 60 kHz MAS to that obtained previously with the ^{1}H DQ CRAMPS experiment at 600 MHz and 12.5 kHz MAS for two forms of an active pharmaceutical ingredient (API);[4] and second, applications at 850 MHz of the ^{1}H DQ CRAMPS – ^{13}C refocused INEPT experiment for the γ polymorph of the pharmaceutical molecule, indomethacin and a guanosine derivative that adopts a ribbon-like self assembly,[5] both at natural isotopic abundance.

Comparing ^{1}H DQ MAS and ^{1}H DQ CRAMPS of an API

Figure 1 compares the resolution in ^{1}H DQ MAS spectra recorded at 60 kHz MAS using a 1.3 mm probe for the anhydrate and hydrate forms of an active pharmaceutical ingredient (as supplied by AstraZeneca), with that in previously presented ^{1}H DQ CRAMPS spectra.[4] While the resolution is still better in the ^{1}H DQ CRAMPS experiment (notably in the crowded low-ppm region), it is sufficient in the "brute-force" high-field fast-MAS approach to resolve the distinct peaks for the anhydrate and hydrate forms, in particular the key differentiating high-ppm DQ peaks involving a hydrogen-bonded proton.

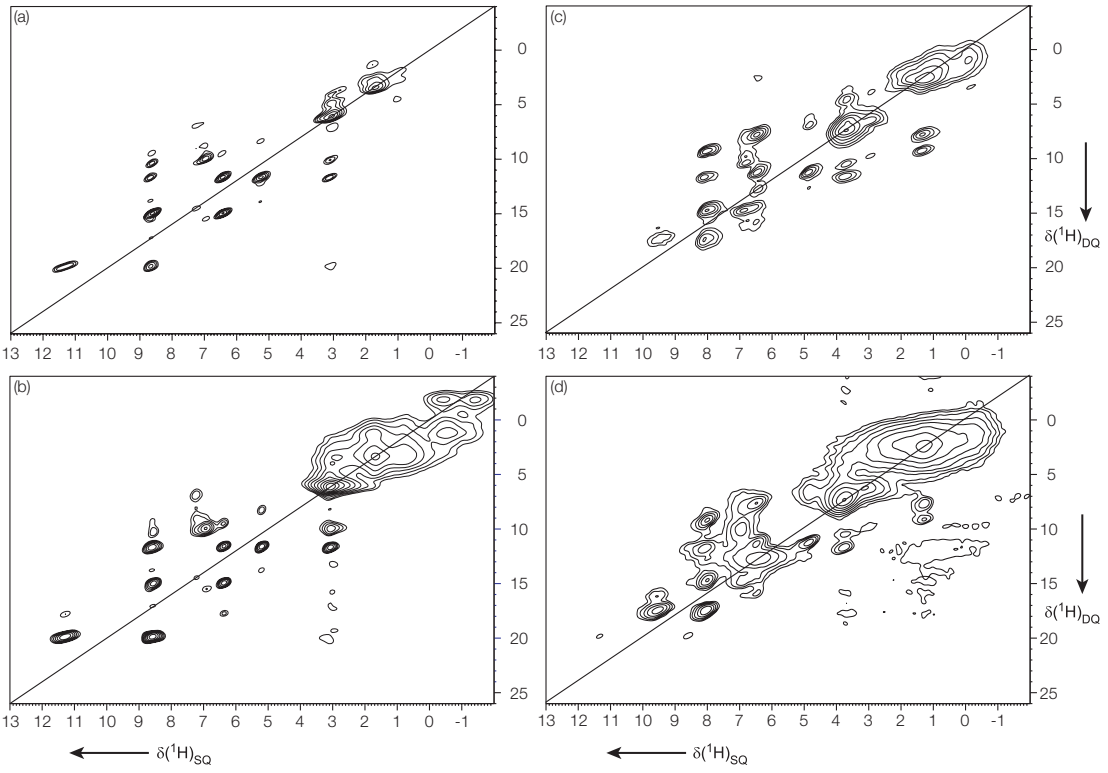

Figure 1. Comparison of (a, c) ^{1}H (600 MHz) DQ CRAMPS spectra at 12.5 kHz MAS[4] and (b, d) ^{1}H (850 MHz) DQ MAS (60 kHz) spectra of (a, b) an anhydrous and (c, d) a monohydrate form of an API.

^{1}H DQ CRAMPS – ^{13}C refocused INEPT spectra

For the γ polymorph of indomethacin, only two distinct resonances can be resolved in a ^{1}H (600 MHz) DQ CRAMPS spectrum (not shown) for the seven aromatic protons. As shown in Figure 2, a ^{1}H (850 MHz) DQ CRAMPS – ^{13}C refocused INEPT spectrum enables separate ^{1}H DQ peaks to be observed for the six resolved ^{13}C aromatic CH resonances. In this way, experimental ^{1}H DQ build-up (as a function of the DQ recoupling time) curves can be extracted, which provide quantitative insight into relative H-H distances:[6] Figure 2 also presents a comparison of experimental and simulated (eight-spin) ^{1}H DQ build-up for the highlighted DQ peak. Figure 3 presents a ^{1}H (DQ) – ^{13}C refocused INEPT spectrum of the guanosine derivative, $dG(C3)_2$ that enables distinct ^{1}H DQ peaks to be identified, notably for the sugar region where there is only limited resolution in a ^{1}H DQ CRAMPS spectrum (not shown).

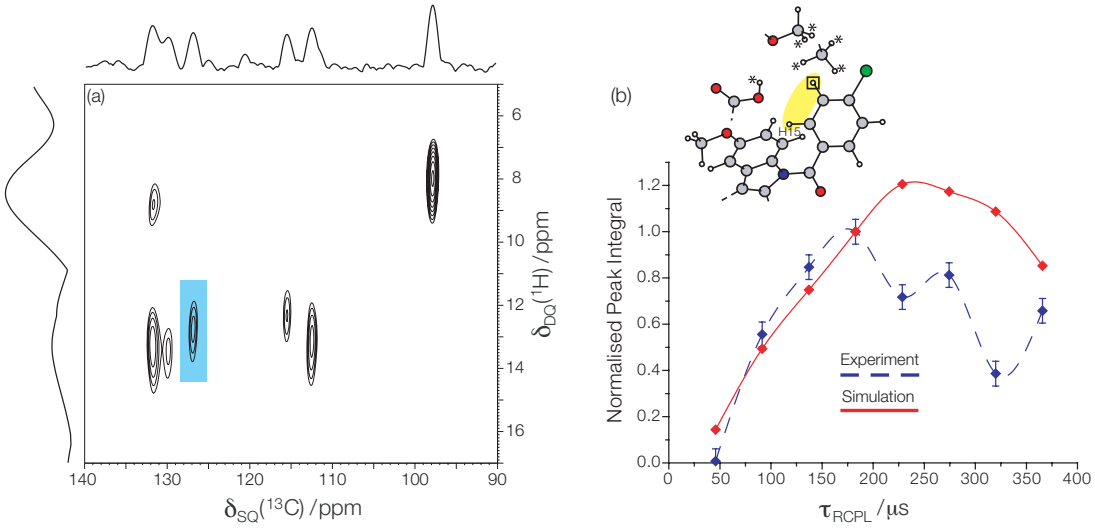

Figure 2. (a) A ^{1}H (DQ) – ^{13}C refocused INEPT spectrum of indomethacin-γ recorded at 850 MHz and 12.5 kHz MAS with a total recoupling time of 183 μs. (b) Experimental (blue) and 8-spin simulated (red) DQ build-up data for the peak highlighted in (a).

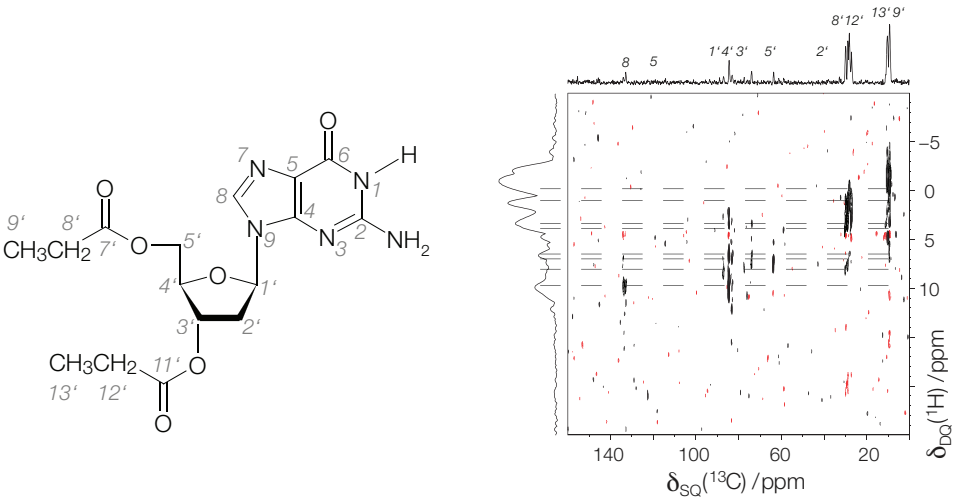

Figure 3. A ^{1}H (DQ) – ^{13}C refocused INEPT spectrum of the guanosine derivative, $dG(C3)_2$, recorded at 850 MHz and 12.5 kHz MAS with a total recoupling time of 137 μs.

References

1. Brown, S. P. *Prog. Nucl. Magn. Reson. Spectrosc.* **2007**, *50*, 199.

2. Brown, S. P.; Lesage, A.; Elena, B.; Emsley, L. *J. Am. Chem. Soc.* **2004**, *126*, 13230.

3. Webber, A. L.; Elena, B.; Griffin, J. M.; Yates, J. R.; Pham, T. N.; Mauri, F.; Pickard, C. J.; Gil, A. M.; Stein, R.; Lesage, A.; Emsley, L.; Brown, S. P. *Phys. Chem. Chem. Phys.* **2010**, *12*, 6970.

4. Griffin, J. M.; Martin, D. R.; Brown, S. P. *Angew. Chem.-Int. Edit.* **2007**, *46*, 8036.

5. Pham, T. N.; Masiero, S.; Gottarelli, G.; Brown, S. P. *J. Am. Chem. Soc.* **2005**, *127*, 16018.

6. Bradley, J. P.; Tripon, C.; Filip, C.; Brown, S. P. *Phys. Chem. Chem. Phys.* **2009**, *11*, 6941.

^{17}O NMR of Biominerals: How are Bone Mineral Particles Cemented Together?

Erika Davies,[1] Sharon E. Ashbrook,[2] Melinda J. Duer,[1] David G. Reid[1]

[1]Department of Chemistry, University of Cambridge, [2]School of Chemistry and EaStCHEM, University of St Andrews

Overview

Bone is a complex organic-inorganic composite consisting primarily of a protein network (collagen type I) on which are deposited nanocrystalline mineral particles. In addition to the collagen network, there are a host of other organic components, including other proteins, proteoglycans and lipids some of which are thought to be important in ordering the mineral crystals, amongst other things. The mineral phase itself has long been described as a calcium phosphate phase similar to hydroxyapatite (HA), but with a recognition that the nanocrystalline nature of the particles means that the "bulk" structure represents a relatively small part of the total particle. The structure at the surface is most unlikely to be that of any lattice plane in the bulk, as cutting the crystal along any plane leaves the surface ions coordinatively unsaturated and thus not in equilibrium positions. The expectation is that surface ions rearrange, and may even be chemically modified in the search for an equilibrium structure. The mineral surface structure is of key importance, both in terms of the material properties of the composite that the mineral forms with the underlying organic matrix, as it determines how the mineral particles can bind into that matrix, and in terms of biology, as the mineral surface will be what cells in the tissue see and recognise.

There is significant evidence in the literature, primarily from ^{1}H and ^{31}P solid-state NMR in conjunction with IR, that the surface of the mineral particles contains an abundance of hydrogen phosphate, i.e., protonated phosphate groups, which have been thought to help stabilise the surface. However, ^{17}O NMR spectra had never been recorded. Results recorded at the National Facility last year suggest that in fact there are no true hydrogen phosphate groups in bone mineral, but rather phosphate groups strongly hydrogen bonded to water and highly mobile protons, the role of which are yet to be fully understood. The conclusions from this work have strong implications for understanding how mineral crystals are organised. It now seems likely that mineral nanoparticles in bone are actually sandwiched together via a layer of water that is strongly hydrogen bonded to mineral surface phosphate groups rather like the way two glass plates can be "stuck" together when their surfaces are dampened with water. This is an entirely different view of bone mineral and, particularly importantly, it suggests that the mineral particle surfaces are stabilised by being in close proximity to other mineral particles, allowing a layer of water "glue" to be trapped where it is needed. If broken apart, one could then expect the mineral nanoparticle surfaces to be highly reactive. This could go a considerable way to explaining why nanocrystalline HA is highly cytotoxic and causes strong inflammatory reactions, both key points in finding proper bone replacement materials and in understanding the effects of joint wear and tear in human patients, as wear produces "free" mineral nanoparticles in joints.

^{17}O NMR of brushite, octacalcium phosphate (OCP) and bone

A double-frequency sweep (DFS) ^{17}O NMR spectrum of brushite ($Ca(HPO_4).2H_2O$) (Figure 1) shows the signals for the ^{17}O-H sites in HPO_4^{2-} ions expected from first principles electronic structure calculations. The crystal structure of OCP ($Ca_8(HPO_4)_2(PO_4)_4.5H_2O$) (Figure 2a) consists of a hydrated layer and a layer with a structure similar to hydroxyapatite, the basis of bone mineral. OCP has long been thought by bone biologists to be involved in the production of bone mineral, perhaps acting as a precursor phase. First-principles electronic structure calculations show the hydrogen phosphate ^{17}O-H sites will have similar chemical shifts to hydrogen phosphates in brushite. Interestingly, the only signal therefore that could be due to ^{17}O-H sites in OCP hydrogen phosphates is a relatively weak and very broad signal centred around 60 ppm (Fig 2b). Two-dimensional ^{1}H-^{31}P HETCOR spectra of OCP (not shown, as not recorded at the Facility) exhibit much broader ^{1}H signals for the hydrogen phosphate ^{1}H and the crystal water than one would expect for a crystalline material and, even at short mixing times, there is a clear cross peak between the hydrogen phosphate ^{31}P signal and water ^{1}H. A consistent explanation of all these observations is that water molecules are strongly hydrogen bonded to the hydrogen phosphate ions and that there is an exchange process between the nominal "hydrogen phosphate" ions and water protons, such that on the timescale of the ^{17}O spectrum, the hydrogen phosphate signal is strongly broadened.

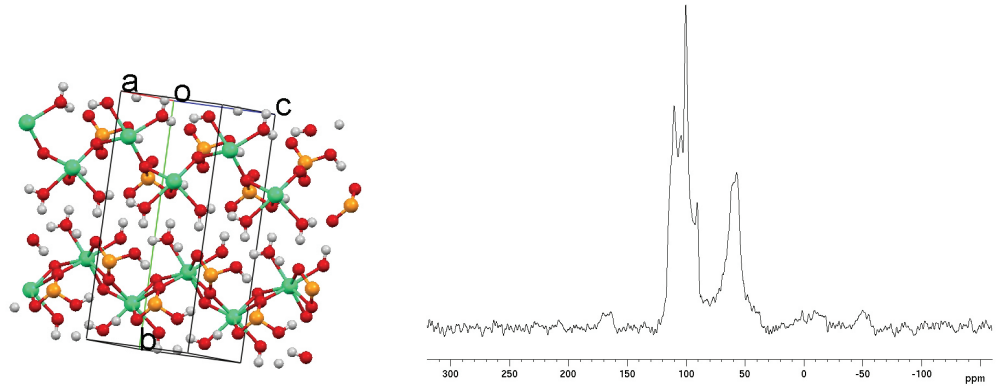

Figure 1. (a) The crystal structure of brushite ($Ca(HPO_4).2H_2O$), (b) DFS ^{17}O NMR spectrum of 20% ^{17}O-enriched brushite showing the expected ^{17}O signals for phosphate oxygens (including phosphate oxygens hydrogen bonded to water) in the region 90 – 110 ppm and ^{17}O-H sites in hydrogen phosphate around 50 - 60 ppm.

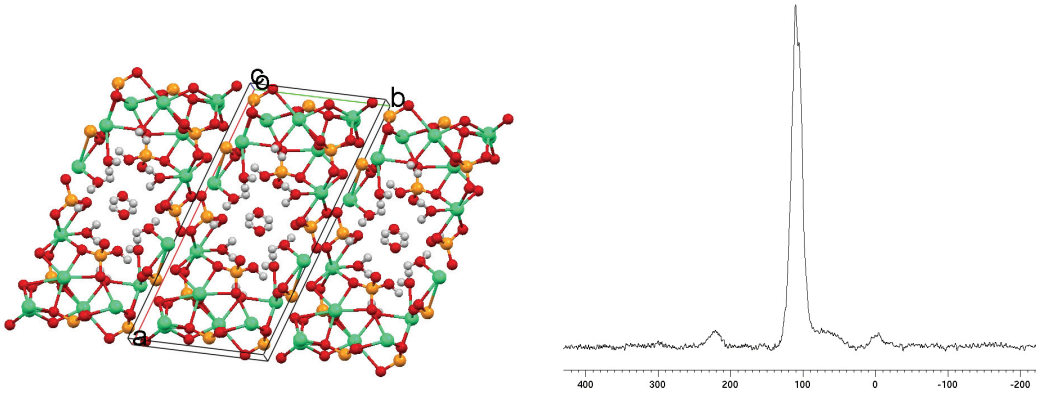

Figure 2. (a) The crystal structure of OCP ($Ca_8(HPO_4)_2(PO_4)_4.5H_2O$)*, (b) DFS ^{17}O NMR spectrum of 10% ^{17}O-enriched OCP showing the expected ^{17}O signals for phosphate oxygens (including phosphate oxygens hydrogen bonded to water) in the region 90 – 110 ppm; signals due to ^{17}O-H sites in hydrogen phosphate around 50 – 60 ppm are highly broadened. Note the water in this sample is not significantly ^{17}O enriched, so appears with weaker intensity (around 0 ppm).*

Interestingly, the ^{17}O DFS NMR spectrum of equine cortical bone (Figure 3) is very similar to that of OCP. It clearly shows the presence of phosphate oxygens (90 – 110 ppm), which is in the region predicted by first-principles electronic structure calculations for hydroxyapatite. However, there are no distinct signals in the expected hydrogen phosphate region (30 – 60 ppm), just a broad shoulder. Two-dimensional ^1H – ^{31}P HETCOR spectra of bone (mineral) always show a cross peak between phosphate ^{31}P and a very broad ^1H signal due to hydrogen phosphate ^1H. Significantly, there is also always a cross peak between ^{31}P phosphate and a broad ^1H water signal, again similar to OCP. Thus, is seems likely that a similar situation exists in bone mineral to that in OCP, i.e., that hydrogen phosphate ions exchange ^1H with water molecules that are strongly hydrogen bonded to them. In OCP, the hydrogen phosphate ions and water form the hydrated layer between apatitic layers. This looks likely to be a model for bone mineral: apatitic layers bound by layers of phosphate cement with strongly-bound water and highly mobile protons.

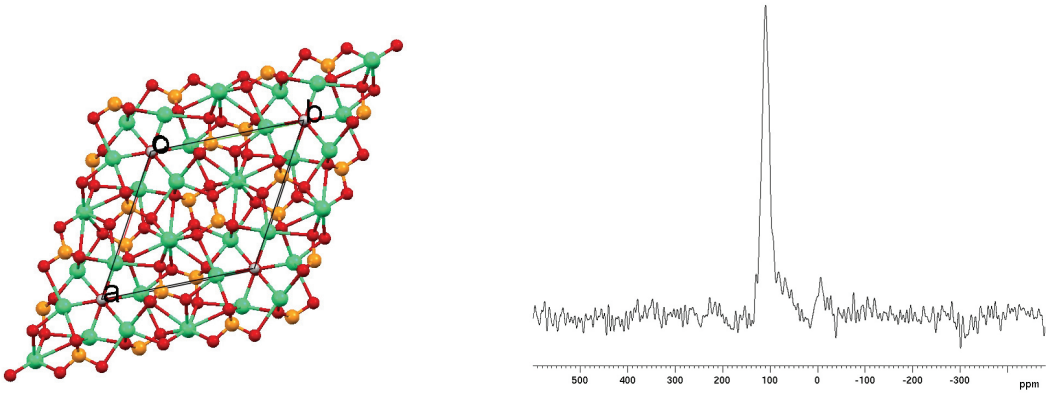

Figure 3. (a) The crystal structure of hydroxyapatite ($Ca_{10}(PO_4)_6(OH)_2$)*, (b) DFS ^{17}O NMR spectrum of bone showing the expected ^{17}O signals for phosphate oxygens (including phosphate oxygens hydrogen bonded to water) in the region 90 – 110 ppm but no signals due to ^{17}O-H sites in hydrogen phosphate around 50 – 60 ppm.*

Double Rotation (DOR) NMR and Spin-Diffusion (SD) DOR NMR of ^{11}B in Glasses and Crystals

Ray Dupree, Diane Holland, Andrew P. Howes, Oliver Alderman

Department of Physics, University of Warwick

The aim of this study was, following the installation and testing of the 850 DOR probe, to implement programs which allow odd-order sideband suppression and spin diffusion to be performed and apply these to some boron containing materials. Implementation was successful and a Pyrex sample was first examined (Figure 1). Pyrex is a commercially important borosilicate glass exploited mainly for its high temperature stability and good thermal shock resistance and further information about its structure is important in developing an understanding of its properties. Whilst use of DOR improves the resolution of the high C_Q peaks (B3) compared with magic-angle-spinning (MAS) NMR, we found no outer rotor speed (within the capability of the current DOR probe) which would move the (even-order) spinning sidebands to a position where there was no overlap with the main peaks (Figure 1a).

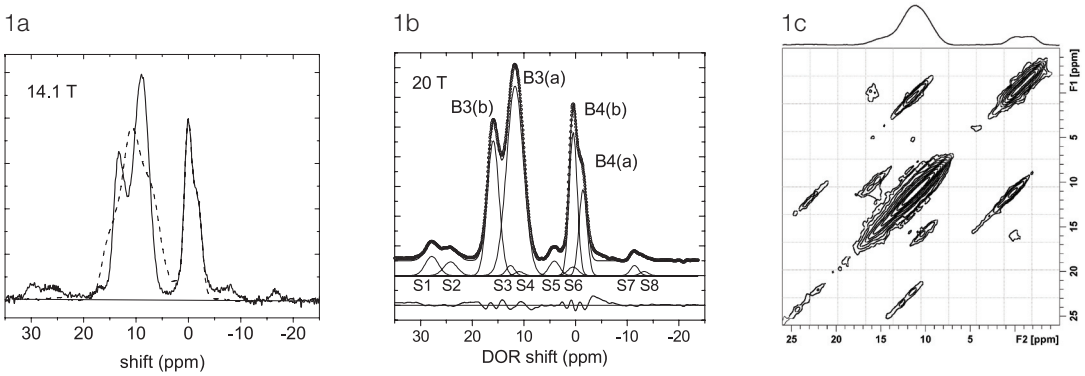

Figure 1. (a) Superposed DOR NMR (solid line) and MAS NMR (dashed line) spectra from pyrex: DOR: 1.6 kHz outer rotor, 4 μs pulse duration, 0.5 s recycle interval, odd-order sideband suppression; MAS: 3.2 mm Bruker probe,12.5 kHz, 1 ms pulse duration, 4 s recycle interval (background subtraction).

(b) DOR spectrum fitted with Gaussian lineshapes, giving intensity ratios: B3b:B3a:B4b:B4a = 24:48:18:10.

(c) SD DOR spectrum with 100 ms mixing time: 1.5 kHz outer rotor, 3 μs pulse, 0.35 s delay, t_1 increment 80 μs, 125 increments, 160 acquisitions per increment.

This compromises the peak resolution to some extent and reduces the accuracy with which the various site abundances can be determined by fitting (Figure 1b). A Spin Diffusion (SD) DOR experiment was performed to investigate the interconnection of the different structural units in the glass (Figure 1c). Clear cross peaks are observed at 100ms mixing time between the more positive B4 at ~0 ppm and the B3 at ~16 ppm and also cross 'ridges' are observed between the B3 at ~17-14 ppm and that from ~12-9 ppm. However although there might be a connection between the B3 from the region near 12 ppm and the B4 peaks, this is uncertain since the cross peaks coincide with regions where contributions from sidebands occur.

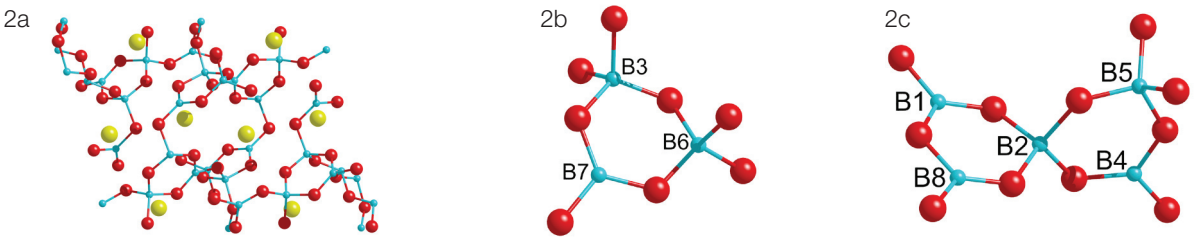

Figure 2. (a) Crystal structure of α-BaB_4O_7; (b) di-triborate superstructural unit; (c) pentaborate superstructural unit. The units are joined (via O) at B5-B6, B5-B7, B6-B8, B3-B1, B3-B4.

As a consequence of this problem, a borate system was chosen which would allow us to resolve sidebands from main peaks at modest spinning speeds and thereby allow cross-peaks in SD DOR to be assigned with confidence. The system chosen was crystalline BaB_4O_7 which has several polymorphs, of which only one has a crystal structure determination. This is α-BaB_4O_7, whose structure contains eight B sites (4 B4 and 4 B3) in two superstructural units, di-triborate and pentaborate (Figure 2)

The MAS and DOR spectra of the α- and γ- polymorphs are compared in Figure 3 which shows the greatly enhanced resolution and simplification of the high C_Q B3 sites under DOR on the 850 MHz spectrometer, with linewidths of ~0.5 ppm and no overlap of the spinning sidebands at an outer rotor speed of 1.4 kHz.

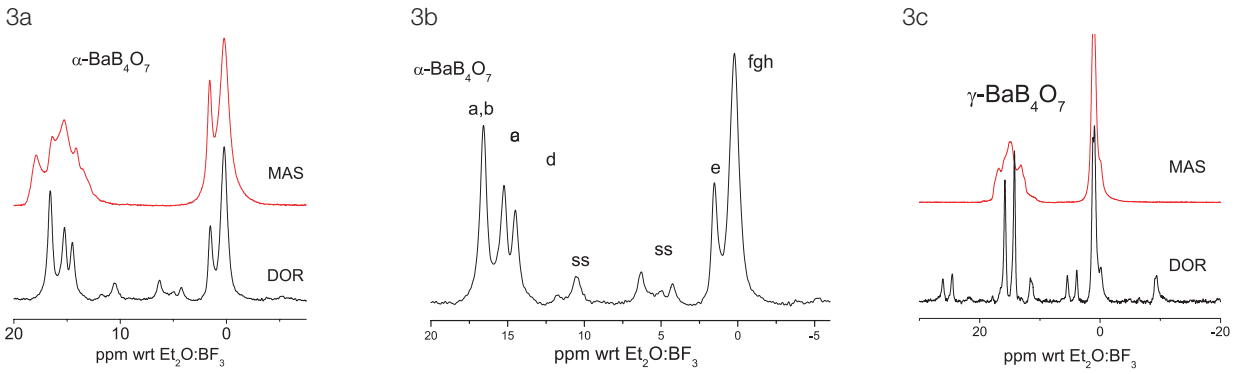

Figure 3. (a) MAS and DOR spectra of α-BaB_4O_7; (b) main peaks labelled; (c) MAS and DOR spectra of γ-BaB_4O_7. Acquisition parameters as in Figure 1a.

This allows the peaks to be fitted and integrated with confidence to give their relative amounts. Those for α-BaB_4O_7 are simple integer ratios, with 3 peaks in the B3 region in the ratio 2:1:1 and 2 B4 peaks in the ratio 1:3 as indicated in Figure 3b. To assign the peaks to specific sites, a series of SD DOR experiments were run at different mixing times. An example SD DOR spectrum with a t_{mix} of 20 ms is shown in Figure 4. Cross-peaks can be seen between B3 and B4 sites and also between two of the B3 sites and between the B4. Using information from SD DOR and the known crystal structure of α-BaB_2O_7, the following preliminary assignment of the peaks in the DOR spectrum (Figure 3b) to the B sites as labelled in Figures 2b, 2c can be made:

a,b = B7,B8; c = B1; d = B4; e = B6; f,g,h = B2,B3,B5

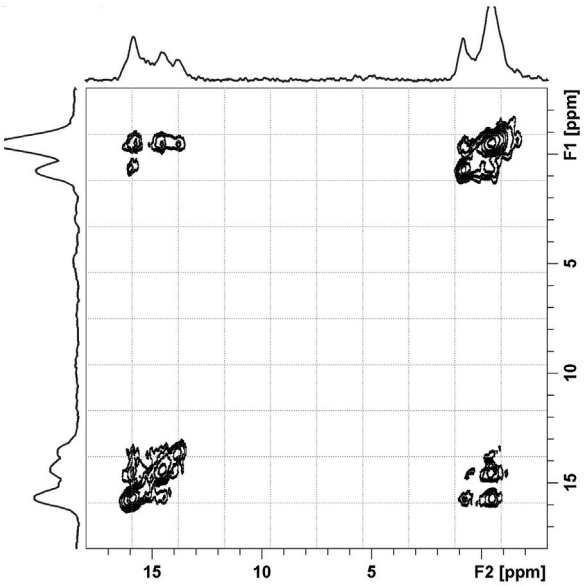

Figure 4. SD DOR spectrum of α-BaB_4O_7 20 ms mixing time: 1.4 kHz outer rotor, 3 μs pulse duration, 1 s recycle interval, t1 increment 100 μs, 80 increments, 384 acquisitions per increment.

High-Field Solid-State NMR Studies of the Defect Chemistry in Perovskites

Frédéric Blanc,[1,2] Lucienne Buannic[2] and Clare P. Grey[1,2]

[1]Department of Chemistry, University of Cambridge, [2]Department of Chemistry, State University of New York, USA

Overview

Solid-state Nuclear Magnetic Resonance (NMR) spectroscopy is a very powerful method for determining the local geometry and coordination number of large range of NMR active nuclei. Nevertheless, certain nuclei are difficult to study due a combination of poor spectroscopic resolution and low sensitivity. Most of these drawbacks could be overcome by the use of high magnetic fields and we demonstrate here their usefulness in the study of the defect chemistry of perovskite systems of general formula ABO_3. This class of materials has application as electrolytes for oxygen and proton transports in solid oxide fuel cells (SOFC) devices, via the so-called defect mechanism. To induce defects, dopant ions are often substituted for higher valent ions in the same crystallographic site (Figure 1a), and therefore observation of any local defects – often present in small amounts – and clustering near the defects using diffraction based techniques is not straightforward. Our NMR approach relies on known correlations between isotropic chemical shift and coordination number[1,2] to identify the sites with defects which thus not only require high resolution but also high sensitivity of the NMR dataset available at high magnetic fields to ensure proper observation of all crystallographic defects.

Observation of crystallographic defects in doped $LaGaO_3$ by ^{71}Ga NMR

The Mg^{2+} and Ga^{3+} local structures of Mg-doped $LaGaO_3$ have been investigated by multinuclear ^{71}Ga and ^{25}Mg studies. Given the dominance of the 6-coordinate sites in the Mg spectra (data not shown), we turn instead to examine the gallium site by using ^{71}Ga static NMR data obtained under various experimental conditions. The static spectra at four fields (Figure 1b) including spectra at our own facility (8.45 T, 9.4 T, 14.1 T) and at the UK high-field facility (20 T), are clearly dominated by a relatively narrow line that may be well-fitted by an EFG tensor with parameters consistent with six–fold coordinated Ga ($\delta_{iso,cs}$ = 59 ± 1 ppm, C_Q = 1.5 ± 0.1 MHz, η_Q = 0.0 ± 0.2, Figure 1b, purple line) and very close to those derived for pure $LaGaO_3$.[3,4] However, closer examination of the lineshape reveals that at least one further Ga environment is present, the associated resonance being much broader than that obtained for the majority GaO_6 sites, with fitted quadrupolar coupling constant of C_Q = 8.3 ± 2.4 MHz and isotropic chemical shift of $\delta_{iso,cs}$ = 72 ± 22 ppm, extracted from the field dependence of the peak position (Figure 1c, blue line). Such values are in keeping with both the experimental[5] and computational[2] results obtained previously for GaO_5 coordination, and so further support the notion that compensating O vacancies occupy sites adjoining Ga cations in the present materials (Figure 1a).

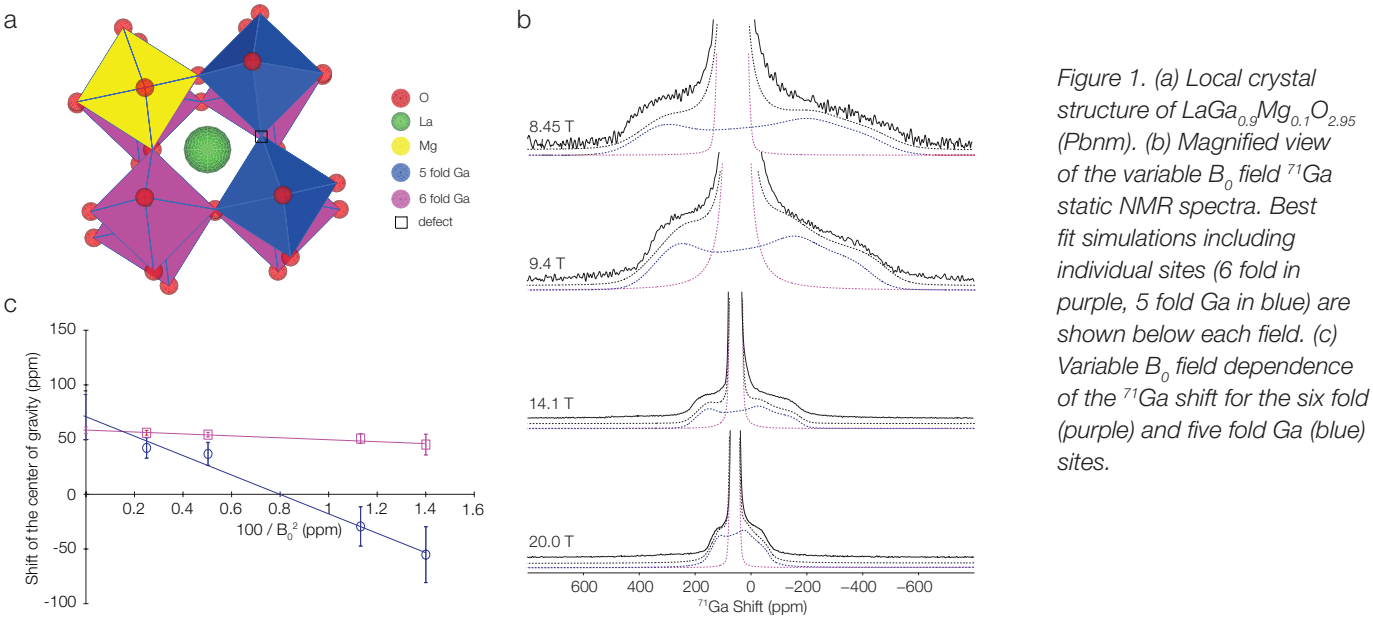

Figure 1. (a) Local crystal structure of $LaGa_{0.9}Mg_{0.1}O_{2.95}$ (Pbnm). (b) Magnified view of the variable B_0 field ^{71}Ga static NMR spectra. Best fit simulations including individual sites (6 fold in purple, 5 fold Ga in blue) are shown below each field. (c) Variable B_0 field dependence of the ^{71}Ga shift for the six fold (purple) and five fold Ga (blue) sites.

Observation of crystallographic defects in Y-doped $BaSnO_3$ by ^{89}Y NMR

The ^{89}Y MAS NMR spectra of $BaSn_{0.90}Y_{0.10}O_{2.95}$ (Figure 2) shows two resonances at about 293 and 105 ppm. While the resonance at 293 ppm is assigned to yttrium in a 6-coordinate environment (as expected for substitution of the B = Sn site of the perovskite by yttrium), the resonance at 105 ppm falls into the region for 12-coordinated yttrium. This could be due to the presence of A = Ba - site substitution[6] but more likely to rotor background that probably arises from yttria stabilized zirconia (YSZ), a material often used to strengthen synthetic zirconia. As the concentration of yttrium increases, the resonance at 293 ppm for 6-coordinate Y in $BaSn_{0.90}Y_{0.10}O_{2.95}$ (Figure 2b) gradually shifts to higher frequencies at 323 and 344 ppm for $BaSn_{0.70}Y_{0.30}O_{2.85}$ and $BaSn_{0.50}Y_{0.50}O_{2.75}$, respectively, and shows a clear tendency of Y to be sensitive to next neighbour cations. More interestingly, ^{89}Y spectra of both $BaSn_{0.70}Y_{0.30}O_{2.85}$ and $BaSn_{0.50}Y_{0.50}O_{2.75}$ show a third resonance at 425 ppm, with increasing intensity at increasing yttrium content. This resonance, at very high field for ^{89}Y NMR has never been seen before, and is assigned to yttrium in five-fold coordination, i.e., a low-coordinate yttrium site hosting an oxygen vacancy nearby and allowing us to answer some important questions of the defect chemistry in this perovskite material.

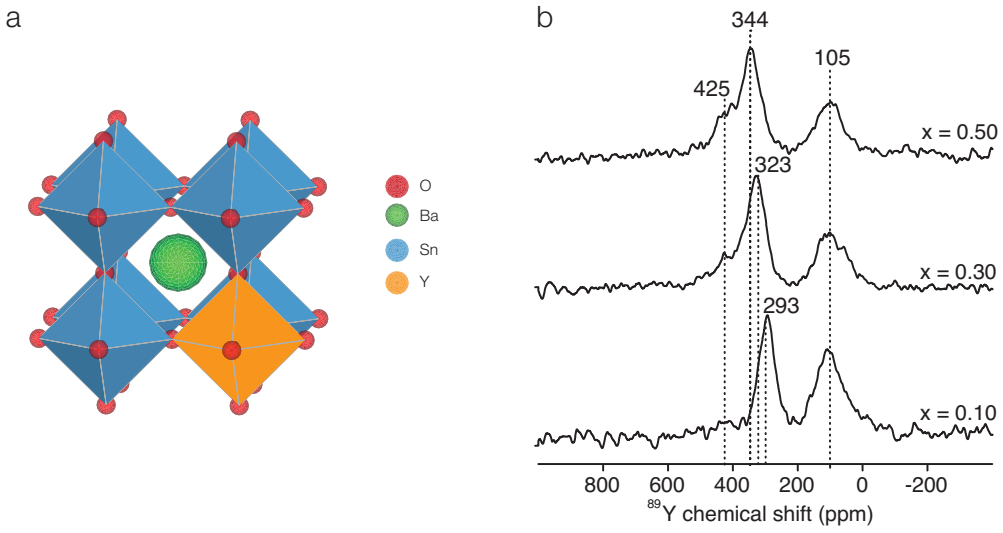

Figure 2. (a) Local crystal structure of Y doped $BaSnO_3$ (space group Pm3m). (b) ^{89}Y MAS NMR spectra of $BaSn_{1-x}Y_xO_{3-x/2}$ (x = 0.1, 0.3 & 0.5).

References

1. MacKenzie, K. J. D.; Smith, M. E. *Multinuclear Solid-State NMR of Inorganic Materials*; Elsevier: Oxford, **2002**; Vol. 43.
2. Middlemiss, D. S.; Blanc, F.; Pickard, C. J.; Grey, C. P. *J. Magn. Reson.* **2010**, *204*, 1.
3. Bastow, T. J.; Mathews, T.; Sellar, J. R. *Solid State Ionics* **2004**, *175*, 129.
4. Ash, J. T.; Grandinetti, P. J. *Magn. Reson. Chem.* **2006**, *44*, 823.
5. Massiot, D.; Vosegaard, T.; Magneron, N.; Trumeau, D.; Montouillout, V.; Berthet, P.; Loiseau, T.; Bujoli, B. *Solid State Nucl. Magn. Reson.* **1999**, *15*, 159.
6. Yamazaki, Y.; Hernandez-Sanchez, R.; Haile, S. M. *J. Mat. Chem.* **2010**, *20*, 8158.

^{93}Nb Static and Ultra-Fast MAS/MQMAS Studies of $A_5B_4O_{15}$ (A=Ba, Sr, Mg, Ca, Zn; B=Nb) Hexagonal Perovskites Employed in Thermoelectric and Microwave Dielectric Devices, and $ABNb_2O_7$ (A=Rb, Cs; B=La, Bi) Layered Perovskites Displaying Proton Conduction and Potential Ferroelectric Properties

John V. Hanna and Dean S. Keeble

Department of Physics, University of Warwick

Overview

Different Nb(V) structural systems play pivotal roles in technologically important materials systems, however there exists a complete dearth pertaining to the accurate ^{93}Nb solid-state NMR characterisation of the many structural polytypes. Serious deficiencies in early ^{93}Nb solid-state NMR studies[1,2] have necessitated that the measurement of the characteristic NMR tensor parameters (in particular δ_{iso}, C_Q and η_Q), and their rationalisation with respect to structural systems and polytypes, be re-evaluated; this has been further aided and verified with DFT computational methods.[3] Many microwave dielectric device materials of nominal composition $A_5Nb_4O_{15}$ (and also $ANbO_3$ and $ANbO_4$) require a complete and exhaustive characterisation because the technological improvement to these systems usually invokes dopants being introduced to the structure, or the original phases becoming incorporated in complex mixtures and solid solutions via co-crystallisation or physical dispersion. The induced disorder and chemically-distinct Nb(V) species that emanate from such synthetic manipulation requires spectroscopic study and evaluation, however this is hampered greatly by the initial lack of accurate characterisation(s) of compositional end-members and ordered systems. The same scenario of difficulties is also encountered in the study of proton conduction/incipient ferroelectric layered perovskite (or Dion-Jacobson (DJ)) systems of the type $ABNb_2O_7$. In addition to the need for characterisation, a broader physical understanding needs to be constructed as to why particular classes of Nb(V) materials yield certain ranges of NMR interaction parameters, and how this related to the structure/function relationship of the material. This is particularly emphasized when comparing and contrasting the ^{93}Nb MAS NMR data from these types of systems.

^{93}Nb static and fast MAS studies

The predominant microwave dielectric materials studied possessed the following nominal stoichiometries $Ba_5Nb_4O_{15}$, $Sr_5Nb_4O_{15}$, $SrNb_2O_6$ and $PbNb_2O_6$, while the DJ layered perovskite suite consisting of the $HLaNb_2O_7$, $KLaNb_2O_7$, $RbLaNb_2O_7$ and $CsLaNb_2O_7$ systems. Figure 1 (below) shows representative ^{93}Nb static and MAS data for (a) $Ba_5Nb_4O_{15}$, (b) $SrNb_2O_6$, (c) $RbLaNb_2O_7$ and (d) $CsLaNb_2O_7$. Initial estimates from these data show that the C_Q values characterising all of these systems are small in magnitude (i.e., ~10-25 MHz), however the F_1 projections of the 3QMAS data (see Figure 2) suggest that there are huge differences in the chemical shift anisotropy/span ($\Delta\delta$ /Ω) parameters that describe these different systems.

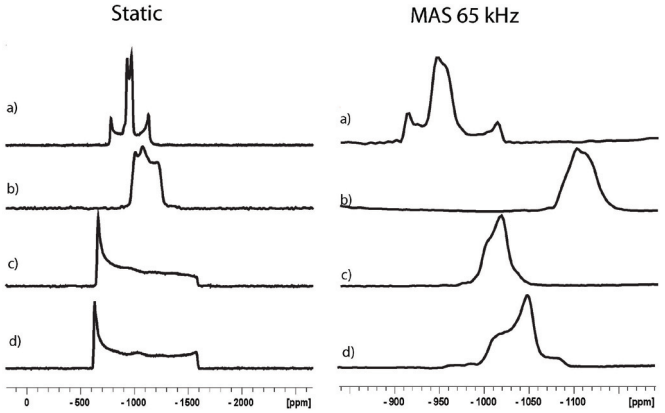

Figure 1. ^{93}Nb static and fast MAS (ν_r = 65 kHz) data for typical microwave dielectric materials (a) $Ba_5Nb_4O_{15}$ and (b) $SrNb_2O_6$, and Dion-Jacobson layered perovskite materials (c) $RbLaNb_2O_7$ and (d) $CsLaNb_2O_7$ acquired at 20 T.

The suite of microwave dielectric materials studied here belong to general families of structures where more than one Nb(V) position exists in the asymmetric unit cell, thus making the ^{93}Nb static data difficult to deconvolute and simulate. However, the increased resolution afforded by the MAS NMR data and the 3QMAS projections is used to elucidate the quadrupolar parameters (C_Q, η_Q) and isotropic chemical shifts (δ_{iso}) for these systems. These data are used to help simulate the full static linewidth which is described by quadrupolar parameters, chemical shift anisotropy/skew parameters ($\Delta\delta$, η_δ / Ω, κ) and the Euler angles (α, β, γ) relating the tensorial frames of each interaction for every Nb(V) position. Initial simulations of the complete unaveraged (static) lineshape indicate that the $A_5Nb_4O_{15}$ microwave dielectric materials exhibit Ω values of ~200 ppm, while the $ABNb_2O_7$ DJ layered perovskite reveal Ω values of > 800 ppm. Of particular note is the contrast in the relative distortion of the immediate oxo environment of each Nb(V) position in these structural classes; each $ABNb_2O_7$ DJ perovskite system exhibits a highly distorted Nb(V) octahedral coordination sphere although this doesn't appear to influence (increase) the field gradient in comparison to the much less distorted $A_5Nb_4O_{15}$ family, but large increases in Ω clearly emanate. These observations will be rationalised in terms of the Jahn-Teller distortions influencing the Nb(V) positions, the concomitant anisotropic/inequivalent contribution of the 3d orbitals and the octahedral tilts thus characteristic of ferroelectric behaviour in other DJ systems. These studies are being assisted with density functional theory (DFT) calculations using both NMR-CASTEP (GIPAW) and WIEN2k (LAPW) methods, and recourse to computed Mulliken populations and other molecular orbital approaches is also being undertaken.

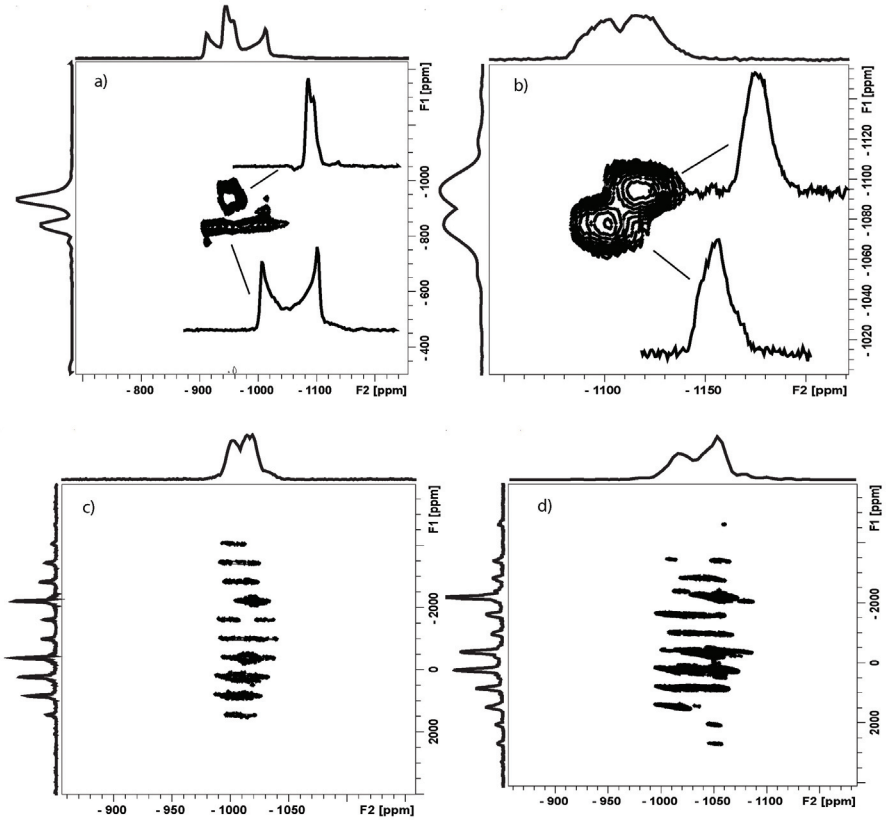

Figure 2. ^{93}Nb z-filtered 3QMAS (ν_r = 65 kHz) for (a) $Ba_5Nb_4O_{15}$, (b) $SrNb_2O_6$, (c) $RbLaNb_2O_7$ and (d) $CsLaNb_2O_7$ acquired at 20 T.

References

1. Lapina, O. B.; Khabibulin, D. F.; Romanenko, K. V.; Gan, Z.; Zuev, M. G.; Krasil'nikov, V. N.; Fedorov, V. E. *Solid State Nucl. Magn. Reson.* **2005**, *28*, 204.
2. Lapina, O. B.; Khabibulin, D. F.; Shubin, A. A.; Terskikh, V. V. *Prog. Nucl. Magn. Reson. Spectrosc.* **2008**, *53*, 128.
3. Hanna, J. V.; Pike, K. J.; Charpentier, T.; Kemp, T. F.; Smith, M. E.; Lucier, B. E.; Schurko, R. W.; Cahill, L. S. *Chem. Eur. J.* **2010**, *16*, 3222.

In-Situ Solid-State NMR Studies of Crystallization of Organic Materials from Solution, and Adsorption in Microporous Solids

Colan E. Hughes, P. Andrew Williams, Mingcan Xu and Kenneth D. M. Harris

School of Chemistry, Cardiff University

Overview

We have developed *in-situ* methods for studying crystallization processes[1,2] and adsorption processes[3,4] by solid-state NMR. In the case of crystallization, results acquired using our spectrometer in Cardiff have demonstrated the ability of our *in-situ* method to observe the formation and growth of crystalline phases, to identify the polymorphs involved, and to follow the evolution of polymorphic forms as a function of time during the crystallization process. However, sensitivity is a substantial barrier in many cases (particularly for samples with natural isotopic abundances), especially as the time-resolution of our method depends on spectroscopic sensitivity. Another difficulty arises for samples with long spin-lattice relaxation times, which also has a detrimental effect on the time-resolution available. To address these problems, we have found the 850 MHz facility to be invaluable. Our work has focused both on crystallization experiments involving the formation of single-component crystals and those involving the formation of co-crystals.

In the case of adsorption processes, we recently proposed and demonstrated[3,4] a new solid-state NMR strategy for *in-situ* studies of adsorption within zeolites and other porous solids, allowing the earliest stages of the adsorption process to be probed, and allowing the subsequent time-evolution of the populations of different adsorption sites within the porous solid to be mapped. In a short allocation of time at the 850 MHz facility for *in-situ* studies of adsorption processes, we focused on *in-situ* ^{23}Na MAS NMR studies of hydration of the zeolite NaY, yielding new insights on changes in the relative populations of the three distinct sodium sites within NaY as a function of time during the hydration process. However, as the majority of our allocated time at the 850 MHz facility has been for *in-situ* studies of crystallization processes, we focus exclusively on these studies in the remainder of this report.

Formation of co-crystals of urea and α,ω-alkanediols

Urea typically forms inclusion compounds with long-chain alkane derivatives. However, even chain-length α,ω-alkanediols are an exception, and instead give rise to a family of stoichiometric co-crystals[5] (see below) in which hydrogen-bonded ribbons of urea molecules are connected into sheets by ladders of α,ω-alkanediol molecules. However, the structures in this homologous family do not form a regular series. For example, the structures of urea/1,6-hexandiol (**U6**), urea/1,8-octandiol (**U8**) and urea/1,10-decandiol (**U10**) display subtle but significant differences. In particular, two different types of urea ribbon are observed, involving either parallel (e.g., **U8**) or anti-parallel (e.g. **U6** and **U10**) alignment of the urea molecules. Furthermore, the angle between the urea ribbons and α,ω-alkanediol molecules can be either acute (e.g., **U6** and **U8**) or obtuse (e.g., **U10**). Despite the family of materials exhibiting a set of well-defined structure types, each member of the family has been found to exhibit only one structure type, and no polymorphism has so far been observed (in spite of extensive explorations).

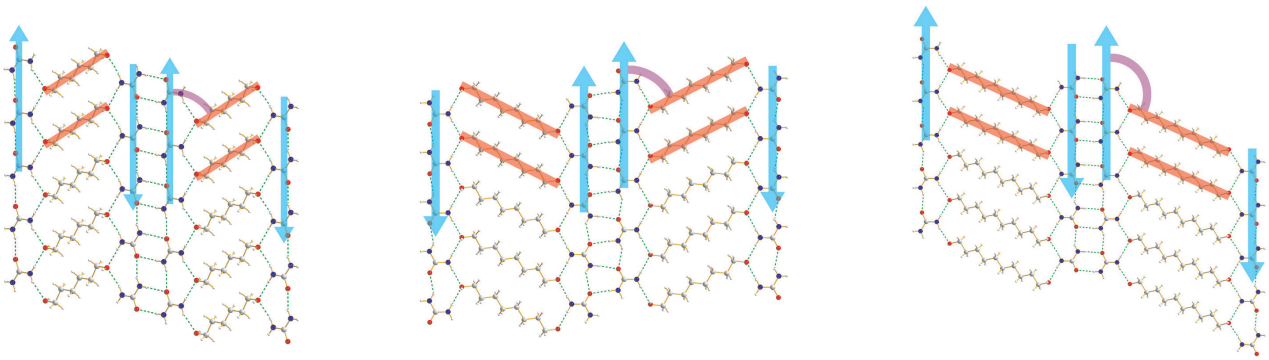

Figure 1. Crystal structures of urea/α,ω-alkanediol co-crystals. Blue arrows show the directions of the strands in the urea ribbons, red bars show the axis of the α,ω-alkanediol molecules, and purple arcs show the angle between the urea ribbon and the axis of the α,ω-alkanediol molecule.

In-situ solid-state ^{13}C CPMAS NMR spectra (see below) were recorded (with ^{1}H-^{13}C CP) for solutions of ^{13}C-labelled urea and different α,ω-alkanediols undergoing crystallization from methanol, induced by cooling. Owing to long spin-lattice relaxation times, a recycle interval of 2 mins was typically used with only 8 scans acquired per time point. Our spectra for crystallization of urea and 1,6-hexandiol reveal the formation of the known **U6** co-crystal phase together with a small amount of pure urea. For urea and 1,8-octandiol, we see only the known **U8** co-crystal phase. However, for urea and 1,10-decandiol, the initial growth of a small amount of an intermediate phase (circled in the figure) is observed, followed by formation of the known **U10** co-crystal phase after *ca*. 1 hour. This observation is the first indication that polymorphism might arise in urea/ α,ω-alkanediol co-crystals. We are currently carrying out wide-ranging experiments to establish the identity and structure of the intermediate phase.

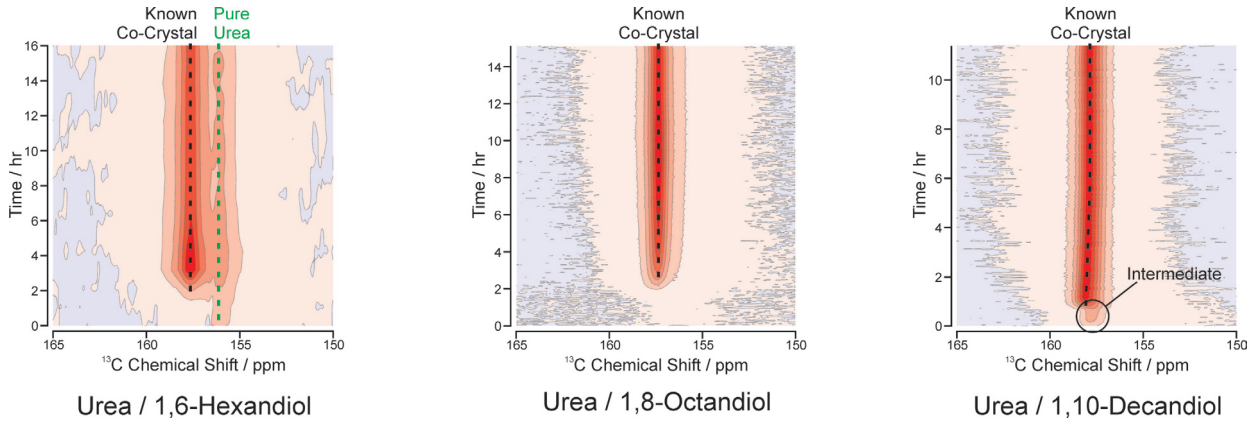

Figure 2. In-situ ^{13}C CPMAS NMR spectra recorded as a function of time during crystallization of three different urea/ α,ω-alkanediol systems. In each case, the final product was the known co-crystal phase (confirmed by powder X-ray diffraction).

Polymorphic evolution of *m*-aminobenzoic acid

We have shown recently that *m*-aminobenzoic acid (*m*-ABA) exhibits a significant degree of polymorphism, with five distinct forms now recognized. Preparing pure samples of the different forms can be challenging due to concomitant crystallization. In particular, forms I, III and IV can all be formed in crystallization from methanol, but it is difficult to control the crystallization so that the less stable forms III and IV are produced. The solid-state ^{13}C NMR spectra of the five polymorphs are distinct, although studies of forms II and V are challenging due to long T_1 values.

Our preliminary *in-situ* solid-state ^{13}C CPMAS NMR spectra recorded during crystallization from a solution of *m*-ABA in methanol show that form I is present in the early stages of crystallization, and then transforms to form III. Improved signal-to-noise is required in order to allow unambiguous assignment of the polymorphs present as a function of time, but these preliminary results give confidence that the 850 MHz facility can yield significant new insights concerning crystallization processes for this complex polymorphic system.

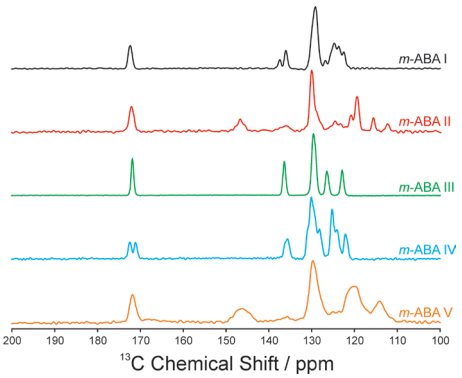

Figure 3. ^{13}C CPMAS NMR spectra of the five polymorphs of m-ABA.

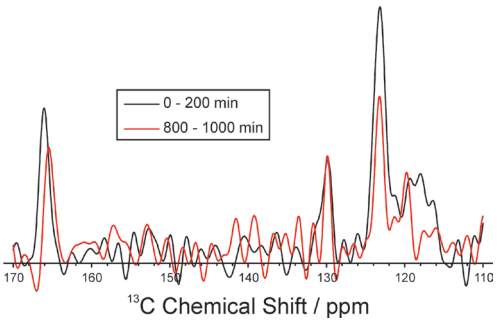

Figure 4. In-situ ^{13}C CPMAS NMR spectra of the early and later products in the crystallization of m-ABA from methanol.

References

1. Hughes, C. E.; Harris, K. D. M. *J. Phys. Chem. A* **2008**, *112*, 6808.
2. Hughes, C.E.; Harris, K.D.M. *Chem. Comm.* **2010**, *46*, 4982.
3. Xu, M.; Harris, K.D.M.; Thomas, J. M.; Vaughan, D.E.W. *ChemPhysChem* **2007**, *8*, 1311.
4. Xu, M.; Harris, K.D.M.; Thomas, J. M. *J. Am. Chem. Soc.* **2008**, *130*, 5880.
5. Martí-Rujas, J.; Kariuki, B. M.; Hughes, C. E.; Morte-Ródenas, A.; Guo, F.; Glavcheva-Laleva, Z.; Taştemür, K.; Ooi, L.; Yeo, L.; Harris, K.D.M. submitted.

^{43}Ca NMR of Substituted Tricalcium Phosphate for Waste Immobilisation

Diane Holland, Ray Dupree, Martin Mee, Andrew Grigg

Department of Physics, University of Warwick

Introduction

The experiment was part of a study of $Ca_3(PO_4)_2$, β-TCP, as an immobilisation host for intermediate-level radioactive waste (ILW). The β-TCP structure contains three phosphorus sites and five calcium sites in a unit cell which is doubled to allow for the half occupancy of the Ca4 site and the ordering of these vacancies on every alternate Ca4 layer. Ca ions have different coordinations to oxygen depending on the site occupied (Table 1) and this determines their likely replacement by waste cations of specific ionic radius. The aim was to identify which of the five Ca sites in β-TCP (Figure 1) are preferentially occupied by the various cations from the waste. Mg^{2+} is a significant component of the waste; Al^{3+} diffuses in from the encapsulating glass; and La^{3+} is a surrogate for plutonium and americium. The sizes of the ions compared with Ca^{2+} in different coordination states are summarised in Table 1.

Table 1. Ionic radii (Å)[1]

cation	CN = 6 Ca4, Ca5	CN = 7 Ca1	CN = 8 Ca2, Ca3
Ca^{2+}	1.0	1.06	1.12
Mg^{2+}	0.72	-	0.89
Al^{3+}	0.535	-	-
La^{3+}	1.032	1.1	1.16

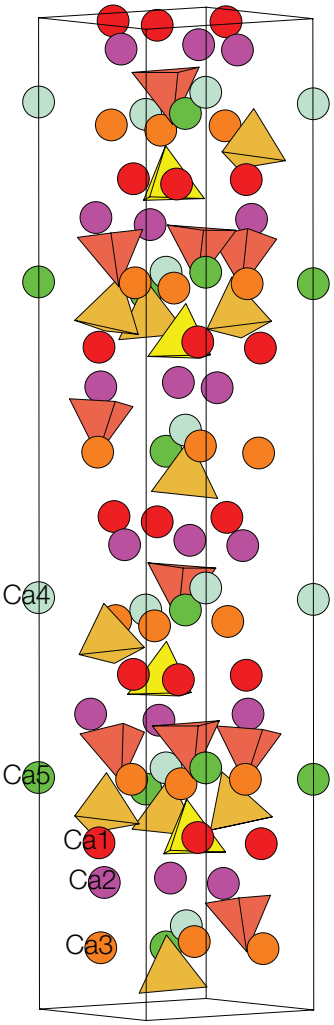

Experimental

Samples were of general formula $Ca_9M_x(PO_4)_{6+x}$ for M^{3+} and $Ca_{3-x}M_x(PO_4)_2$ for M^{2+}. Substitution of M^{3+} for Ca^{2+} leads to the creation of vacancies and the site preference of these also needs to be established. MAS spectra were obtained with a 7 mm-probe and an MAS rate of 5 kHz. Signal enhancement was achieved using RAPT. Spectra were acquired using a 1.5 μs pulse duration, 5 s or 8 s recycle interval and are referenced to 2 M $CaCl_2$ (aq) solution. Owing to the low natural abundance of ^{43}Ca (0.135%), its high spin (7/2) and very low γ (–1.8 10^7 rad $T^{-1}s^{-1}$), the spectra shown took 1.5 days each to acquire.

Figure 1. β-TCP structure showing $[PO_4]^{3-}$ tetrahedra and Ca^{2+} ions. Every alternate layer of Ca4 sites are empty.

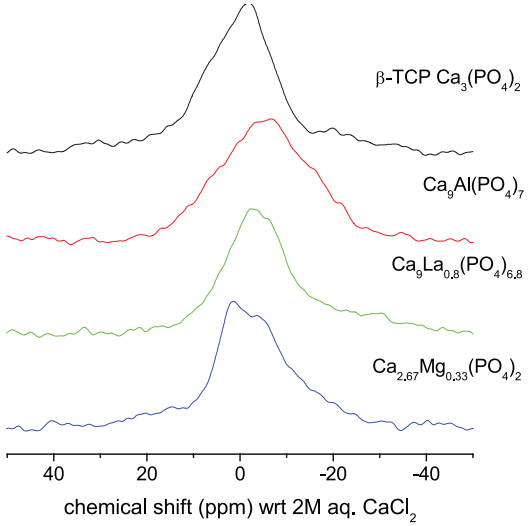

Figure 2. ^{43}Ca spectra of pure and doped TCP.

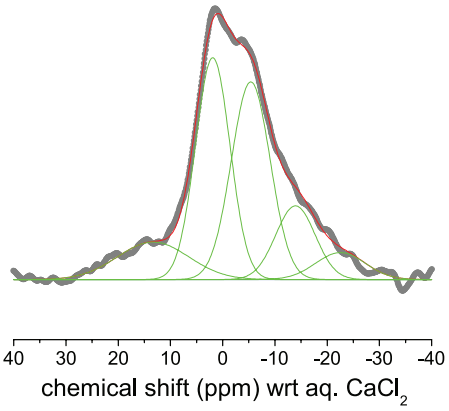

Figure 3. Gaussian fits to the ^{43}Ca spectrum from $Ca_{2.67}Mg_{0.33}(PO_4)_2$.

Results and discussion

The spectra obtained are shown in Figure 2 for the samples studied and a typical fit, using Gaussian lineshapes, is shown in Figure 3. The fitted peaks are assigned to the Ca sites on the basis of the shift/Ca-O distance relation[2]. Site preference is most likely to be determined by the relevant Shannon radii which are shown in Table 1 for the site coordination numbers relevant to this structure.

Conclusions

Natural abundance ^{43}Ca spectra can be obtained from doped TCP to investigate substitution by ILW surrogates. Fitting/simulation of these spectra indicates that La^{3+} goes onto the Ca3 site, Al^{3+} goes onto the Ca5 site and Mg^{2+} goes onto the Ca3 site. The latter is surprising given the smaller ionic radius of Mg^{2+} compared to Ca^{2+} and contradicts information from ^{31}P MAS NMR and X-ray diffraction.

Table 2. Results of fitting of the spectra

Ca site	Ca-O av. distance	$Ca_3(PO_4)_2$		$Ca_9La_{0.8}(PO_4)_{6.8}$		$Ca_9Al(PO_4)_7$		$Ca_{2.67}Mg_{0.33}(PO_4)_2$	
	(Å)	shift (ppm)	% (theory)	shift (ppm)	%	shift (ppm)	%	shift (ppm)	%
5	2.26	15.4 (9)	9 (9.5)	6.3	11	14.7	4	13.3	12
1	2.43	5.5 (30)	30 (28.6)	0.1	30	3.4	32	1.9	34
2	2.48	–1.3 (27)	27 (28.6)	–5.8	31	–5.5	33	–5.3	34
3	2.54	–6.3 (28)	28 (28.6)	–16.4	21	–5.0	29	–13.9	13
4	2.83	–20.5 (6)	6 (4.8)	–32.4	6	–25.5	2	–22.6	6

Acknowledgements

We acknowledge AWE plc and EPSRC for funding.

References

1. Shannon, R. D. *Acta Cryst.* **1976**, *A32*, 751.
2. Gervais, C.; Laurencin, D.; Wong, A.; Pourpoint, .; Labram, J.; Woodward, B.; Howes, A. P.; Pike, K. J.; Dupree, R.; Mauri, F.; Bonhomme, C.; Smith, M. E. *Chem. Phys. Lett.* **2008**, *464*, 42.

NMR Study of Medium Structure in Glasses of the $CaAl_2Si_2O_8$–CaF_2–P_2O_5 System

Natalia Karpukhina,[1] Robert V. Law,[2] Robert G. Hill[1]

[1]Institute of Dentistry, Queen Mary University of London, [2]Department of Chemistry, Imperial College London

Background

Fluoro-phospho-alumino-silicate glasses constitute the basis of acid-degradable ionomer glasses used commercially for producing glass ionomer or polyalkenoate dental cements. The cements form following the acid hydrolysis of the Si-O-Si and Al-O-Si linkages in the glass network which results in the leaching of the Al^{3+} and alkali earth cations for crosslinking the polymeric chains. Presence of phosphorus in the glass composition has a drastic effect on the formation of the cements. This is assumed to be due to the formation of the Al-O-P linkages in the glass that do not hydrolyse immediately. This fluoro-phospho-alumino-silicate system is also of practical interest due to formation of fluoroapatite-anorthite glass ceramics on crystallisation.[1] However, the fraction of the ceramic and the mechanism of nucleation vary depending upon the ratio of Ca/P.

The structural study is presented on glasses with compositions restricted by ternary stoichiometry, anorthite ($CaAl_2Si_2O_8$) – fluorite (CaF_2) – phosphorus pentoxide (P_2O_5) (Figure 1a). This ternary system is used as a model to study the simultaneous presence of F and P in alumino-silicate glasses and the role of both components in the structure of these cation deficient compositions. The aim of the project was to determine presence of the Al-O-P and Al-F linkages in the fluoro-phospho-alumino-silicate glasses using solid-state $^{27}Al/^{31}P$ and $^{27}Al/^{19}F$ double resonance NMR techniques and establish the evolution of these linkages within the compositional variations. Taking into account the high C_Q value (> 5MHz) estimated from the preliminary ^{27}Al NMR single resonance data, the good resolution between three different coordination of the Al species can be beneficially achieved at the very high field.

Establishing the Al-O-P linkages by ^{27}Al–^{31}P double resonance

The double resonance data obtained from both HMQC and REDOR measurements unambiguously showed the presence of the Al-O-P linkages in all of the glasses in the ternary system. The REDOR curves for the variety of glasses are presented in Figure 1b. Qualitatively, glasses in the B series show weaker interaction between the two nuclei mainly due to smaller P_2O_5 content compared to the other compositions. The HMQC spectra, e.g., in Figure 1c for the D6 composition, showed only Al(IV) signal present indicating that it is mainly Al(IV)-O-P linkages. However, absence of the other Al coordinations could be due to the low fraction of the Al(V) and Al(VI) in the glasses in addition to the low resolution of the two-dimensional experiment.

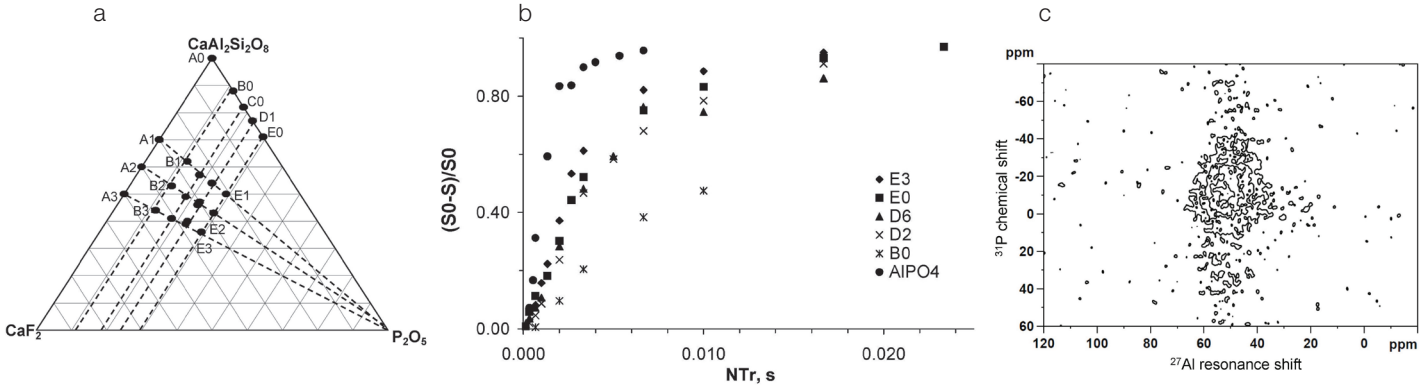

Figure 1. (a) Ternary compositional diagram. (b) $^{27}Al\{^{31}P\}$ REDOR curves obtained for the selected compositions. (c) ^{27}Al-^{31}P HMQC spectrum for the D6 glass composition.

Establishing the Al-F linkages by $^{27}Al–^{19}F$ double resonance

The results of the $^{27}Al\{^{19}F\}$ REDOR measurements indicate the presence of direct Al-F linkages in the glasses. The data in Figure 2 shows that it was possible to distinguish the contribution from the different coordinations of Al at this very high field. However, the difference in the interaction depends on the quadrupolar coupling. The latter was significantly lower for the Al(VI) than for the Al(IV) species.

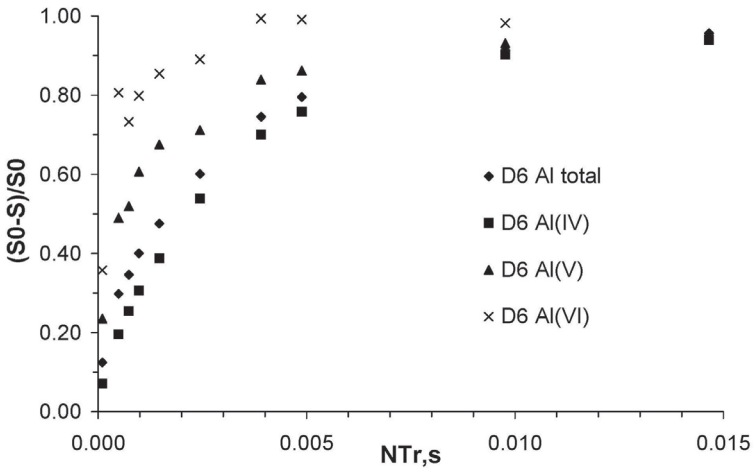

Figure 2. $^{27}Al\{^{19}F\}$ REDOR curves for three coordination environments of Al obtained for the D6 glass compositions.

The obtained results show an excellent correlation with the previously acquired single resonance data and provide with unambiguous proof for existence of Al-O-P and Al-F linkages in the ionomer glasses.

References

1. Clifford, A.; Hill, R.G.; Towler, M.R.; Wood, D.J. *J. Mater. Sci.* **2001**, 36, 3955.

High-Field ^{13}C Solid-State NMR Reveals Glycosaminoglycan-Polypeptide Interactions in Alzheimer's Amyloid Fibrils

Jillian Madine,[1] Maya Pandya,[2] Sheena Radford[2] and David Middleton[1]

[1]*Institute of Integrative Biology, University of Liverpool,* [2]*Astbury Centre for Structural Molecular Biology, University of Leeds.*

Overview

A small number of proteins and peptides are currently known to assemble into amyloid fibrils that are the pathological hallmark of human disease. The relationship between the structural and toxicological properties of amyloid fibrils, a question that is central to our understanding of misfolding diseases, remains unresolved. Equally important, yet completely unexplored at a structural level, is how fibril assembly is modulated by factors ubiquitously associated with amyloid *in vivo*, including other associated proteins, nucleic acids and oligosaccharides including glycosaminoglycans (GAGs). The presence of factors such as GAGs during aggregation profoundly influences the growth rate, gross morphology and toxicity of amyloid fibrils.[1] The molecular details behind these observations are entirely unknown, principally because detailed atomistic studies of amyloid fibrils to date have focused on material formed from pure peptides/proteins in isolation of their natural biological ligands under non-physiological, conditions. Here high-field ^{13}C solid-state NMR is used to examine, for the first time, the molecular sites of interaction between the GAG and polypeptide components of amyloid fibrils. The work focuses on fibrils formed by the polypeptide $A\beta_{1\text{-}40}$ famously associated with Alzheimer's disease.

GAGs associate with $A\beta_{1\text{-}40}$ during and after fibril assembly

Low molecular weight (6 kDa) heparin (LMWH) was identified as a biologically relevant and experimentally tractable GAG analogue which binds to $A\beta_{1\text{-}40}$, affects the rate of aggregation and alters the morphology of the fibril deposits compared to $A\beta_{1\text{-}40}$ in isolation (Figure 1a). Biochemical analysis reveals that LMWH binds to $A\beta_{1\text{-}40}$ during the fibril assembly process; interestingly, LMWH also binds in equal measure to the mature, fully formed fibrils (Figure 1b). These results imply that LMWH associates with $A\beta_{1\text{-}40}$ at sites constituting the external face of the mature fibrils or protofilaments. SSNMR could in principle pinpoint which amino acid residues are involved in the association with GAGs by reporting on selective changes in ^{13}C frequencies for uniformly ^{13}C labelled $A\beta_{1\text{-}40}$. Initial dipolar assisted rotational resonance (DARR) SSNMR measurements on LMWH/$A\beta_{1\text{-}40}$ fibrils using the in-house 400 MHz instrument in Liverpool were inconclusive owing to low resolution and sensitivity. Further experiments were therefore conducted at 850 MHz.

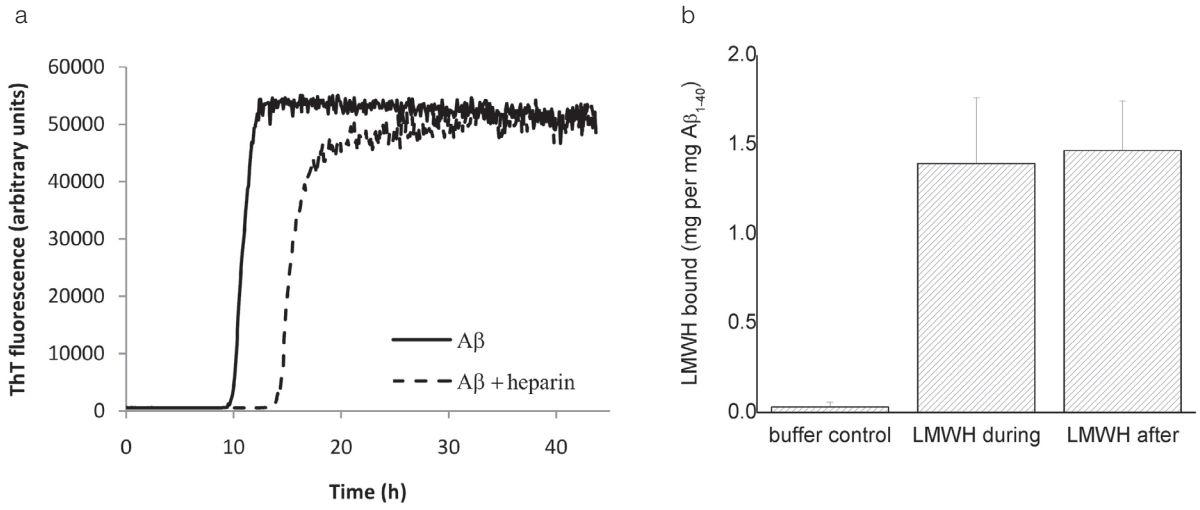

Figure 1. (a) Effect of LMWH on the rate of $A\beta_{1\text{-}40}$ aggregation, assessed by thioflavin T fluorescence. (b) Association of LMWH with $A\beta_{1\text{-}40}$ during fibril growth and with the mature fibrils, as determined by a heparinase functional assay

Sites of GAG-A$\beta_{1\text{-}40}$ interactions

Depending on the growth conditions, A$\beta_{1\text{-}40}$ fibrils can assume different morphologies which have been traced to the level of packing and structure of the A$\beta_{1\text{-}40}$ molecules.[2] Specific, homogeneous fibril species can be propagated by seeding with pre-formed fibrils of the required morphology.[2] Here, fibrils corresponding to the 3-fold symmetry packing structure[3] were selected by addition of the appropriate seed (kindly provided by Dr R. Tycko). The excellent resolution and sensitivity of the high-field DARR spectra of seeded A$\beta_{1\text{-}40}$ fibrils permitted approximately 70 % of the spectrum to be assigned with reference to the chemical shift values previously tabulated[3-4] (Figure 2a). Fibrils grown without seeding were highly heterogeneous and spectra were too broad to yield useful information (data not presented). Comparison of the DARR spectra for fully-formed A$\beta_{1\text{-}40}$ fibrils before and after the addition of LMWH reveals movements and/or changes in intensity of several of the peaks after adding the GAG (Figure 2b). Similar trends are seen for fibrils grown in the presence of LMWH (data not presented). Mapping the chemical shift changes onto the current structural model indicates that the greatest perturbations correspond to the putative loop regions and, notably, the salt bridge between D23 and K28 side-groups.

Further work is underway to map the GAG-polypeptide interface in greater detail by measuring intermolecular couplings between ^{13}C labelled A$\beta_{1\text{-}40}$ and novel heparin analogues substituted with ^{13}C, ^{2}H and ^{19}F labelled acetyl groups.[5]

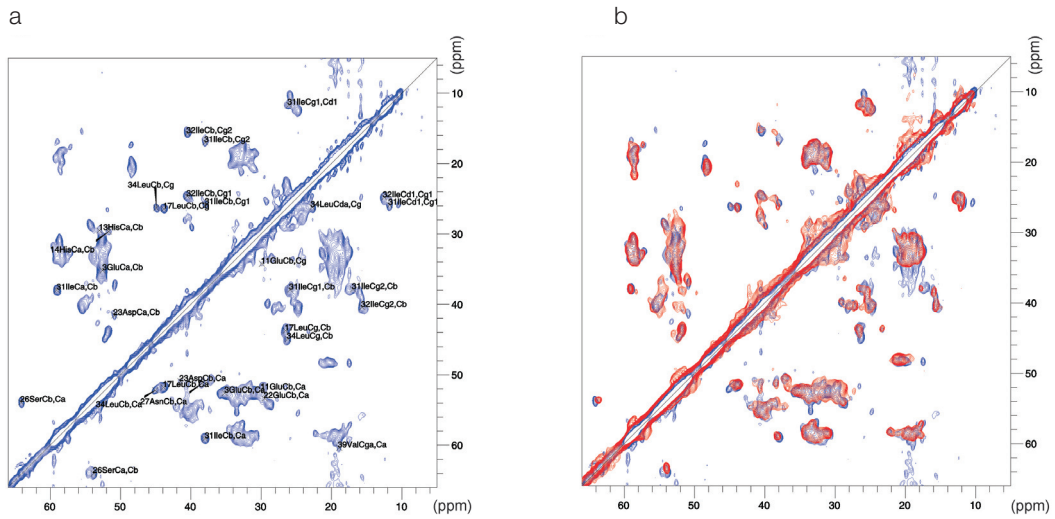

Figure 2. (a) ^{13}C DARR spectrum for seeded A$\beta_{1\text{-}40}$ fibrils with peaks assigned so far labelled. (b) Superposition of DARR spectra for seeded A$\beta_{1\text{-}40}$ fibrils before (blue) and after (red) addition of LWMH.

References

1. Alexandrescu, A. T. *Protein Sci.* **2005**, *14*, 1-12.
2. Petkova, A. T.; Leapman, R. D.; Guo, Z. H.; Yau, W. M.; Mattson, M. P.; Tycko, R. *Science* **2005**, *307*, 262-265.
3. Paravastu, A. K.; Leapman, R. D.; Yau, W. M.; Tycko, R. *Proc. Natl. Acad. Sci. USA* **2008**, *105*.
4. Petkova, A. T.; Yau, W. M.; Tycko, R. *Biochemistry* **2006**, *45*, 498-512.
5. Madine, J.; Clayton, J. C.; Yates, E. A.; Middleton, D. A. *Organic & Biomolecular Chemistry* **2009**, *7*, 2414-2420.

^{17}O Solid-State NMR of Ionothermally-Prepared $AlPO_4$ Zeolites

Valerie R. Seymour, John M. Griffin, Daniel M. Dawson, Sharon E. Ashbrook and Russell E. Morris

School of Chemistry and EaStCHEM, University of St Andrews

Overview

Zeolites, including aluminosilicates and aluminophosphates (AlPOs), are an important class of microporous materials with applications in medicine, catalysis, separation and ion exchange. Zeolites consist of frameworks containing pores and channels of molecular dimensions, allowing chemistry to take place at their internal surface and giving rise to many useful properties. Solid-state NMR is a valuable tool for studying such materials, as the basic constituents of their frameworks are NMR-active nuclei: ^{29}Si, ^{27}Al ^{31}P and ^{17}O. Whilst many of these nuclei are commonly studied, the exception is ^{17}O, for which there are few studies on framework materials. This is unfortunate as oxygen atoms line the internal surface of zeolites, and it is here that the interesting chemistry occurs. Studying the local environment of oxygen nuclei can, therefore, yield important information relating to the function and applications of zeolites.

There are several reasons why ^{17}O NMR has been poorly exploited for the study of microporous materials. It has a low natural abundance (0.037%) and high spin quantum number (I = 5/2), meaning that more complex two-dimensional NMR experiments such as MQMAS[1] are required to obtain high-resolution spectra. Although financially costly, zeolites may be enriched using either ^{17}O-enriched O_2 or H_2O.[2] Enrichment levels obtained using post-synthetic approaches are often low. This difficulty in enrichment with ^{17}O is a major obstacle to full characterisation of zeolites by NMR. Since the synthesis of zeolites involves hydrolysis, the use of ^{17}O-enriched H_2O in the synthesis medium increases enrichment considerably. However, the large excess of water required for hydrothermal synthesis makes this approach prohibitively costly. In recent years we have developed the use of ionic liquids in the synthesis of zeolites.[3] This approach has produced new zeotypes, analogues of catalysts already used in industry, *e.g.*, CHA, (SIZ-4) and AEL (SIZ-3), as well as other zeolite-related materials with unusual chemical features. In the context of ^{17}O-enrichment during synthesis, the ionothermal method has the advantage of providing a higher degree of control over water as a reagent than the hydrothermal route, where water is present in excess.

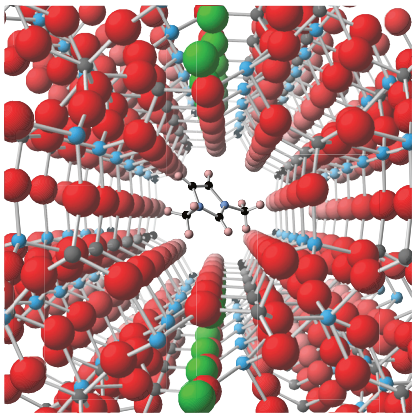

Figure 1. A template molecule within an AlPO pore.

We aimed to investigate the use of ^{17}O NMR to study ionothermally prepared zeotypes. Where crystal structures are known, experimentally-measured NMR parameters have been compared with those calculated by density functional theory (DFT) using the *ab initio* CASTEP code.

Results

Over two visits to the Facility, we acquired ^{17}O NMR spectra of ^{17}O-enriched samples of SIZ-3 (AEL framework containing methyl-ethyl imidazolium) and calcined SIZ-4 (CHA framework with vacant pores). ^{17}O MAS NMR spectra recorded at 14.1 T and 20.0 T confirm enrichment in ^{17}O and demonstrate the sensitivity gain and line-narrowing effect of the high magnetic field (Figures 2 and 3). Template disorder in SIZ-3 means that a crystal structure is unavailable. However, the obtained spectra show broad agreement with DFT calculations performed on other templated AlPOs, which predict ^{17}O quadrupolar coupling (C_Q) values of between 5 and 7 MHz. C_Q values of this magnitude require relatively fast MAS and, correspondingly, relatively small sample volumes. This, together with the moderate gyromagnetic ratio of ^{17}O ($\omega_0/2\pi$ = 115.2 MHz at 20.0 T), hinders sensitivity. The use of higher fields mitigates this by increasing sensitivity and narrowing second-order-broadened quadrupolar lineshapes. Indeed, we obtained a ^{17}O MQMAS NMR spectrum of templated SIZ-3 at 20.0 T in 7 days using a 2.5 mm probe. This spectrum separates resonances in the indirect dimension, revealing four distinct groups of sites. However, template disorder means that individual sites are unresolved.

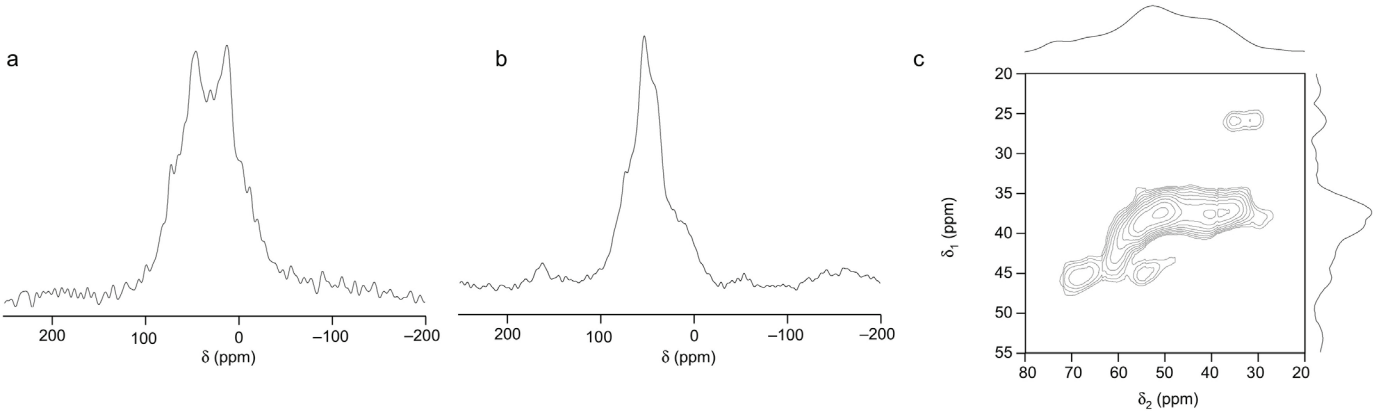

Figure 2. ^{17}O MAS NMR spectra of templated SIZ-3 recorded at (a) 14.1 T and (b) 20.0 T. (c) A ^{17}O MQMAS NMR spectrum of templated SIZ-3 recorded at 20.0 T. Experimental acquisition times were (a, b) 15 hours and (c) 7 days.

From the crystal structure of calcined SIZ-4, four ^{17}O resonances are expected. While resolution afforded in the indirect dimension of the 3QMAS NMR spectrum acquired (with an acquisition time of just 22 hours) would have been insufficient fully to resolve these sites, only a single lineshape is observed. As the spectrum is inconsistent with DFT results, further characterization of the sample is now required.

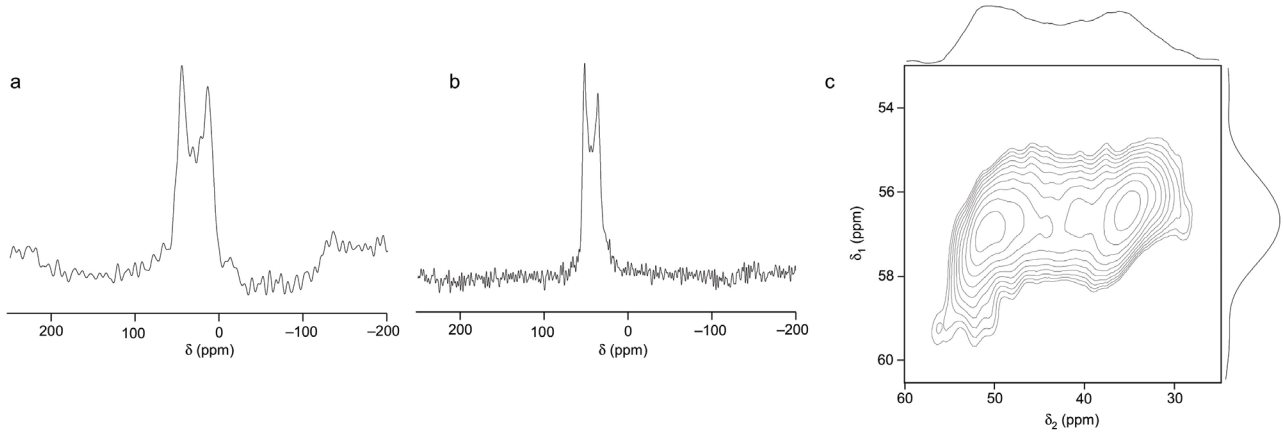

Figure 3. ^{17}O MAS NMR spectra of calcined SIZ-4 recorded at (a) 14.1 T and (b) 20.0 T. (c) A ^{17}O MQMAS NMR spectrum of calcined SIZ-4 recorded at 20.0 T. Experimental acquisition times were (a, b) 1.5 hours and (c) 22 hours.

References

1. Frydman, L.; Harwood, J. S. *J. Am. Chem. Soc.* **1995**, *117*, 5367.

2. Readman, J. E.; Grey, C. P.; Ziliox, M.; Bull, L. M.; Samoson, A. *Solid State Nucl. Magn. Reson.* **2004**, *26*, 153.

3. Cooper, E. R.; Andrews, C. D.; Wheatley, P. S.; Webb, P. B.; Wormald, P.; Morris, R. E. *Nature* **2004**, *430*, 1012.

High-Field ^{87}Sr Solid-State NMR for the Characterization of Inorganic and Hybrid Materials

Christian Bonhomme,[1] Danielle Laurencin,[2] John V. Hanna[3] and Mark E. Smith[4]

[1]LCMCP UMR CNRS 7574, University Paris 06, France, [2]Institut Charles Gerhardt de Montpellier, France, [3]Department of Physics, University of Warwick

Overview

Hydroxyapatite derived materials and bioactive glasses are of paramount importance in the field of bone tissue regeneration. In particular, anionic and/or cationic substituted HAp are of great interest in biomaterials science. Recently, it has been suggested that *strontium* is an important element to incorporate in biomaterials and apatites, because of its antiosteoporotic properties. Very few techniques are available to characterize the local structure around this ion. The goal of this work is to characterize Sr local environments in inorganic and hybrid biomaterials using solid state NMR. Strontium-87 is characterised by a strong nuclear quadrupole moment (~ 8 times higher than that of ^{43}Ca), a low γ (36.8 MHz at 19.9 T) and a moderate natural abundance (7.0%). The use of very high magnetic field is clearly necessary in order to reduce second-order quadrupolar effects.[1] The NMR spectra of a series of crystalline samples were recorded, as detailed below. Moreover, GIPAW calculations[2] (using CASTEP and the "on the fly" pseudopotential for Sr) were systematically performed for a large number of Sr derivatives ($SrCl_2$, $SrCl_2$, SrO, $SrCO_3$, $Sr(NO_3)_2$, $SrSO_4$, SrP_2O_6, $Sr_2P_2O_7$, $SrHPO_4$, SrS, Sr malonate, Sr phosphonate and $Sr_{10}(PO_4)_6(OH)_2$). GIPAW calculations were not only used for the validation of the Sr pseudopotential but also for the safe prediction of quadrupolar parameters. Such predictions are crucial for the implementation of the ^{87}Sr DFS-QCPMG-VOCS experiments, which can be time-consuming.

Standard samples and validation of ^{87}Sr GIPAW calculations

In Figure 1, ^{87}Sr NMR data of compounds with increasing C_Q ((a) → (c)) are presented. As expected from the reported cubic structure, SrS exhibits a very small C_Q (Figure 1a: MAS, 4mm, $\delta_{iso.}$ = 322 ± 1 ppm). Strontianite, $SrCO_3$ is characterized by: $\delta_{iso.}$ = 0 ± 5 ppm, C_Q = 8.5 ± 0.3 MHz, η_Q ~ 0 (Figure 1b: DFS static echo, 7 mm). $Sr(NO_3)_2$ is characterized by: $\delta_{iso.}$ = –75 ± 5 ppm, C_Q = 15.3 ± 0.3 MHz, η_Q ~ 0 (Figure 1(c): DFS-QCPMG, 7 mm). MAS spectra (4 mm) were also recorded for SrB_6, with C_Q ~ 0 (as expected from the crystallographic structure). A sharp line at $\delta_{iso.}$ = 95 ± 3 ppm is observed, as well as a small quadrupolar distribution (data not shown). These results show that: (i) the ^{87}Sr chemical shift range is limited to several hundreds of ppm, for a very large variety of Sr chemical environments, which is quite unusual as ^{87}Sr can be considered as a heavy nucleus. (ii) SrS and SrB_6 exhibit the most deshielded resonances when compared to all ^{87}Sr data already published in the literature. Points (i) and (ii) are in full agreement with our preliminary ^{87}Sr GIPAW calculations. Moreover, GIPAW C_Q values show correct trends when compared to experimental ones (0.00, 5.66 and –19.5 MHz for SrS, $SrCO_3$ and $Sr(NO_3)_2$, respectively).

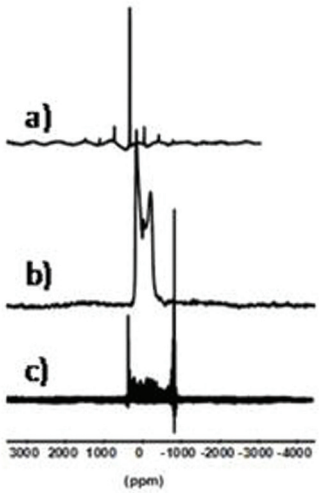

Figure 1. ^{87}Sr spectra of (a) SrS (MAS), (b) $SrCO_3$ (static) and (c)$Sr(NO_3)_2$ (static).

Predictions of C_Q parameters for α-SrP_2O_6

In the case of α-SrP_2O_6 (for crystallographic sites), ^{87}Sr GIPAW calculations give: C_Q = 32.9, 35.5, 35.6 and 40.7 MHz (η_Q ranging from 0.08 to 0.62). Starting from these predictions, the expected static line width can be estimated as ~ 370 kHz. It follows that a *variable offset* QCPMG experiment is necessary in order to recover undistorted lineshapes. The corresponding ^{87}Sr spectrum is presented in Figure 2. The spectral extension of the central transitions is about 350 kHz, in very good agreement with the experiment. One notes that partial excitation of the satellite transitions is effective.[3] It seems difficult to analyse the spectrum as four crystallographic sites are involved. In a very near future, the spectrum will be recorded with a much smaller frequency interval between the QCPMG spikelets, in order to recover all the discontinuities of the lineshape.

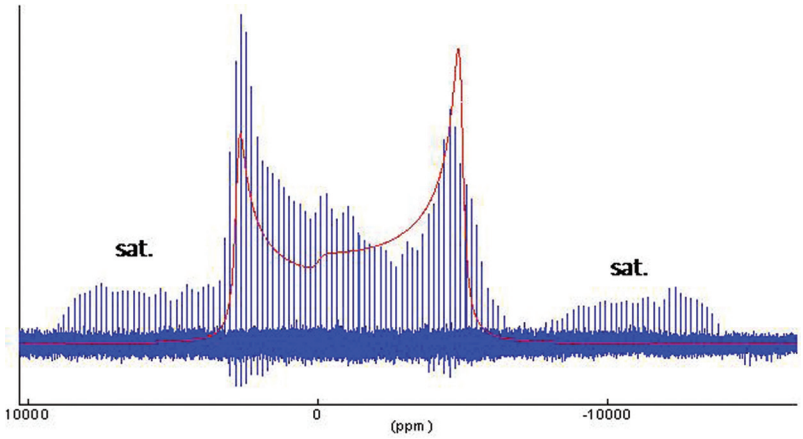

Figure 2. ^{87}Sr DFS-QCPMG-VOCS of α-SrP_2O_6. The simulation (in red) corresponds to a unique crystallographic site with: C_Q = 38.0 MHz, η_Q = 0.0.

^{87}Sr study of Sr malonate

The ^{87}Sr static NMR spectrum of Sr malonate ($Sr(C_3H_2O_4)$) is presented in Figure 3. It corresponds to a labelled sample (90% in ^{87}Sr – starting material: commercial strontianite, $SrCO_3$). The combination of very high field and labelling allowed for a very precise description of the quadrupolar lineshape, in a reasonable amount of time. GIPAW calculations (corresponding to a relaxed Sr malonate structure in VASP) lead to: C_Q = –28.1 MHz, η_Q = 0.97. Again, the calculated data are in very good agreement with the experimental ones. It demonstrates unambiguously that the GIPAW approach is suitable not only for inorganic Sr derived phases, but also for hybrid compounds.

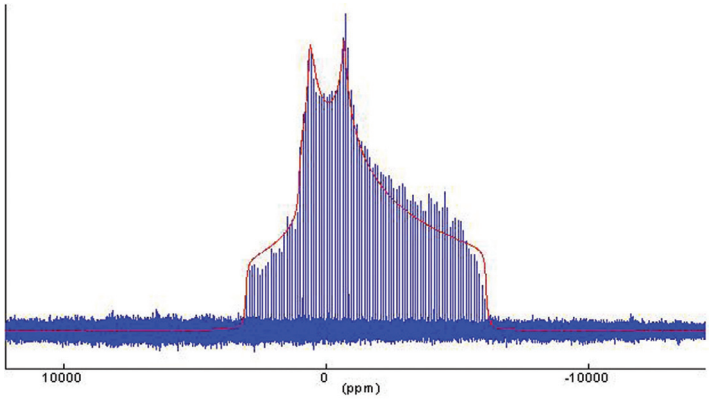

Figure 3. ^{87}Sr DFS-QCPMG-VOCS of Sr malonate. The simulation (in red) corresponds to a unique crystallographic site with: C_Q = 31.5 MHz, η_Q = 0.8.

References

1. Bowers, G. M.; Lipton, A. S.; Mueller, K. T. *Solid State Nucl. Magn. Reson.* **2006**, 29, 95.
2. Gervais, C.; Laurencin, D.; Wong, A.; Pourpoint, F.; Labram, J.; Woodward, B.; Howes, A. P.; Pike, K. J.; Dupree, R.; Mauri, F.; Bonhomme, C.; Smith, M. E. *Chem. Phys. Lett.* **2008**, 464, 42.
3. Hamaed, H.; Laschuk, M. W.; Terskikh, V. V.; Schurko, R. W. *J. Am. Chem. Soc*. **2009**, 131, 8271.

High-Field ^{43}Ca Solid-State NMR for the Characterization of Biomaterials

Danielle Laurencin,[1] Dong Qiu,[2] Christian Bonhomme[3] and Mark E. Smith[4]

[1]Institut Charles Gerhardt de Montpellier, France, [2]Institute of Chemistry, Chinese Academy of Sciences, Beijing 100190, China, [3]LCMCP UMR CNRS 7574, University Paris 06, France, [4]Department of Physics, University of Warwick

Overview

Calcium is one of the key elements present in implant materials which are used for bone substitution, such as bioactive glasses. Indeed, its presence has been found to be essential for the formation of new bone. However, the *in vitro* performance and dissolution properties of bioactive glasses strongly rely on their composition and structure, and it thus appears crucial to analyze their structural features in detail, and in particular to investigate the local environment of calcium.

In this context, ^{43}Ca solid-state NMR has been shown to be a particularly powerful technique to analyze Ca local environments.[1,2] However, ^{43}Ca solid-state NMR is challenging, because it is a "low-gamma" nucleus with very low natural abundance (~0.14%). Fortunately, significant progress has been made in the past few years, both from the point of view of instrumental advances (e.g., access to higher magnetic fields, large-volume magic-angle spinning (MAS) probes), and new pulse sequences (enhancement sequences for quadrupolar nuclei via population transfer),[3] which has rendered ^{43}Ca NMR more accessible. Here, we show how natural abundance ^{43}Ca NMR spectra recorded at 20 T can be used to characterize different biomaterials, and in particular a calcium phosphosilicate bioglass of low calcium content (~7%wt Ca).[4]

Optimization of the signal enhancement conditions using ^{43}Ca-labelled monetite ($CaHPO_4$)

Given the difficulties of natural abundance ^{43}Ca experiments, signal enhancement schemes like FSG-RAPT have been developed. These were tested and optimized at 20 T on the signal of a ^{43}Ca-enriched calcium phosphate, monetite, a constituent of certain cements used for tissue repair. As shown in Figure 1, there is a significant increase in signal-to-noise on using the enhancement sequence, which will be particularly valuable in view of experiments on the non-enriched samples.

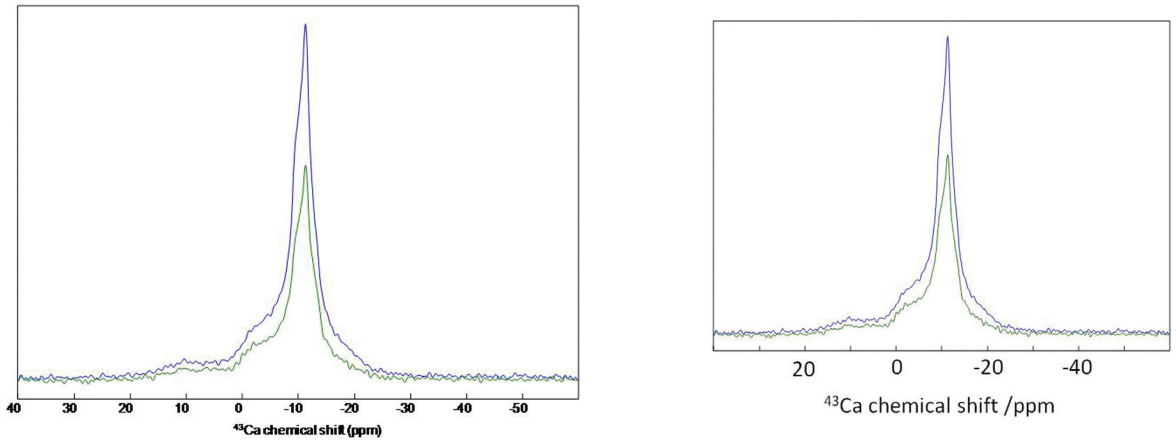

Figure 1. ^{43}Ca MAS (20 T) NMR spectrum of monetite with (blue) and without (green) the FSG-RAPT enhancement scheme.

Natural abundance ^{43}Ca NMR spectra of a calcium phosphosilicate bioglass

The ^{43}Ca MAS NMR spectrum of a calcium phosphosilicate bioglass (noted SG1-120°C) was recorded and compared to those of hydroxyapatite ($Ca_{10}(PO_4)_6(OH)_2$) and pseudowollastonite ($CaSiO_3$), in order to gain insight into the calcium local environment. As shown in Figure 2, NMR shows that the calcium environments in these three materials differ: the ^{43}Ca NMR signal observed for SG-1 (after heat treatment at 350 °C) is at a significantly different chemical shift position than for the two model samples. Further information can be derived from the ^{43}Ca NMR spectrum of SG-1: the ^{43}Ca NMR signal of SG-1 appears in the range expected for calcium phosphates/silicates,[1] but the peak is fairly narrow, which is rather surprising given the amorphous nature of these glasses. It is possible that other calcium local environments are also present in the bioglass sample, leading to a chemical shift distribution that is not visible in the ^{43}Ca NMR spectrum recorded at natural abundance, despite having acquired the data for over 14 hours at a very high magnetic field. Synthesis using expensive ^{43}Ca-labelled precursors would probably be necessary to confirm this point.

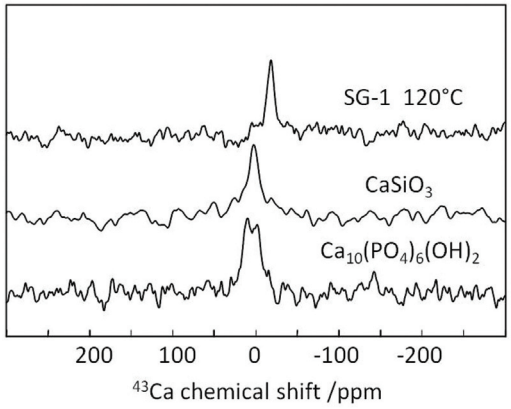

Figure 2. Natural abundance ^{43}Ca MAS NMR spectra of hydroxyapatite ($Ca_{10}(PO_4)_6(OH)_2$), pseudowollastonite ($CaSiO_3$), and a calcium phosphosilicate bioglass (SG1-120°C), recorded at 20 T, using the FSG-RAPT enhancement scheme.

References

1. Gervais, C.; Laurencin, D.; Wong, A.; Pourpoint, F.; Labram, J.; Woodward, B.; Howes, A. P.; Pike, K. J.; Dupree, R.; Mauri, F.; Bonhomme, C.; Smith, M. E. *Chem. Phys. Lett.* **2008**, 464, 42.
2. Bryce, D. *Dalton Trans.* **2010**, 8593.
3. Siegel, R.; Nakashima, T. T.; Wasylishen, R.E. *Concepts Magn. Reson. A* **2005**, 26A, 47.
4. Li, A.; Wang, D.; Xiang, J.; Newport, R. J.; Reinholdt, M. X.; Mutin, P. H.; Vantelon, D.; Bonhomme,C.; Smith, M. E.; Laurencin, D.; Qiu D. submitted to *Acta Biomaterialia*.

Studying Hydrogen Bonds by Solid-State NMR: Recoupling Proton-Oxygen-17 Dipolar Interactions

David Bennett and Jeremy Titman

School of Chemistry, University of Nottingham

Introduction

Hydrogen bonding plays a critical role in molecular self assembly, particularly in biological systems. Recently, Brinkmann and Kentgens have described a novel solid-state NMR approach to the measurement of ^{1}H–^{17}O internuclear distances in hydrogen bonds.[1] The method involves sequences of rotor-synchronized rf pulses designed to reintroduce the MAS-averaged dipolar interactions between protons and quadrupolar nuclei. These sequences can be incorporated into a selective spin-echo experiment, as shown in Figure 1, where the ^{17}O rf pulses are selective for the central transition. If necessary, coherence associated with the central transition can be enhanced prior to the spin echo using a method such as a double frequency sweep (DFS). During the echo time a heteronuclear recoupling sequence is applied on the proton channel for a period τ. The recoupling is suspended while a frequency-selective proton π pulse is applied at the midpoint of the spin echo. As a consequence ^{17}O magnetization is modulated solely by the heteronuclear dipolar interaction to the selected proton during τ. The ^{17}O dephasing curve which results can be used to extract the heteronuclear dipolar coupling and hence the internuclear distance. Brinkmann and Kentgens demonstrated this experiment using a supercycled $SR4_1^2$ recoupling sequence in order to measure the medium range distance (170 pm) associated with the ^{1}H"–$^{17}O^{\eta}$ (carboxylic acid proton – hydroxyl oxygen) hydrogen bond in $^{17}O^{\eta}$ enriched tyrosine.

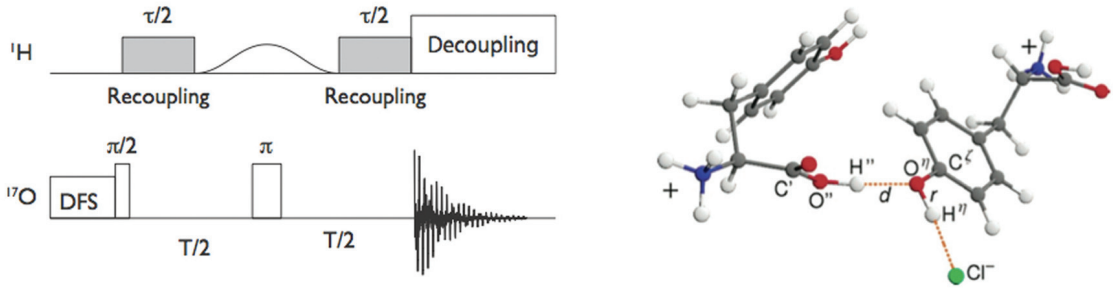

Figure 1. Pulse sequence (left) for selectively measuring heteronuclear dipolar couplings between protons and ^{17}O nuclei and tyrosine molecular structure (right) by neutron diffraction.

New recoupling sequences

Recoupling sequences which are suitable for measuring ^{1}H–^{17}O distances must fulfil certain criteria. Firstly, the pulse sequence symmetry must ensure that proton shift anisotropies and homonuclear dipolar couplings are not reintroduced. Secondly, weak heteronuclear couplings must be measured in the presence of strong ones which implies that the recoupled heteronuclear interactions must commute with each other. Finally, to simplify the design of the sequence, rf pulses are only applied to the protons because the spin dynamics of quadrupolar nuclei are more difficult to predict.

Using SIMPSON[3] simulations of the ^{17}O dephasing curve a number of symmetries were identified which satisfied these criteria and which had not been previously investigated by Brinkmann and Kentgens.[2] Of these a subset of γ-encoded[4] R sequences[5] gave a clean oscillatory dephasing curve under ideal conditions but suffered from poor compensation for B_1 inhomogeneity. This suggested a strategy for the design of new R sequences incorporating composite pulses to provide this compensation, rather than the supercycling approach of Brinkmann and Kentgens. The performance of a number of these new composite R sequences was tested using a (simpler) non-selective variant of the experiment in Figure 1 on 20% ^{17}O- enriched tyrosine. For a non-selective experiment the dephasing curve is dominated by the effect of the large $^1H^{\eta}$–$^{17}O^{\eta}$ (hydroxyl proton – hydroxyl oxygen) dipolar coupling. For example, Figure 2 shows the experimental dephasing curve (blue circles) obtained using a $R10_3^9$ sequence with $180_{104.5}360_{313.4}180_{104.5}180_0$ composite R elements.[6] In order to accommodate the long duration of the individual R elements and to preserve the required symmetry these experiments were carried out at a relatively slow MAS rate of 30 kHz. Note the oscillatory dephasing behaviour which results in negative ^{17}O intensity around 500 μs.

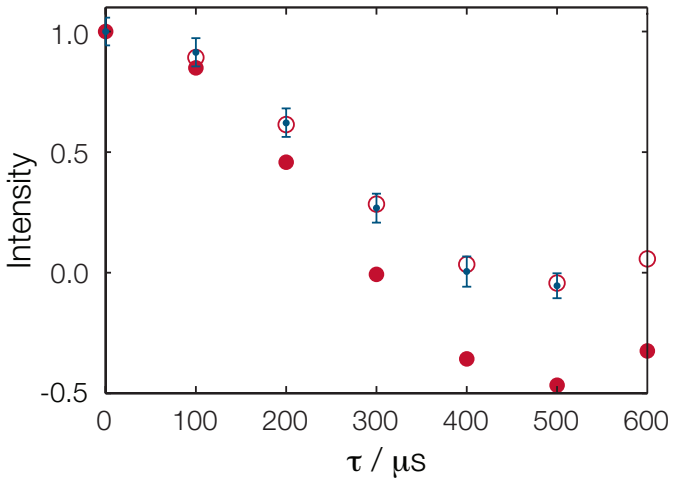

Figure 2. Comparison between experimental and simulated ^{17}O peak intensities as a function of recoupling time τ obtained for 20% ^{17}O- enriched tyrosine with a non-selective variant of the experiment in Figure 1. The experiments (small blue circles) were carried out at the UK High-field Solid-state NMR Facility (^{17}O Larmor frequency 115.3 MHz) using a $R10_3^9$ sequence with the R elements constructed from $180_{104.5}360_{313.4}180_{104.5}180_0$ composite pulses. SIMPSON simulations carried out under ideal conditions (filled red circles) were damped with a simple exponential function to produce the best-fit dephasing curve (open red circles) as described in the text. In this case the best-fit curve corresponds to a ^1H – ^{17}O dipolar coupling constant of 15.61 ± 0.47 kHz.

Following Brinkmann and Kentgens,[2] the dephasing curve simulated under ideal conditions (filled red circles) was damped with a simple exponential function in order to take account of experimental imperfections such as B_1 inhomogeneity. The ^1H–^{17}O dipolar coupling constant and the time constant for the damping function were allowed to vary in a least squares fit to the experimental data. The best fit simulated dephasing curve (open red circles) gave a ^1H–^{17}O dipolar coupling constant of 15.61 ± 0.47 kHz corresponding to an internuclear distance of 101.4 ± 0.9 pm. This value is close to that expected from the neutron structure, but the NMR measurement underestimates the neutron distance by about 3 %. This scale of discrepancy has been explained previously[7] by the librational motion of (in this case) the O–H bond.

References

1. Brinkmann, A.; Kentgens, A. P. M. *J. Am. Chem. Soc.* **2006**, *128,* 14758.
2. Brinkmann, A.; Kentgens, A. P. M. *J. Phys. Chem. B* **2006**, *110*, 16089.
3. Bak, M.; Rasmussen, T. J.; Nielsen, N. C. *J. Magn. Reson.* **2000**, *147*, 296.
4. Lee, Y. K.; Kurur, N. D.; Helmle, M.; Johannesen, O.; Nielsen N. C.; Levitt, M. H. *Chem. Phys. Lett.* **1995**, *242*, 304.
5. Carravetta, M.; Edén, M.; Zhao, X.; Brinkmann A.; Levitt, M. H. *Chem. Phys. Lett.* **2000**, *321*, 205.
6. Wimperis, S. *J. Magn. Reson. Ser. A* **1994**, *109*, 221.
7. Ishii, Y.; Terao, T.; Hayashi, S. *J. Chem. Phys.* **1997**, *107*, 2760.

Understanding the Role of Serum Amyloid P Component in the Stabilization of Amyloid Deposits

Garrick F. Taylor[1], Joern M. Werner[1], Stephen P. Wood[2], Philip T. F. Williamson[1]

[1]School of Biological Sciences, University of Southampton, [2]Centre for Amyloidosis and Acute Phase Protein, Division of Medicine, University College London Medical School.

Overview

Amyloidosis is a family of pathological condition characterised by the formation of insoluble deposits that lead to the disruption of local tissue. The formation of these deposits has been linked to the mis-folding of normally soluble proteins that results in the formation of large fibrillar structures. Over 20 such diseases have been identified and are linked to a number of socio-economically relevant diseases including Alzheimer's disease, Parkinson's disease, reactive systemic amyloidosis and dialysis related amyloidosis.[1] These serious and often fatal diseases have proved difficult to treat frequently organ transplantation or the use of extremely toxic and dangerous drugs. Although each of these diseases are characterised by the mis-folding of a particular protein, common to all amyloid deposits irrespective to the type of disease is the presence of the protein serum amyloid-P component (SAP). *In-vivo* the binding of SAP is thought to stabilize the fibrillar structures found in these amyloid deposits inhibiting the host's ability to clear them. Accordingly, SAP represents an attractive target for therapeutic intervention, with application across a broad spectrum of amyloid disease.[2] Despite this the development of drugs that inhibit the binding of SAP to amyloid fibrils is challenging as although high-resolution crystal structures are readily available for the soluble SAP,[3] structural studies of amyloid fibrils and their interactions with other partners found *in-vivo* has been hindered by the intractability of these systems to modern methods in structure biology. However, utilizing high-magnetic fields together with NMR probes optimized to work with challenging biological samples we have been able to obtain well-resolved spectra of fibrils composed of β_2-microglobulin which are typically found in patients suffering from dialysis related amyloidosis. Changes in the spectra observed upon the binding of SAP are providing valuable insights at a molecular level into the recognition of amyloid fibrils by SAP.

Interaction of β_2-microglobulin fibrils with SAP

Solid-state NMR studies are being conducted on fibrils composed of β_2-microglobulin in the presence and absence of SAP. To maintain the integrity of the complex and ensure that the proteins remain stable it has proved necessary to perform NMR studies under near physiological conditions (neutral pH, high salt). Typically such studies are experimentally challenging as the high salt reduces the efficiency of the NMR probes. However, utilizing the E-free probe installed on the 850 MHz spectrometer we have been able to obtain good quality ^{13}C-^{13}C homo-nuclear correlation spectra of the β_2-microglobulin fibrils with (Figure 1, red) and without SAP (Figure 1, black). Despite the size of the protein (99 residues) many sites are resolved with linewidths of some residues approaching ~0.5 ppm. This indicates that within the fibrils the β_2-microglobulin is relatively structurally homogeneous. On the basis of their characteristic chemical shifts and correlation patterns many of the resonances can be attributed to particular types of amino acids.

Most interesting though are the large perturbations in chemical shift that are observed when the β_2-microglobulin fibrils are complexed with SAP. The most significant of these arise in a spectral region whose resonances are attributed to the proteins acidic side chains. This suggests that interactions between SAP and β_2-microglobulin fibrils may be mediated through charged interactions in agreement with on-going biochemical studies. Also apparent are significant increases in intensity in regions associated with aliphatic sidechains.

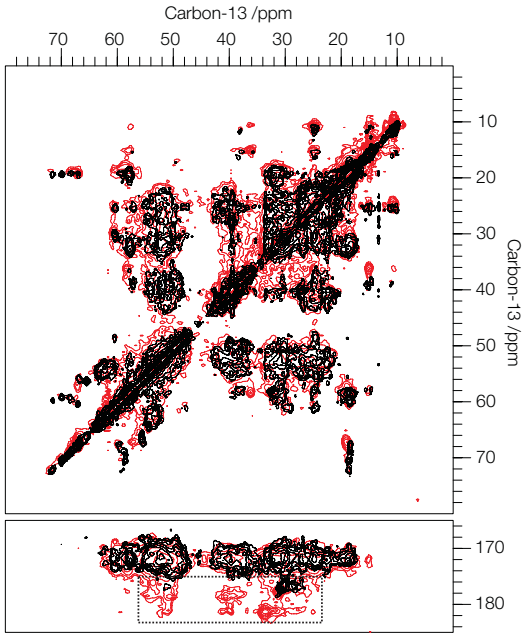

Figure 1. Comparison of ^{13}C-^{13}C correlation spectra of U-^{13}C/^{15}N labelled β_2-microglobulin fibrils in the presence (red) and absence (black) of SAP. Large perturbations in chemical shift are observed in areas assigned to the acidic sidechain (boxed area) highlighting the importance in SAP binding.

This suggests that upon the binding of SAP these residues are becoming more ordered; leading to enhanced cross-polarisation efficiency and proton driven spin diffusion. Interestingly analysis of the sequence indicates several tracts of protein that are rich in acidic and aliphatic residues enabling us to tentatively map potential SAP binding sites onto the β_2-microglobulin.

Identification of residues in β_2-microglobulin involved in SAP binding

To identify exactly which residues are implicated in the binding of SAP to β_2-microglobulin fibrils it is necessary to attribute each resonance in the $^{13}C/^{13}C$ correlation spectrum to a particular amino acid within the protein. To achieve this we are conducting a range of 3D experiments including NCOCX and NCACX. In addition we have recorded data on selectively and extensively labelled samples[4,5] (β_2-microglobulin expressed grown on media with 1,2- and 3-^{13}C glycerol as their carbon source) which significantly reduces the complexity and spectral overlap. Together these techniques are facilitating the assignment of the β_2-microglobulin fibrils (Figure 2). This data will not only identify which particular residues are important in SAP binding but will also inform on the conformation of the β_2-microglobulin within the fibrils. Comparison of chemical shifts with those obtained for β_2-microglobulin in solution will provide insights into the structural rearrangements that occur upon fibrillogenesis.

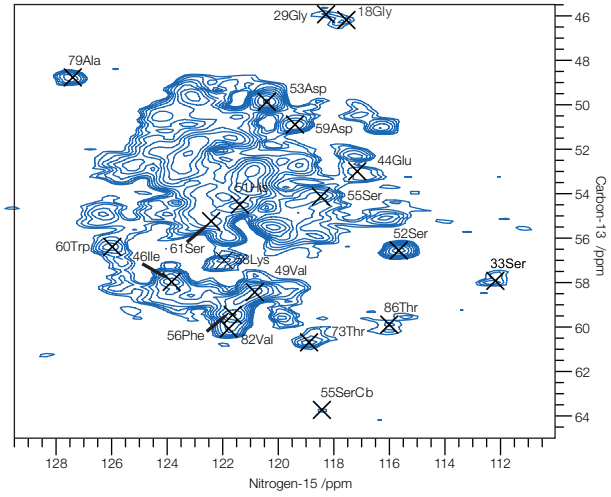

Figure 2. Expansion of the N/Cα region of a $^{13}C/^{15}N$ correlation spectrum showing some of the assignments made of the β_2-microglobulin fibrils.

Summary

Recent improvements in NMR hardware including access to higher magnetic fields and NMR probes tailored to work on biological samples coupled with new labeling strategies is enabling significant progress to be made in understanding how *in-vivo* factors, such as SAP, interact with amyloid fibrils and the role this may play in their formation of stability. To date our findings suggest that the interaction of SAP is mediated by through electrostatic interactions with acidic sidechains that are presumably exposed on the fibril surface. Completion of a full assignment of the β_2-microglobulin fibrils at neutral pH will allow us to unambiguously identify which acidic residues are responsible and identify the types of motifs recognized by SAP. We envisage that this will assist in the development of novel therapeutic strategies that will disrupt the interaction of SAP with amyloid fibrils helping the host's own defenses clear the amyloid deposit.

References

1. Chiti, F.; Dobson, C. M. *Ann. Rev. Biochem.* **2006**, *75*, 333
2. Bodin, K.; Ellmerich, S.; Kahan, M. C.; Tennent, G. A.; Loesch, A.; Gilbertson, J. A.; Hutchinson, W. L.; Mangione, P. P.; Gallimore, J. R.; Millar, D. J.; Minogue, S.; Dhillon, A. P.; Taylor, G. W.; Bradwell, A. R.; Petrie, A.; Gillmore, J. D.; Bellotti, V.; Botto, M.; Hawkins, P. N.; Pepys, M. B. *Nature* **2010**, *468*, 93.
3. Emsley, J.; White, H. E.; O'Hara, B. P.; Oliva, G.; Srinivasan, N.; Tickle, I. J.; Blundell, T. L.; Pepys, M. B.; Wood, S. P. *Nature* **1994**, *367*, 338.
4. Hong, M.; Jakes, K. *J. Biomol. NMR* **1999**, *14*, 71.
5. Higman, V. A.; Flinders, J.; Hiller, M.; Jehle, S.; Markovic, S.; Fiedler, S.; van Rossum, B. J.; Oschkinat, H. *J. Biomol. NMR* **2009**, *44*, 245.

High-Resolution ^{1}H and ^{17}O Solid-State NMR Studies of Hydrous Wadsleyite

Sharon Ashbrook,[1] Andrew Berry,[2] John M. Griffin[1] and Stephen Wimperis[3]

[1]School of Chemistry and EaStCHEM, University of St Andrews, [2]Department of Earth Sciences and Engineering, Imperial College London, [3]School of Chemistry and WestCHEM, University of Glasgow

Overview

It is easier to study the chemistry of Jupiter's atmosphere than it is to study the chemistry of the Earth's mantle, just 50 km or so beneath our feet. Space probes can be sent to Jupiter, but no drill bit has ever penetrated much more than about 10 km into the Earth's crust. Currently, everything we know about mantle chemistry has had to be inferred by secondary means. These include studies of rocks found in the crust but derived from the upper mantle, seismological measurements, and laboratory measurements on minerals under conditions of extreme pressure and temperature.

The Earth's upper mantle consists mainly of olivine, or α-$(Mg,Fe)_2SiO_4$. However, as shown in Figure 1, a seismic discontinuity at a depth of 410 km is believed to correspond to a phase transition to a denser polymorph called wadsleyite, or β-$(Mg,Fe)_2SiO_4$. It is thought that the Earth may contain many times the amount of water than is accounted for by the oceans and atmosphere. A variety of experimental observations indicate that this 'hidden water' is likely to be dissolved in the mantle. Laboratory studies have shown that olivine can accommodate substantial amounts of water but that it is wadsleyite that has the highest affinity, containing up to 3.3% of water by weight. However, the question of how wadsleyite might accommodate water (or, equivalently, hydrogen) has yet to be fully answered. Hydrous wadsleyite can be synthesised in the laboratory, yet many standard techniques for structure determination then fail. Indeed, X-ray diffraction has yielded the structure of anhydrous wadsleyite but cannot tell us where low concentrations of H atoms are located in the hydrous form.

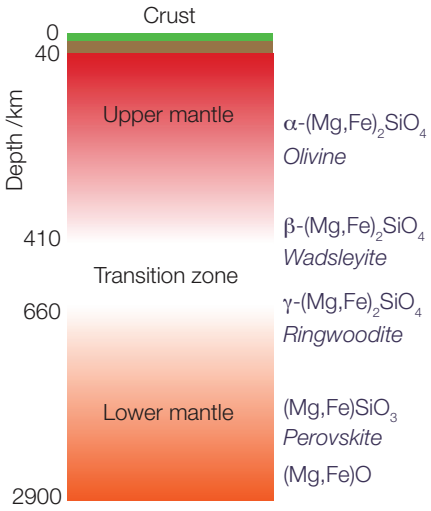

Figure 1. The structure of the Earth's mantle

Solid-state NMR offers a powerful alternative technique for the study of inner-Earth minerals. Indeed, ^{1}H solid-state NMR can yield detailed information about proton chemical environments and hydrogen-bonding interactions. Furthermore, the ^{17}O nucleus (spin I = 5/2) also provides a highly sensitive probe of oxygen bonding geometry and coordination through changes in the chemical shift and second-order quadrupolar interactions. However, the low natural abundance of ^{17}O (0.037%) means that isotopic enrichment is usually required for observation of the NMR signal. In previous studies, we have successfully used this method to provide structural insight into a range of synthetic anhydrous silicate systems by ^{17}O solid-state NMR.[1,2] Nevertheless, characterisation of subtle structural changes upon hydration remains a challenge due to the typically small sample volumes available. In the current work, we have attempted to address this problem by exploiting the significant signal enhancement achievable at a magnetic field strength of 20.0 T.

Experimental results

The anhydrous wadsleyite structure, shown in Figure 2a, consists of pyrosilicate $Si_2O_7^{6-}$ units (sites O2 – O4) and a five-coordinate O^{2-} site (O1) surrounded by magnesium cations. A number of experimental and theoretical studies have identified the under-bonded crystallographic O1 site as a favourable location for protonation upon removal of a nearby magnesium cation from the Mg3 site.[3,4] Full hydration of the structure in this way leads to two slightly different hydroxyl group hydrogen sites in the structure and gives a theoretical maximum hydration level of 3.3 wt%, in agreement with maximum hydration levels achieved in experimental studies.

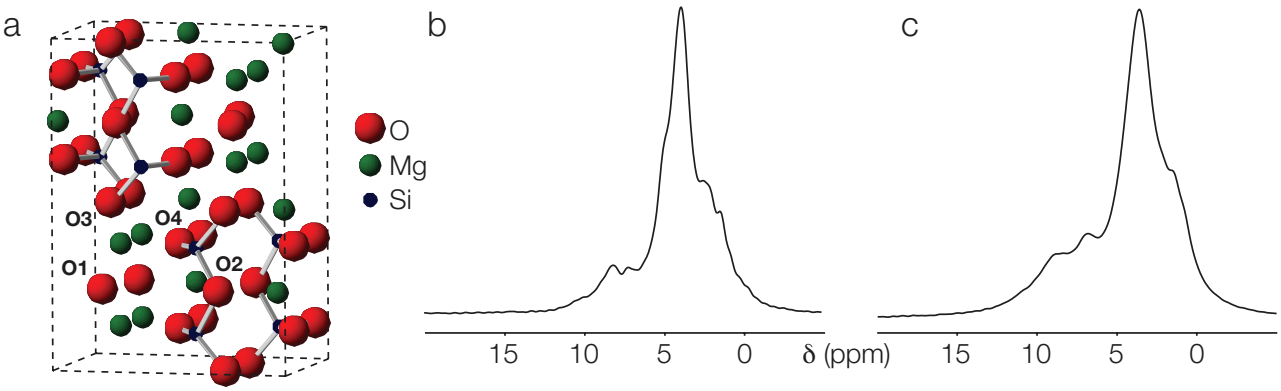

Figure 2. (a) Crystal structure of anhydrous wadsleyite. ^{1}H MAS NMR spectra of hydrous wadsleyite recorded at 20.0 T are shown for samples with hydration levels of (b) 1.5 and (c) 3 wt% hydrogen.

^{1}H MAS NMR spectra of synthetic samples of ^{17}O-enriched hydrous wadsleyite are shown in Figures 2b and c. In these spectra, strong intensity is observed around ~3.5 ppm, consistent with the presence of OH hydroxyl protons in the structure. These shifts are in agreement with density functional theory (DFT) calculations on a crystal structure of hydrous wadsleyite with full hydration on the O1 site. However, lower intensity peaks between 7 and 9 ppm are also observed in both spectra. DFT calculations for model structures indicate that these shifts are more characteristic of protons in Si-OH environments, suggesting low-level protonation of the pyrosilicate group oxygen sites.

Further insight into the proton locations is provided by comparison of ^{17}O MAS and satellite-transition (ST)MAS NMR spectra obtained for both anhydrous and hydrous wadsleyite. The proposed hydration of the O1 site is consistent with the observed reduction in intensity of the narrow O1 signal in ^{17}O MAS NMR spectra of hydrous wadsleyite samples as compared to the anhydrous form (Figures 3a-c), and the concomitant increase in the quadrupolar-broadened OH hydroxyl group intensity. However, ^{17}O STMAS NMR spectra also reveal extensive broadening of the silicate oxygen sites O3 and O4 in the hydrous samples. This indicates disorder in the structure, with the possible protonation of these sites to form silanol groups.

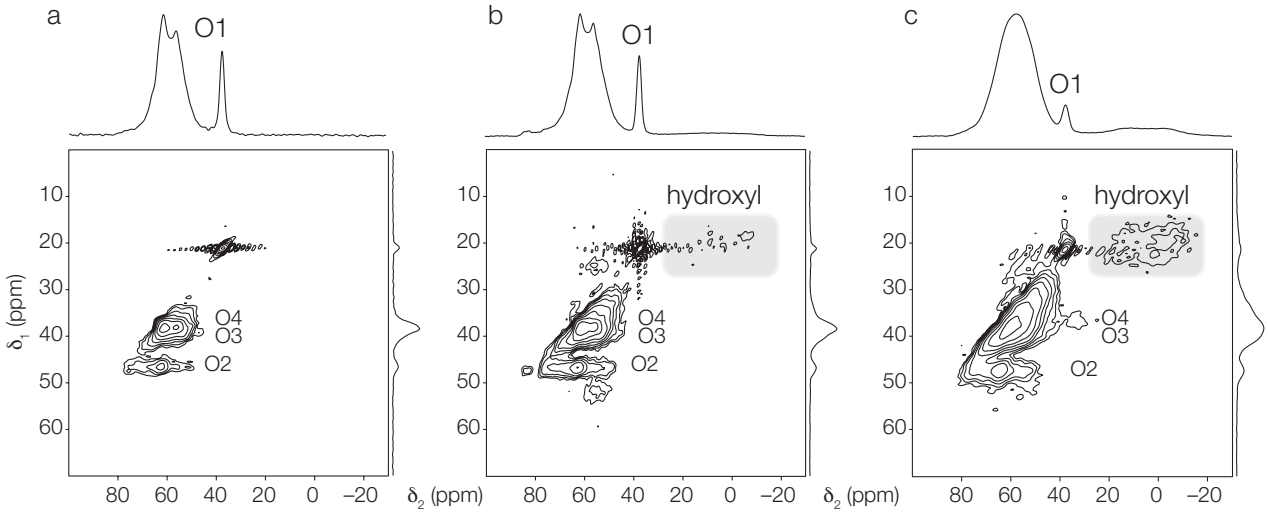

Figure 3. ^{17}O STMAS NMR spectra of (a) anhydrous, and (b) 1.5 wt% and (c) 3 wt% hydrous wadsleyite, recorded at 20.0 T. ^{17}O MAS NMR spectra are shown above.

References

1. Ashbrook, S. E.; Berry, A. J.; Hibberson, W. O.; Steuernagel, S.; Wimperis, S. *J. Am. Chem. Soc.* **2003**, *125*, 11824.
2. Ashbrook, S. E.; Berry, A. J.; Frost, D. J.; Gregorovic, A.; Pickard, C. J.; Readman, J. E.; Wimperis, S. *J. Am. Chem. Soc.* **2007**, *129*, 13213.
3. Smyth, J. R. *Am. Mineral.* **1994**, *79*, 1021.
4. Ross, N. L.; Gibbs, G. V.; Rosso, K. M. *Am. Mineral.* **2003**, *88*, 1452.

^{14}N and ^{2}H NMR Studies of Microsecond Timescale Dynamics in Solid Peptides

Luminita Duma[1] and Stephen Wimperis[2]

[1]Department of Chemistry, Ecole Normale Supérieure, Paris, France, [2]School of Chemistry and WestCHEM, University of Glasgow

Overview

Most molecules of interest are not soluble and therefore solid-state nuclear magnetic resonance (NMR) is an attractive tool to study dynamics of solid compounds. Anisotropic nuclear spin interactions (e.g., dipole-dipole and quadrupolar couplings) often match the timescales of different kinds of dynamic processes occurring in solids. These dynamic processes affect various spectral features, such as lineshapes and relaxation rates, whenever their rate constants are close to the characteristic frequency of the experiment. Therefore, NMR has a variety of applications in different areas of science.

One of the quadrupolar nuclei extensively exploited in the past to probe dynamics in solids is deuterium (^{2}H). A recent method,[1] based on the comparison of single-quantum (SQ) and double-quantum (DQ) spectra of ^{2}H under magic angle spinning (MAS), easily reveals slow dynamics in solids. The same principle was recently applied to ^{14}N solid-state NMR to characterise this time much faster processes.[2] Hence, ^{2}H and ^{14}N quadrupolar nuclei, which both have a spin quantum number $I = 1$ and quadrupolar interactions that vary between 10^{3} and 10^{7} Hz, can be exploited to monitor dynamic timescales ranging from microsecond (μs) to millisecond (ms).

Indirect detection of ^{14}N MAS NMR spectra of L-histidine

Despite its high abundance (99.6%), ^{14}N has been rarely studied in the past because of its low gyromagnetic ratio ($\gamma_{^{14}N}/\gamma_{^{1}H} = 0.07$) and relatively large quadrupolar coupling (few MHz). In contrast to half-integer quadrupolar nuclei that have a central transition with vanishing first-order quadrupolar broadening, the energy levels of ^{14}N lack a central transition since ^{14}N is a spin $I = 1$ nucleus. Hence, ^{14}N spectra at high magnetic fields are often several MHz wide, making direct NMR detection extremely difficult. First-order quadrupolar broadening can in principle be avoided by the observation of the overtone transitions, but the overtone signal intensity and excitation are second-order effects that diminish with increasing magnetic field. The indirect detection techniques introduced recently can overcome the limitations in sensitivity and resolution of ^{14}N NMR spectra under MAS.[2] Indeed, indirect ^{14}N detection through nearby "spy" nuclei such as ^{1}H or ^{13}C under MAS considerably enhances spectral resolution and sensitivity, making measurements of large quadrupolar couplings such as those of amide ^{14}N nuclei in small molecules possible.

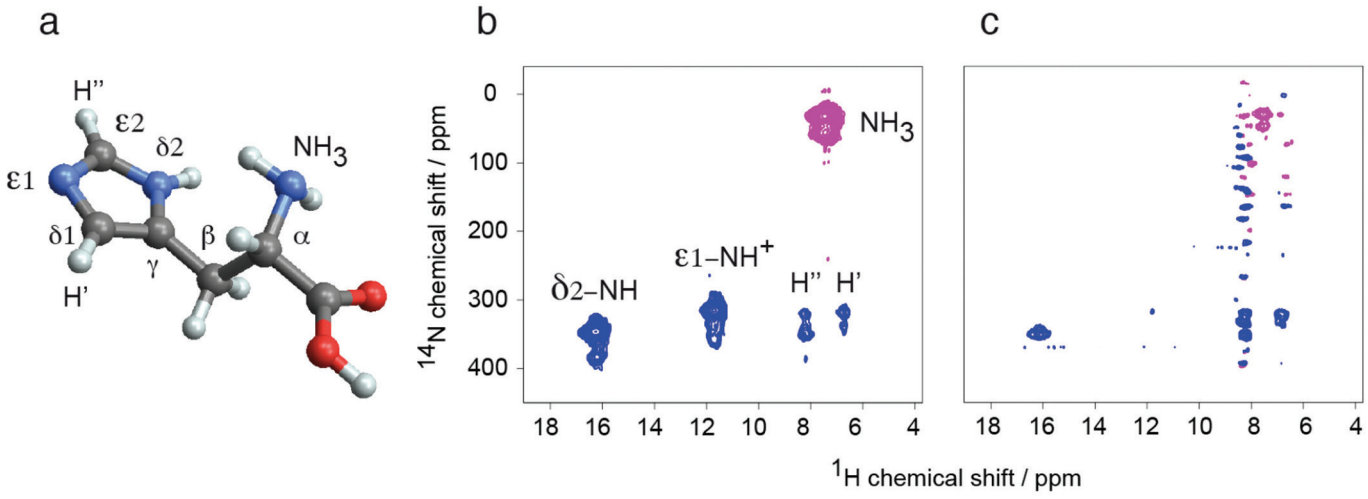

Figure 1. (a) L-histidine molecule. ^{1}H–^{14}N SQ HMQC MAS NMR spectra of the (b) protonated and (c) exchange-deuterated L-histidine recorded at 20 T and 55 kHz MAS spinning frequency.

In order to combine ^{2}H and ^{14}N MAS NMR studies for probing dynamic processes, the feasibility of ^{13}C and ^{1}H indirect detection of ^{14}N NMR spectra has to be demonstrated on deuterated molecules where the exchangeable protons were replaced by deuterons. ^{1}H–^{14}N HMQC SQ correlation MAS spectra were recorded at 55 kHz spinning frequency and 20 T magnetic field on protonated (Figure 1b) and exchange-deuterated L-histidine samples (Figure 1c). A rotary resonance recoupling scheme[3] has been used to transfer the magnetisation from protons to nitrogens. Both spectra show correlation peaks not only for the three directly bound ^{1}H – ^{14}N but also the two bonds $^{1}H'$–$^{14}N^{\varepsilon 1}$ and $^{1}H''$–$^{14}N^{\delta 2}$ (Figure 1a, b) pairs which can thus be easily assigned. The NH_3^+ correlation peak is negative because of a spectral aliasing associated with a different second-order isotropic chemical shift when compared to the aromatic nitrogens. However, the correlations peaks of the directly bound ^{1}H–^{14}N pairs in the aromatic ring are lower in intensity suggesting a less efficient magnetisation transfer. As expected, the sensitivity for the directly bound ^{1}H–^{14}N pairs decreases considerably for spectra recorded on the deuterated L-histidine sample. In addition, artefacts at the ^{1}H carrier position which evolve in the indirect dimension affect the spectrum obtained on the exchange-deuterated sample.

References

1. Cutajar M.; Ashbrook S. E.; Wimperis S. *Chem. Phys. Lett.* **2006**, *423*, 276.
2. Cavadini S.; Lupulescu, A.; Antonijevic, S.; Bodenhausen, G. *J. Am. Chem. Soc.* **2006**, *128*, 7706.
3. Oas T. G.; Griffin R. G.; Levitt M. H. *J. Chem. Phys.* **1988**, *89*, 692.

^{71}Ga NMR of Microporous Gallium Phosphates (GaPOs)

Sharon Ashbrook,[1] Richard Walton[2] and Stephen Wimperis[3]

[1]School of Chemistry and EaStCHEM, University of St Andrews, [2]Department of Chemistry, University of Warwick, [3]School of Chemistry and WestCHEM, University of Glasgow

Overview

Gallium phosphates (GaPOs) are a novel class of microporous solid, with possible practical applications in, for example, separation and catalysis. A number of GaPO structures are made up exclusively of corner-sharing tetrahedral units (GaO_4 and PO_4) and are thus direct analogues of aluminosilicate zeolites. However, unique GaPO forms, not seen in aluminosilicate chemistry, are also found, with some arising from the possibility of gallium occurring in five- and six-coordination sites. GaPOs are normally synthesized hydrothermally. An amine or quaternary ammonium salt is also added and the presence of this organic "template" molecule, which is incorporated into the cavities within the structure, is essential in producing the microporous framework. The thermal stabilities of GaPOs are similar to those of the better known aluminium phosphates (AlPOs) and hence calcination at 500-600 °C can be used to remove the template molecule and any occluded water.

Investigations of host-guest interactions in microporous solids are important in understanding the sorption and any catalytic properties of the materials. However, it is often difficult to study template or adsorbed guest molecules in porous solids using standard diffraction techniques, owing to the considerable positional and/or dynamic disorder of the guest species. It is therefore necessary to turn to methods, such as solid-state magic angle spinning (MAS) NMR spectroscopy, that directly probe the local environments of individual atom types and are sensitive to dynamic behaviour. In the case of GaPOs, ^{31}P MAS NMR has been widely used to study the microporous framework, but gallium NMR has presented a number of difficulties.

The two stable isotopes of gallium are ^{69}Ga and ^{71}Ga, both with spin quantum number I = 3/2. The natural abundance of ^{71}Ga (40%) is smaller than that of ^{69}Ga (60%) but its Larmor frequency is higher (122 MHz at B_0 = 9.4 T, as opposed to 96 MHz for ^{69}Ga) making ^{71}Ga generally the nucleus of choice for NMR. However, solid-state ^{69}Ga and ^{71}Ga MAS NMR studies remain rare as very large quadrupolar interactions are the norm and lead to poor sensitivity and resolution, with the second-order quadrupolar broadening often so large that achievable spinning rates are insufficient to average the lines to the forms expected under MAS. For example, we encountered these difficulties in a 2002 study of sodium gallium silicate zeolite precursors.[1]

Recently, we have been studying dynamics in an aluminophosphate known as AlPO-34, synthesized with various template molecules. We decided to revisit ^{71}Ga MAS NMR and investigate if the same dynamics are observed in the isostructural material known as GaPO-34, which again can be synthesized with a variety of template molecules.

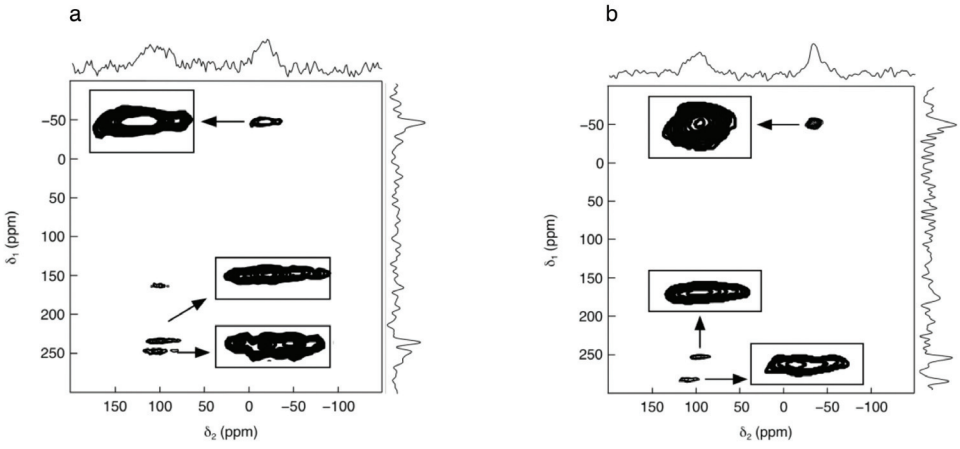

Figure 1. ^{71}Ga MQMAS spectra of (a) GaPO-34 with a methylimidazole template and (b) GaPO-34 with a pyridine template, recorded at B_0 = 20.0 T and a MAS rate of 33 kHz.

^{71}Ga multiple-quantum MAS NMR

^{71}Ga multiple-quantum (MQ) MAS spectra of two templated forms of GaPO-34 are shown in Figure 1. These spectra were recorded overnight, at a magnetic field strength of 20.0 T using a 2.5-mm MAS probehead. In each spectrum, the predicted three Ga sites are resolved: two 4-coordinate and one 6-coordinate. With the feasibility of high-resolution ^{71}Ga NMR now proven for these materials, we can now attempt to apply ^{71}Ga satellite-transition (ST) MAS NMR to the study of solid-state dynamics on the microsecond timescale.[2]

^{69}Ga MAS NMR

^{69}Ga MAS NMR spectra of two templated forms of GaPO-34 are shown in Figure 2. These spectra were recorded at a magnetic field strength of 20.0 T using a 1.3-mm MAS probehead. Using a very high MAS rate (65 kHz) combined with the high magnetic field strength, it is possible to resolve the 4-coordinate and 6-coordinate Ga sites into separate lineshapes for the first time using ^{69}Ga NMR. However, in view of the more favourable NMR properties of the ^{71}Ga nuclide, ^{69}Ga NMR is likely to remain as only of minor interest.

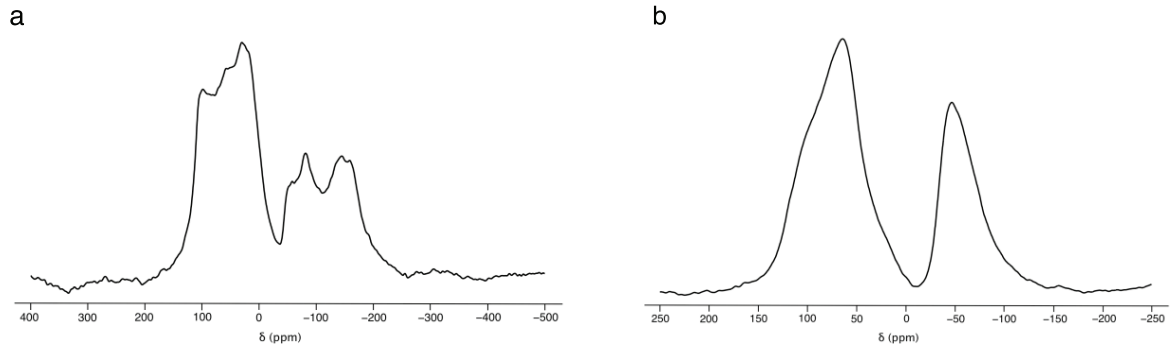

Figure 2. ^{69}Ga MAS NMR spectra of (a) (a) GaPO-34 with a methylimidazole template and (b) GaPO-34 with a pyridine template, recorded at B_0 = 20.0 T and a MAS rate of 65 kHz.

References

1. Antonijevic, S.; Ashbrook, S. E.; Walton, R. I.; Wimperis, S. *J. Mater. Chem.* **2002**, *12*, 1469.

2. Antonijevic, S.; Ashbrook, S. E.; Biedasek, S.; Walton, R. I.; Wimperis, S.; Yang, H. Y. *J. Am. Chem. Soc.* **2006**, *128*, 8054.

Solid-State NMR Investigation of Proteins Bound to F-Actin

Mark Pfuhl[1] and Steven Brown[2]

[1]King's College London, [2]Department of Physics, University of Warwick

Overview

Actin is a key protein without which even the most simple processes in a eukaryotic cell would be impossible. Its strong tendency to polymerise and the inability to crystallise polymeric F-actin have made structural studies very difficult with only low resolution methods such as electron microscopy or fibre diffraction available. The observation of proteins bound to F-actin is even more difficult, especially for small or actin binding proteins that are unfolded in the free state such as Calponin and Nebulin.[1,2]

F-actin and its complexes have so far been very little explored by solid-state NMR[3,4] so that we set out to first of all establish a simple model system to explore the possibilities. We selected the small, well structured (PDB entry: 2L3X) villin head piece domain (VHD) from human ABLIM2 because it is very small, very stable, highly soluble, binds tightly to F-actin and can be expressed in high yields in bacteria.

Results

Samples of about 4 mg of $^{15}N/^{13}C$ labelled VHD bound to about 30 mg F-actin were produced by cosedimentation. The pellet was then transferred into a 3.2 mm rotor provided by the facility. A fresh sample was produced for each of the two NMR time slots. After an initial period of spinning at 15 kHz and 3 ºC in the magnet excess liquid was removed before resuming the experiment. This was undertaken to see if more space for more protein can be made without causing problems and to reduce the arcing that was observed in the $^{15}N/^{13}C$ correlation experiment. In the two sessions 1D ^{13}C spectra were recorded, and linewidths of < 50Hz could be measured for resolved lines. A 50 ms mixing time 2D PDSD ^{13}C-^{13}C experiment was recorded to better resolve the signals so that assignments from the solution experiments (BMRB: 17206) could be transferred. This was supplemented by a ^{15}N-^{13}C correlation experiment to produce selective N-Cα correlations. The clear appearance of the two glycines in the latter is a good indication of its quality. Consequently, several cross peaks could be assigned immediately and work is now continuing towards a more complete assignment in the complex.

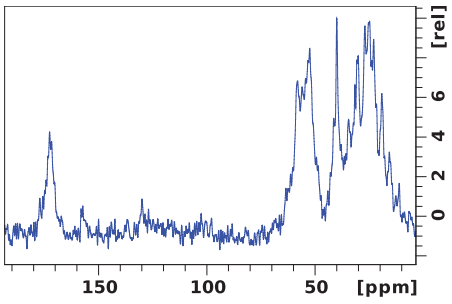

Figure 1. ^{13}C CP-MAS (15 kHz) at 3 ºC.

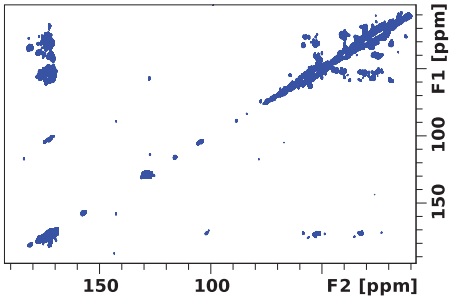

Figure 2. ^{13}C 2D PDSD 15 kHz -15 ºC (50 ms mixing time).

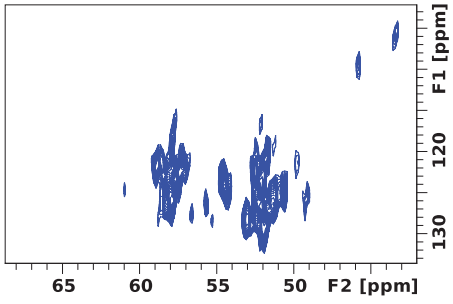

Figure 3. 2D N-Cα correlation 15 kHz at –15 ºC.

References

1. Pfuhl, M.; Winder, S. J.; Pastore, A. Nebulin, *EMBO J.* **1994**, *13*, 1782.
2. Pfuhl, M.; Al-Sarayreh, S.; El-Mezgueldi, M. *Biophys. J.* in the press, 2011.
3. Phillips, L.; Separovic, F.; Cornell, B. A.; Barden, J. A.; dos Remedios, C. G. *Eur. Biophys. J.* **1991**, *19*, 147-155.
4. Ahmed, M. A.; Bamm, V. V.; Shi, L.; Steiner-Mosonyi, M.; Dawson, J. F.; Brown, L.; Harauz, G.; Ladizhansky, V. *Biophys. J.* **2009**, *96*, 180-191.

BRUKER

Analytical Results Driven by Performance

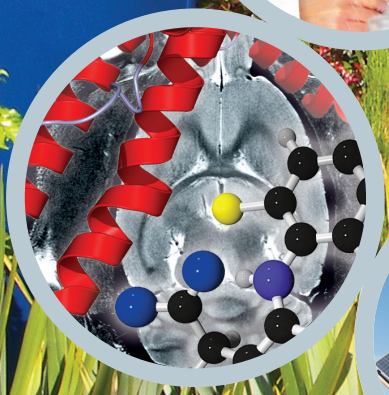

The ideal technological solution for each analytical question

Magnetic Resonance
- Nuclear Magnetic Resonance (NMR)
- Electron Paramagnetic Resonance (EPR)
- Magnetic Resonance Imaging (MRI)
- Time Domain-NMR (TD-NMR)

Analytical X-Ray
- X-Ray Diffraction (XRD)
- Chemical Crystallography
- Biological Crystallography
- X-Ray Fluorescence (XRF)
- Handheld X-Ray Spectrometry
- Microanalysis (EDS)
- Atomic Force and Scanning Probe Microscopy
- Optical Emission Spectroscopy (OES)
- Elemental Analysis

Vibrational Spectroscopy
- FT-IR Spectrometry and Microscopy
- Near-Infrared Spectrometry (NIR)
- Raman Spectrometry and Microscopy

Mass Spectrometry
- MALDI-MS
- Ion Trap MS
- ESI TOF MS
- Ultra High Resolution ESI TOF MS
- Fourier-Transform MS
- Gas Chromatography MS (GC-MS)
- Inductively Coupled Plasma MS (ICP-MS)
- Gas Chromatography

Contact us for more details: +44 (0)24 7685 5200
info@bruker.co.uk bruker.com/uk

Innovation with Integrity

Design by Mustard: www.mustardhot.com

Advantage West Midlands
www.advantagewm.co.uk

BBSRC
bioscience for the future

EPSRC
Engineering and Physical Sciences Research Council

investing in your future
European Regional Development Fund
European Union

Dr Dinu Iuga (Facility Manager)
Department of Physics
University of Warwick
Coventry CV4 7AL

T +44 (0) 24 761 50814
F +44 (0) 24 761 50897
E D.Iuga@warwick.ac.uk
W http://go.warwick.ac.uk/850mhz/

UNIVERSITY OF CAMBRIDGE
Durham University
University of Glasgow
The University of Nottingham
UNITED KINGDOM · CHINA · MALAYSIA
University of St Andrews
THE UNIVERSITY OF WARWICK